Effects of clinically-relevant electrical stimulation of macaque sensorimotor cortex on neural activity and behavior

Andrew R. Bogaard

A dissertation
submitted in partial fulfillment of the
requirements for the degree of

Doctor of Philosophy
University of Washington
2018

Reading Committee:

Eberhard E. Fetz, Chair
Steven I. Perlmutter
Stavros Zanos

Program Authorized to Offer Degree:
Department of Physiology & Biophysics

University of Washington

Abstract

Effects of clinically-relevant electrical stimulation of macaque sensorimotor cortex on neural activity and behavior

Andrew Robert Bogaard

Chair of the Supervisory Committee:
Professor Eberhard E. Fetz
Physiology & Biophysics

Electrical stimulation is a popular technique for neuromodulation in research, but the scope of approved therapeutic devices is extremely limited. For conditions where direct stimulation of the cortex may alleviate symptoms, such as stroke, clinical trials testing electrical cortical stimulation (CS) have produced mixed effects. These protocols may be less refined than other types of neurostimulation because basic physiological effects are not well understood, and because responses in the cortex are less predictable than other types of neurostimulation (e.g. to nerves). The following dissertation outlines experiments in non-human primates designed to document the physiological and behavioral effects of two types of CS. First, we adopt a tonic

form of CS common among clinical trials, transcranial direct current stimulation, and demonstrate how polarity and dose influence neural activity. Second, we test two forms of phasic CS: one that is timed relative to unilateral hand movements in a reaction time task, and another that is triggered by muscle activity. “Activity-dependent” CS such as these can be used to probe the functional roles of dynamic brain signals, or to induce plasticity. Our monkey model provides direct physiological evidence that is often lacking in human research, and reveals that, under certain conditions, CS produces repeatable changes in brain activity by facilitating or disrupting natural physiological processes. These insights may be useful towards the design of future CS-based therapies.

TABLE OF CONTENTS

LIST OF FIGURES

ACKNOWLEDGEMENTS

I thank the people who helped bring me to Dr. Eberhard Fetz' lab, and who made this research possible. Dr. Fetz was always available and enthusiastic about our research. I remember exchanging emails multiple times daily as we wrote our first grant together, all while he simultaneously visited labs in Europe. This was one of the first lessons Eb taught me – if he could respond to email promptly, in the midst of all his responsibilities, so could I. Eb helped me improve my writing, both for grants and papers, but also for getting my point across. I also hope to emulate Eb's scientific philosophy, which is mechanistic and critical, yet open and undevoted to hypotheses. Eb, thank you for taking me into your lab. Your theories regarding distributed neural coding have shaped my understanding of the brain in a profound way.

Thank you also to my fellow lab members in the Fetz and Perlmutter labs. Dr. Steve Perlmutter always kept lab meeting conversations grounded and provided down-to-earth feedback. I am very grateful to have had a second advisor such as Steve for support and scientific ideas. Dr. Stavros Zanos also dedicated a great deal of time mentoring me: we collected data reported in Chapter 3, planned experiments in Chapter 2, and he trained me to perform monkey surgery for which I was later certified at the WaNPRC. Rebekah Schaefer helped train me in monkey handling and provided support around the lab. Larry Shupe wrote the code responsible for monkey tasks reported in this dissertation, and provided patient, efficient, and expert technical support. Dr. Matthew Edwardson and Rebekah Schaefer contributed data presented in Chapter 1. Andrew Morse and Hayley Boyd helped collect data presented in Chapter 1. Richy Yun contributed data, code, and critical discussion underlying Chapter 3. Thanks to Dr. Irene Rembado for regular discussion and support. Thanks to Dr. Guillaume Lajoie who performed the population analysis in Chapter 1, and who became a friend along the way. Finally, thank you to committee members Drs. Elizabeth Buffalo, Jeff Ojemann, and Mark Holmes for guidance and support during my PhD.

I would like to mention the scientists who dedicated time and trust in my early training. Dr. Michal Zochowski and Dr. Victoria Booth at the University of Michigan sat patiently with me, every week, as I learned the principles of computational neuroscience and found my desire to study systems neuroscience. Dr. Jim Heys and Dr. Florian Mormann brought me back into the fold after some time brewing beer. Dr. Michael Hasselmo, Dr. Howard Eichenbaum, and Dr. Chantal Stern invited me to join a wonderful group of neuroscientists at Boston University where I learned how to analyze neural and behavioral data. Of the community in Boston I want to thank Dr. Hasselmo, as well as Drs. Konstantin Bakhurin, Claudia Cherici, Mark Brandon, Ehren Newman, and Sam Mckenzie.

Finally, thank you to my parents Tom and Karen, and to my siblings, John, Erik, and Katherine. I am fortunate to have such an inspiring and caring family.

I should also acknowledge serendipity, my personal source of strategy and planning.

DEDICATION

I dedicate this work to my family, to those who have trained me, and to the animals we use to learn about neuroscience.

GLOSSARY

a-tDCS	anodal transcranial direct current stimulation
c-tDCS	cathodal transcranial direct current stimulation
CC	corpus callosum
CCEP	cortico-cortical evoked potential
CS	cortical stimulation
ECS	epidural cortical stimulation
EMG	electromyography
FE	flexion/extension torque
FS neuron	fast spiking neuron (fast spike, putatative interneuron)
ICMS	intracortical microstimulation
IHI	interhemispheric inhibition
ISI	interspike interval
ISP	ipsilateral silent period
LFP	local field potential
LTD	long term depression
LTP	long term potentiation
NC	neurochip
NMDA	n-methyl-d-aspartate
M1	primary motor cortex
MEP	motor evoked potential
MRV	mean resultant vector
PCA	principle component analysis
PMBR	post-movement beta rebound
PS	pronation/supination
PT	pyramidal tract
RS neuron	regular spiking neuron (slow spike, putative principle cell)
RT	reaction time
RU	radial/ulnar torque
S1	primary sensory cortex
SNR	signal to noise ratio
st-LFP	spike-triggered LFP
SUA	single unit activity
tDCS	transcranial direct current stimulation
TMS	transcranial magnetic stimulation
Utah array	microelectrode array (100 channels, 3x3mm)
wst-LFP	whitened spike-triggered LFP

INTRODUCTION

Electrical stimulation is a common experimental technique in neuroscience, but its use in medicine is mostly limited to a handful of approved devices that can alleviate symptoms such as pain, deafness, and bladder incontinence by targeting peripheral nerves. Devices that target the brain directly, such as deep brain stimulation, or electro-convulsive therapy, are limited in scope. Some medical conditions of the central nervous system that are currently untreated by CS may benefit from this approach, but the protocols and parameters are not well established. This is partly because the effects of electrical cortical stimulation (CS) are less understood than those following activation of nerves or subcortical structures with more rudimentary function. In this dissertation, we explore whether CS is effective at modulating brain activity for functional gain, either by recruiting natural processes or by disrupting them.

The following experiments were conducted in the motor cortex, which can adapt and reorganize to compensate for injury to body and brain[1]. Despite these natural mechanisms, many patients are left with incomplete motor recovery following accidents like stroke or traumatic brain injury, and doctors can do little to ameliorate the damage. CS holds promise to help patients boost beneficial brain processes, such as synaptic reorganization, or inhibit maladaptive ones, such as aberrant inhibition[2] by non-specific excitation or inhibition of motor cortex[3–5]. The most popular method behind this approach, transcranial direct current stimulation (tDCS), delivers tonic stimulation for 20 minutes at a time. Although tDCS showed early promise, it has become the center of intense debate because results are variable and direct evidence of physiological effects is lacking. In *Chapter one* of this dissertation, I describe a monkey model for tDCS designed to bridge this translational gap with the goal of elucidating the parameters and mechanism of action underlying tDCS efficacy.

There is an alternative to preprogrammed stimulation, namely activity-dependent stimulation, that may produce longer and more robust effects[6]. This approach differs from most protocols in neurostimulation because delivery is spatiotemporally defined by neural activity within the brain, muscles, or behavior[7,8]. The Fetz lab has shown that the activity-dependent intracortical micro-stimulation is effective in producing predictable plastic changes, but these experiments required invasive implants. Experiments described in *Chapter two* extend this line of work by applying the same activity-dependent stimulation protocol with CS surface electrodes that are more suited for clinical use. Finally, *Chapter three* presents effects of activity-dependent stimulation delivered to motor cortex timed relative to unilateral movements in a reaction time task. These experiments demonstrate that the effects of CS vary with behavioral state and can modulate ongoing communication between cortical areas.

GENERAL METHODS

SUBJECTS AND BEHAVIORAL TASKS

All experiments were conducted with male Macaca nemestrina monkeys (N=5). Procedures conformed to the National Institutes of Health 'Guide for the Care and Use of Laboratory Animals' and were approved by the University of Washington Institutional Animal Care and Use Committee.

Monkeys were trained in visuomotor target tracking tasks conducted in a primate behavior booth equipped with a computer monitor (30 cm × 23 cm), tones for audio feedback, and a computer-controlled feeder dispensing fruit smoothie as a reward. One or more computer cursors were used to direct the monkey to produce torques about the forearm(s) and were controlled by accelerometers affixed to the dorsum of the hand, or by a manipulandum capable of registering isometric torque (flexion/extension, FE; radial/ulnar, RU) and grip force. Details pertaining to the behavioral task are outlined for each experiment under *Specific Methods*.

SURGICAL PROCEDURES

For all surgical procedures, the skin around the surgical site was shaved and scrubbed with betadine. Sterile surgery was performed with the animal under 1–1.5% isoflurane anesthesia (95:5 O2:CO2). Cardiac waveform, heart rate, respiratory frequency, blood-pressure and end-tidal CO_2 was monitored continuously. Post-operative care included recovery in a padded cage, administration of analgesics (ketoprofen 5 mg/kg), additional doses of antibiotics (cephalexin 25 mg kg−1 PO), and careful overnight observation by trained personnel. After recovery, monkeys showed no signs of discomfort related to any of the implanted devices.

IN-VIVO NEURAL RECORDINGS

We used a 256 channel digital data acquisition system (Tucker-Davis Technologies) to record neural, behavioral, and task data in the primate booth. Data from the manipulandum (isometric torque) and behavioral task (target number, cursor position, task condition) was sampled at 3kHz. Voltage signals from the microelectrodes were amplified, digitized, and streamed to the TDT base station with a sampling rate of 25kHz. The data streams from each electrode was processed and saved as local field potential (LFP) and single unit activity (SUA). To extract the LFP, signals were band-pass filtered (0.25 – 500 Hz), down-sampled (3 kHz), and saved to hard disk. To extract SUA, signals were band-passed filtered (0.5-4 kHz), and a threshold unique to each channel was used to detect action potentials by negative threshold crossing. Thresholds were initially estimated automatically as minus three times the standard deviation estimated from 10 seconds of the SUA filtered signal, and the first five minutes of recording was used to ensure that thresholds were appropriately set outside of the baseline noise and to detect spikes. When a spike was detected, a snippet of SUA signal was recorded to the disk corresponding to 8 samples before the threshold crossing and 22 samples after the threshold crossing (1.2ms window)

DATA AND STATISTICAL ANALYSES

All figures, data analysis, and statistical comparisons were calculated using MATLAB R2017a unless otherwise stated. When applicable, paired statistical tests were used, and normality was never assumed. In particular, Wilcoxon's paired, two-sided sign rank test (signrank, MATLAB) was used when comparing cells across conditions, and the Wilcoxon's two sided rank sum test (ranksum, MATLAB) was used when comparing the behavioral and neural activity across sessions. Unless otherwise noted, data and error bars depict the median and the 95% confidence interval of the median, respectively.

Chapter 1. NEURAL EFFECTS OF CLINICAL-TYPE TRANSCRANIAL DIRECT CURRENT STIMULATION

Transcranial direct current stimulation (tDCS) is the focus of intense debate because polarization experiments in animals clearly demonstrate neuromodulation, but results across human trials are inconsistent. To address this translational gap, we designed a clinically realistic non-human primate model of tDCS to target sensorimotor cortex and analyzed changes in neural firing during anodal (a-) and cathodal (c-) tDCS ranging from clinical to supraclinical intensities. We found that tDCS reproducibly affected firing rate in a dose-dependent manner that depends on polarity and cell type. Changes were significant above scalp current densities of 0.1 mA/cm^2, which is higher than doses usually applied to humans. Single-cell encoding of sensorimotor task variables was largely unaffected by tDCS, but network-level population dynamics were altered. Our results suggest that many human trials may not be delivering sufficient current, and that both a-tDCS and c-tDCS produce a mix of excitatory and inhibitory effects.

BACKGROUND

Modern direct current stimulation began with the application of polarizing electrodes to the pia of sensorimotor cortex in anesthetized animals over 50 years ago[9–11]. Early findings demonstrated that anodal currents of sufficient duration produced hours-long increases in neuron spike rates and the amplitude of cortico-cortical evoked potentials, while cathodal currents produced the opposite effect[10,12,13]. Recently, this technique was adapted for noninvasive use in humans[14,15] with doses that are orders of magnitude lower than those used in animals[16,17]. These studies reported that motor cortical excitability, estimated by the amplitude of the motor evoked potential using transcranial magnetic stimulation (TMS-MEP), was increased under the anode, and decreased under the cathode[15]. In line with the earliest results in rodents, these changes could be made to last hours if tDCS was applied for long enough (over 10 minutes). Interest in tDCS skyrocketed after these seminal reports, and over 1000 papers have reported its use as a tool in neuroscience[18,19] and also in clinical trials for many neurological[20–22] and psychiatric conditions[23].

Recent tDCS research in humans often relies on cognitive and behavioral effects to infer its action, probably because it is difficult to record directly from the human brain. Moreover, it was already generally accepted in clinical settings that one could "tune" brain excitability "up" with anodal stimulation and "down" with cathodal stimulation. This theory of tDCS informed the design and interpretation of many studies. For example, the relative advantage/disadvantage of anodal/cathodal tDCS was shown in stroke recovery[2,3,5,24], in a memory task[25,26], and performance measures like reaction time and force production[27]. Unfortunately, follow-up studies suggest that these effects are not very reliable[20,28–30], a problem that may be addressed by future experiments that explain the physiological mechanisms of human tDCS.

There are some direct recordings of changes in evoked and oscillatory EEG activity and fMRI-based measures in humans[31–34], but simultaneous recording and stimulation is rare. Instead, direct neurophysiological measurement during tDCS in humans is largely limited to measuring responses evoked by TMS[35], and are recorded in the periphery. Although evoked activity is a more direct measure than behavior, interpreting these results is difficult because they do not reflect natural neural activity[36]. And while individual experiments reported significant results in one or more aspect of their studies, taken together, the picture is unclear. Recent metaanalyses[35,37] suggest that physiological results are also variable. The sources of this variability may include the paucity of subjects in most human trials, inconsistencies in tDCS protocol (such as duration and dose), and the possibility that clinical-type tDCS is too weak or non-specific to produce reliable effects.

As interest in human tDCS grew, a second wave of animal polarization studies started anew, and these studies elaborated on early mechanistic findings in significant ways. In particular, controlled experiments in animals have elucidated the ways in which neurons[38,39] and synapses[40–42] are modulated by a uniform electric field, and paint an intriguing picture for how this seemingly nonspecific (both temporally and spatially) stimulation paradigm may actually produce task-specific effects[19,40,42]. Furthermore, these studies challenge the notion that anodal and cathodal stimulation may be applied to turn brain excitability up and down, instead, they present a nuanced description of how certain cell compartments are hyperpolarized while others are simultaneously depolarized. This pattern of polarization depends upon the cells morphology and orientation in the field, and affects its excitability as well as plasticity at its synapses. Furthermore, it is expected (but so far undemonstrated) that the effects at single neurons may be

amplified by the network, producing larger effects in spatiotemporal activity of the brain than might be expected given the relatively small effects on single neurons themselves.

While research on the basic science of polarization is well developed and clinical and behavioral research in humans abounds, translational research that characterizes the effects in the parameter space of clinical-type tDCS is lacking[16,17]. There are concerns about the translatability of animal polarization studies, including: vastly different current intensities, different methods of delivery (the skin, which shunts current, is typically bypassed), differences in the shape and organization of rodent and primate brains, and limited understanding about effects in active, un-anaesthetized brains. One important study recently measured the current shunting effects of the skin: in cadavers, they found that over 75% of applied currents are lost when tDCS is delivered to the scalp as opposed to the skull, and confirmed these effects in the spiking activity of anesthetized rodents across a range of currents and polarity[43]. Another study applied anodal tDCS at a human-like dose to the scalp of monkeys to target prefrontal cortex, and reported neurophysiological effects in the spontaneous LFP that corresponded with learning gains[44]. Intracranial electric fields induced by transcranial alternating current stimulation applied at clinical doses have been recently reported in humans[45] and monkeys[46]. This small collection of new experiments provide important evidence to validate claims made by computational methods[47,48]. However, many basic questions about clinical-type tDCS remain to be addressed. Do neural responses change across a range of potential clinical tDCS doses in the un-anaesthetized primate brain[49]? Does switching polarity broadly modulate excitability, or is there evidence for cell by cell modulation by somatic polarization or other mechanisms? Do changes in spontaneous activity persist after tDCS is turned off? How consistent are the effects within subjects, furthermore, is the spiking of single neurons consistently affected during repeated

sessions? How does tDCS affect coding and correlations between neurons in the active cortex? These are the questions addressed in the present study.

The sensorimotor cortex is a common target for tDCS, particularly in stroke trials[2,50]; the most common montage places one pad over sensorimotor cortex, and the other over the contralateral supraorbital area[15,24,51] (**Figure 1.1C**). Human tDCS electrodes are roughly 5x7cm in size, and current densities are low (0.028mA/cm^2 to ~0.1mA/cm^2)[35]. In the present study, we designed a non-human primate model of unihemispheric tDCS for targeting left sensorimotor cortex that matched human studies as closely as possible. tDCS electrodes were made from saline-soaked cellulose sponge electrodes (**Figure 1.1D**) and were 3x3cm in size to accommodate for the smaller skull. tDCS intensity ranged from low in human studies (0.027 mA/cm^2, 0.25mA) to about four times the maximal current density currently used in humans (0.44 mA/cm^2; 4mA). Neural data (local field potential, LFP and single unit activity, SUA) were recorded intracortically before (Pre, 20 minutes), during (Stim/Sham, 25 minutes) and after (Post, 30+ minutes) tDCS.

The present study aimed to document the changes in neuronal activity while the network was engaged in a motor task. Monkeys were trained in a visuomotor target tracking task in which the position of a cursor was controlled by a 2-axis manipulandum that registered isometric wrist torques (**Figure 1.1E**). During each trial, the monkey was cued to move the cursor to one of eight targets by contracting his forearm muscles to produce isomentric torques in wrist flexion/extension and radial/ulnar deviation. We found that tDCS modulated cortical single neuron spiking and population dynamics in a dose dependent manner that persisted for minutes after stimulation, with significant differences emerging at current densities that were higher than the majority of human trials. Responses during tDCS were similar across precentral and

postcentral gyrus, suggesting that effects may be generalized to other cortical structures with similar microanatomy. Both a-tDCS and c-tDCS produced mixed excitatory/inhibitory effects that were consistent across days and depended on cell type.

We also analyzed how tDCS affects neural coding of wrist torques using classical single cell tuning measures, as well as recently established techniques for quantifying neural population dynamics during movements[52]. We find that tDCS affects the way in which populations of cells coordinate their spiking activity during stereotyped movement, despite the fact that the tuning of individual cells is preserved. We also find that single-cell effects vary with the phase of movement generation. These results suggest that modulation by tDCS arises through an interaction of single cell and network effects.

SPECIFIC METHODS

Experiment timeline and behavioral task

During each experiment, the monkey voluntarily climbed from the cage into a primate chair for transport to the primate booth. Once in the booth, the head was fixed using two plastic bars which flexibly yet securely connected the halo to the chair. A feeder tube was placed in front of the monkey's mouth to deliver fruit smoothie reward. Finally, we prepared the scalp and placed the tDCS pads (see **tDCS**, above), and connected the recording system to the microelectrode array.

The behavioral task required the monkey to use his right hand to use a manipulandum to control a single cursor on the screen. The left arm was gently restrained in a tube. Trials in the task consisted of four phases: OFF, START, CONTRACT, and RELAX. At the beginning of a trial, the screen was blank for five seconds (OFF), followed by a cue (START) that indicated the

monkey would soon have to produce a torque about the wrist to one of eight possible targets (CONTRACT). During the START condition, the monkeys had to keep the cursor in a center target (no contraction) for a variable period of time (0.5-2 seconds) so that we could measure response time. During the CONTRACT condition, targets pseudo-randomly selected from one of eight targets in FE and RU were presented. After holding the cursor in the CONTRACT target box for 1 second, the RELAX target would appear in the center of the screen, cueing the monkey to relax his wrist to receive a reward. The monkeys performed the task continuously for the entire duration of the experiment, and each experiment consisted of roughly 1000 trials.

At the start of the experiment, we initialized the behavioral task, which ran without interruption until the experiment ended. Sample data recorded during epochs 1-3 are shown in **Figure 1.3A**. Epoch 1 (Pre) lasted 20 minutes, and established baseline activity. Epoch 2 (Stim/Sham) lasted for 25 minutes, and had three possible conditions: a-tDCS, c-tDCS, or sham. Epoch 3 (Post), lasted over 30 minutes, and until the monkey showed signs of fatigue or disinterest in the task. The monkeys would often perform the task for up to an hour following tDCS.*Surgical methods: halo*Both monkeys underwent a two-stage implantation schedule. During the first surgery, four 1.25x4mm perforated titanium craniofacial ties were affixed to the skull by 3 2x6mm titanium bone screws each. Two were implanted bilaterally over the occipital ridge, and two were placed temporally bilaterally. The plates integrated with the skull for 6 weeks and were used to reinforce the four points of contact for the surgical halo.During the second surgery, the 96-channel microelectrode arrays (length = 1.5mm, Blackrock Microsystems, Salt Lake City, UT) were implanted (left M1, Monkey S; left S1, monkey W) using the pneumatic insertion technique[53]. To implant the array, a bone flap (1.5x1.5cm) was removed from an area of the skull located stereotactically. Electrode arrays were placed in hand/wrist sites in pre and postcentral gyrus, located in precentral gyrus from the line extending from the genu of the arcuate sulcus

posteriorly to the central sulcus, and in the adjacent location in postcentral gyrus. After placement of the array, the dura was reapproximated over the array and the bone flap was replaced in the craniotomy with two 1mm screws and a single strip of thin titanium mesh plate together with hydroxyapatite to promote reintegration. At the end of experiments, the skull was inspected and there were no remaining defects or holes in the skull except for the hole permitting passage of the wire bundle. One connector pedestal was fixed to the skull caudal to ear-bar-zero. Finally, a lightweight aluminum halo system used for head fixation and mounting the tDCS pads was mounted with four pins seated in each of the four bone straps implanted during the first surgery. These pins were low on the head and separated by >2 cm from the tDCS pads.

Daily recording sessions began after the monkey had completely recovered from surgery. Monkeys voluntarily crawled from the cage to a primate chair adjusted so that each monkey sat upright comfortably. The left arm was loosely restrained in the plastic tube, and the monkey placed his right arm into a manipulandum. The head was restrained for the duration of experiments to promote attention in the task and for stability of neural recordings.*Transcranial direct current stimulation*

tDCS was designed to match human trials as closely as possible. Scalp pads were made from cellulose sponges soaked in 0.9% NaCl solution with inlaid copper wire, and were cut to a smaller size to accommodate the smaller anatomy of the monkey brain and skull (**Figure 1.1d**; 3x3cm versus ~5x7cm. Sponges were checked so as to be moist throughout but not wet or dripping onto the scalp to avoid any undesired current spread. Similar to the classic sensorimotor cortex/contralateral supraorbital montage used in human trials[3,51], we used placed one pad over the implanted array in sensorimotor cortex (anode: a-tDCS, cathode:c-tDCS), and a second pad over the right supraorbital ridge (main text **Figure 1.1c**). Proper location of pads was easily determined relative to landmarks (halo, pins, and connector pedestal) each day. As necessary,

hair was removed with Nair™ (Church & Dwight Co.), and the was skin rinsed and dried. At the onset of tDCS, current was delivered by a programmable stimulator (IZ2, Tucker-Davis Technologies) or a manual stimulator as previously used in clinical trials (Phoresor II autostimulator, IOMED, Salt Lake City, UT) and was slowly ramped up over 1 minute to a predetermined current to decrease the chance of the animal perceiving the stimulation. Voltage delivered to the pads was monitored to ensure that the proper current was delivered throughout the experiment (i.e. proper pad contact and circuit impedance such that the compliance voltage of the stimulator was never reached). If noise was observed in the neural recording as tDCS current was ramped (3 experiments), stimulation was decreased to the nearest dose that did not affect recording. Similar to human trials[3], the duration of tDCS was 25 minutes, and we explored doses ranging from the lowest delivered to human subjects (0.027 mA/cm^2) to roughly four times the highest dose currently delivered to humans (0.44 mA/cm^2).*Single unit identification and inclusion.*

Snippets of detected spikes in the SUA signal were sorted offline with Offline Sorter v4 (Plexon Co, Dallas, TX) using the template matching method. For each neuron, the signal to noise ratio (spike SNR)[54] was calculated by equation 1:

$$SNR = \frac{\max(\bar{W}) - \min(\bar{W})}{2 \cdot SD_{\varepsilon}}, \quad (1.\ 1)$$

where W the collection of all spike waveforms, $\bar{W}$ is the average waveform, and ε is the matrix of noise values calculated as deviations from the mean:

$$\varepsilon = W - \begin{bmatrix} \bar{W} \\ \vdots \\ \bar{W} \end{bmatrix}, \quad (1.\ 2)$$

Only neurons with >1000 spikes, an average peak height of >50uV, and spike SNR >3 were included for analysis.

Changes in firing rate

Data depicted in **Figure 1.3** were generated by compiling data across multiple experiments for each current step. The data from each individual experiment can be seen in **Figure 1.4**. For these analyses, we calculated ΔF, which describes the percent change in firing from Pre to Post, and was calculated by equation 1.3:

$$\Delta F = 100\ \frac{F_{Stim} - F_{Pre}}{\max(F_{Pre}, F_{PStim})}, \text{ (1.4)}$$

where f_{Pre} and f_{Stim} are the median firing rates for the Pre and Stim/Sham epochs, normalized by the larger of the two. Equation 1 is bound between -100 and 100, and represents the percent change in firing from the first epoch to the second.

We fit a sigmoid function to the data presented in Figure 1.3B, defined by equation 1.5:

$$\Delta F = \frac{A_M - A_0}{1 + 10^{b(x50 - x)}} + A_0, \text{ (1.6)}$$

where A_0 is a fixed parameter defined by ΔF during Sham epochs for each monkey, and A_M, $x50$, and b are free parameters describing the maximal value, inflection point and inflection point slope, respectively.

Longitudinal cell identification

The microelectrode arrays used in these experiments are chronic, immovable, and record stable SUA for years under ideal circumstances[55]. Considering that the area of tissue recorded by any given electrode is unchanging, it is likely that some neurons are recorded across many days. We

leveraged this to investigate whether a-tDCS or c-tDCS reliably affected individual neurons in a reliable manner across experiments.

Studies have used various spiking statistics such as waveform shape, inter-spike interval distribution, autocorrelation, and firing rate to identify which spikes might originate from the same neuron across days[56–58]. We performed a similar analysis, depicted in **Figure 1.8**. First, we calculated five metrics for each neuron: the mean waveform, spike rate during Pre, refractory period-timescale autocorrelation (bins logarithmically spaced from decades $10^{-3.6889}$ to 10^{-1}ms), regular-timescale autocorrelation (bins linearly spaced from 0 to 100ms), and ISI distribution (bins logarithmically spaced from decades 10^{-3} to $10^{1.5}$ms). Logarithmic spacing was used for short-timescale autocorrelation and ISI histogram so that the shape of short time interval features (where many important dynamics are reflected) were weighted similarly to slower ones.

The distance between each of the five metrics was calculated pairwise across all neurons. The L^2 norm was used for ISI distribution, autocorrelation, and firing rate, whereas the distance between spike waveforms was defined as 1 - sample correlation. The reason for this was the amplitude of the spike often changed day to day, but the shape generally does not, and the L^2 norm is sensitive to changes in amplitude, but the sample correlation is not. Each paired distance was z-scored for normalization, and we calculated the dot product between the four distances and a weighting vector **w** to favor the most consistent features, namely the spike time autocorrelation and interspike interval distribution,

$$d_i = \vec{d}_i \cdot \vec{w}, \quad (1.7)$$

Where

$\bar{d} = \left[d_{waveform}, d_{ISI}, d_{ACORR1}, d_{ACORR2}, d_F\right]$, and $\bar{w} = [1,1.3,2,2,0.75]$

D was larger for neurons recorded on different channels than for neurons recorded on the same channel for both monkeys **Figure 1.8Ci-ii**). This difference likely reflects that some neurons recorded across days were the same. We performed complete-linkage hierarchical clustering on the set of *D* for each channel, and clusters were cut from the cluster tree using a threshold for a distance criteria of 4 (see **Figure 1.8B)**, which corresponded to D most likely to be observed between neurons on the same channel as compared with neurons on different channels (**Figure 1.8Ci-ii**). Out of a total of 2671 neurons, the algorithm detected 1178 unique cells. **Figure 1.9** shows how many neurons were recorded for a given number of sessions. **Figure 1.10** shows channels with the most repeat recorded neurons detected by the algorithm.

Shuffle distributions for estimating statistical significance of repeated effects across sessions

For each condition (a-tDCS, c-tDCS, Sham), we calculated ΔF for all cells recorded more than once, and noted the percent of cells that were always modulated up or down by a given threshold *T*. We used a range of *T* (from 0-10%) to avoid arbitrary parametrization. To determine whether repeat changes in ΔF were more consistent than statistically expected, we shuffled all cells recorded more than once during a given condition (10,000 iterations) to generate a distribution of repeat ΔF for each *T*. Thus, we calculated the probability that observed repeat ΔF occurred by chance given the measured ΔF *in that condition*, thereby accounting for differences in ΔF across conditions (for instance, the chance level of repeat increases during a-tDCS is higher than c-tDCS because more cells tended to increase their firing).

Torque Directionality

Polar plots of firing rate by torque direction were generated to visualize the pattern of spiking dependent upon the animal's direction of wrist torque. To construct the rate map, torque direction was collected into bins of 6 degrees and the number of spikes in each bin was divided

by the time spent torqueing in that direction. To quantify the degree of directional selectivity, we calculated the mean resultant, R_m, of the directional firing rate map:

$$R_m = \frac{\cos(\bar{\theta})\sum_{i=1}^{n} F_i \cos(\theta_i) + \sin(\bar{\theta})\sum_{i=1}^{n} F_i \sin(\theta_i)}{\sum_{i=1}^{n} F_i}, \quad (1.8)$$

where $\bar{\theta}$ represents the preferred firing direction of the cell, and is calculated by

$$\bar{\theta} = \arctan\left(\frac{\sum_{i=1}^{n} F_i \sin(\theta_i)}{\sum_{i=1}^{n} F_i \cos(\theta_i)}\right), \quad (1.9)$$

Tuning rate functions

Firing rate maps of cell spiking in torque space were constructed by dividing the spike count within pixels of two dimensional torque data by the time spent by the cursor in that bin. Data were smoothed by a two-dimensional convolution with a pseudo-Gaussian kernel with a standard deviation of one pixel. Rate maps were compared across epochs using Pearson's correlation coefficient, ρ, calculated by the MATLAB function *corrcoef*. The torque vector information per spike was inspired by[59], and is defined in equation 5:

$$I = \sum_{i=1}^{N} p_i \frac{\lambda_i}{\lambda} log_2 \frac{\lambda_i}{\lambda}, \quad (1.10)$$

where the torque space was divided into N nonoverlapping pixels, p_i is the cursor occupancy probability of bin i, λ_i is the mean firing rate for bin i, and λ is the overall mean firing rate of the cell.

Spike-triggered LFP and unitary spiking contribution to LFP

We calculated whitened spike triggered LFP (wst-LFP) features as described in[60]. The wst-LFP technique applies spatial filters that decorrelate LFP signals in space, thereby eliminating features such as beta oscillations that are broadly distributed across the array. After this filtering ("whitening") step, features in the spike-triggered averages are limited to electrodes adjacent to the triggering neuron, and peak at lag times that match predicted propagation speeds of axonal conduction. It appears that these features represent the unitary contribution of the single neuron to the LFP, reflected by post-synaptic currents following spikes.

The algorithm for calculating the wst-LFP has been described previously[60]. Briefly, the LFP was bandpass filtered (15-300Hz, 3rd order elliptic filter, results are similar with Butterworth), and we calculated the covariance matrix (*C*) of the continuous LFP across the 96 channels (bad channels removed by visual inspection). Averages of the ongoing LFP about spikes (st-LFP; -50 to 50 ms) are calculated for each cell, and the wst-LFP are calculated by the matrix product of the st-LFP and a whitening matrix (*W*) derived from the covariance matrix:

$$wstLFP_i = \sum_{j=1}^{96}(W)_{ij} \times stLFP_j, \text{ (1.11)}$$

where

$$W = E \times D^{-\frac{1}{2}} \times E^T \text{ , (1. 12)}$$

and E is the matrix of eigenvectors of the covariance matrix, and D is a diagonal matrix of eigenvalues.

To calculate the change in wst-LFP trough about spiking, we averaged all electrodes separated from the triggering neuron position by the same L_1 (Manhattan) distance and took the minimum

amplitude from lags 0-6ms relative to spike time. This window contains the full range of delays reported previously and observed in our data (**Figure 1.17B**).

	High dose a-tDCS		*High dose c-tDCS*	
	N	λ_{pre}, λ_{post} *(mm)*	*N*	λ_{pre}, λ_{post} *(mm)*
All cells	111	0.21, 0.21	324	0.28, 0.28
FS	38	0.18, 0.24	107	0.37, 0.31
RS	73	0.33, 0.19	217	0.25, 0.24

Table 1.1. Fit parameters for Figure 1.17. The data is fitted with an exponential $A\ exp(-x/\lambda)+C$, where x is the distance and λ is the space constant. N_{cells} for this analysis are less than for others because some experiments were omitted due to poor LFP signal quality (N omitted, Sham: 8, a-tDCS: 10, c-tDCS: 15)

Neural population dynamics dimensionality reduction and analysis.

Population spiking activity during the target tracking task was analyzed with a focus on neural dynamics surrounding each cursor movement. **Figure 1.13a** shows data for an example trial where time *t = 0* when the target appears on screen. The top panel of **Figure 1.13a** shows the *FE*- and *RU-torques* registered by the manipulandum while the second panel shows a raster plot of spike times for all recorded neurons (*N = 49*) during that experiment. Similar to other studies[52], the instantaneous firing rate of each neuron is approximated by convolving its spike train with a Gaussian filter with σ = 100 milliseconds and temporal resolution of *dt* =1 millisecond, as illustrated in the third panel in **Figure 1.13a**. We verified that changing the definition of instantaneous rate did not change the qualitative nature of our results by testing one-sided Gaussian and Exponential filters, as well as spike counts in sliding windows of width σ ranging from 10-100ms. On each trial, the firing rate curve of every neuron was normalized to zero mean and unit variance (over the time course of the trial) to mitigate the biasing effects

heterogeneous spike counts across neurons and tDCS induced changes. Neural population activity during trials was thus described by a time-dependent, *N*-dimensional rate vector, as depicted in the bottom panel of **Figure 1.13a** (not normalized for illustration). The trial-averaged mean firing rate of a neuron was computed by averaging the rates at each time point across aligned trials. Target-conditioned mean rates were obtained by only including trials with the same target in the averaging. **Figure 1.13b** shows the mean rate aligned on target 1, for two example neurons (one is up-modulated and the other is down-modulated). For all following analysis, only the activity taking place between $t = 0$ (target onset) and $t = 0.5$ seconds was considered. **Figure 1.13c** shows the mean rates of all neurons ($N_{cells} = 49$) for each target.

Rate averaging was further conditioned on the four experimental epochs (Pre, tDCS/Sham, Post). We performed a principal component analysis (PCA) of neural dynamics for each epoch by concatenating all target-conditioned mean rates vectors into a large set of N_{cell}-dimensional vectors. This procedure is a version of demixed PCA[61,62] and extracts relevant subspaces where population coding takes place by taking task parameters into account. **Figure 1.15** illustrates the results of this analysis for three experimental sessions with different tDCS modalities (sham, a-tDCS, c-tDCS) where we plot the projection of the target-conditioned population rates in the space spanned by the first two principal components (PC), alongside the target-conditioned mean torques for the corresponding tDCS epochs (**Figure 1.15a**). Thus, for each epoch, a different PCA model was computed. Even if the shape of projected activity differed from one model to the next, the first two PCs were often sufficient to decode direction of motion for any tDCS modality since the task has two degrees of freedom. To check this, we trained a linear classifier to predict target label from the single-trial activity projected in the first two demixed PCs and found that the average of the 80%-20% split, cross-validated performance was between 80% and 95%

(close to monkey performance) for all sessions. Trials where the monkey failed to reach the appropriate target were included in this spot check.

We estimated the dimensionality of ensemble trajectories using previously reported methods[63,64]. The dimension *D* of a set of points in *N* dimensions is computed as:

$$D = \frac{\left(\sum_{i=1}^{N} \mu_i\right)^2}{\sum_{i=1}^{N} {\mu_i}^2}, \quad (1.13)$$

where μ_i represents the eigenvalues of the covariance matrix of the data used in the PCA model. If the *N* coordinates are statistically independent from one another, *D*=*N*, and if they are perfectly correlated, *D*=1.

To quantify how individual neurons contributed to a subspace spanned by a given set of PCs, we defined the neuron's ***participation score***: the norm of the canonical neural vector v_i (*N*-dimensional vector with zeros everywhere but at the i^{th} position) linearly projected in the subspace. **Figure 1.15c** shows the participation score of all *N* neurons for the space spanned by the first two PCs in each epoch-specific PCA models (neurons are ordered by their participation score in the *PRE* model). Some neurons were more informative than others, and the spread in participation scores reflects that. In contrast, if all neurons contributed equally to the subspace, their scores would all be $\sqrt{d/N}$ where *d* is the dimension of the subspace ($1 \leq d \leq N$, see dashed line in **Figure 1.15c**). For a given subspace dimension *d*, we measured the difference in participation scores between two epoch-specific PCA models by computing the Pearson correlation coefficient, C_{part}, of the pairs $\{(s(d)_i^a, s(d)_i^b)\}_1^N$ where $s(d)_i^a$ denotes the participation score of neuron *i* in the first *d*-dimensions of PCA model *a*. A high correlation coefficient indicates that neurons have similar participation scores in models *a* and *b*, while a low coefficient indicates a big change in participation. Variability in participation score is expected

between epochs, even for sham sessions where no stimulation is administered since neural activity is noisy and drifts during the course of the experiment. This is especially true for $d \ll N$ since low-dimensional subspaces have many "free degrees of freedom" to move in (i.e. *N*-*d*). Nevertheless, we concentrate on *d*=2 since the task itself involves two degrees of freedom (i.e *x*- and *y*-torques), a fact that should be recovered in task-relevant neural activity. We find that tDCS stimulation can induce greater-than-normal variability in participation score for *d*=2, indicating a rearrangement of neurons' roles in supporting task-relevant subspace (see statistical tests reported in **Figure 1.16**). We verified that these results generally hold for *d* up to 5.

Beyond the contribution of neurons to coding subspaces, we investigated the geometry of subspaces themselves. PCA produces linear subspaces (hyperplanes) whose orientation can be measured by principal angles. To measure how similarly oriented are two *d*-dimensional PC subspaces, we measured the *d* principal angles between them $\{\theta_1, \dots, \theta_d\}$ and define their ***orientation similarity***, S_{ori}, as the mean cosine of these angles: $\frac{1}{d}\sum_{i=1}^{d}\cos(\theta_i)$. Identical subspace will have $S_{ori} = 1$, while orthogonal spaces will have $S_{ori} = 0$ (see **Figure 1.16**).

We computed the three comparative quantities described above, (i) explained variance ratio difference, D_{var}, (ii) correlation of participation score, C_{part}, and (iii) orientation similarity, S_{ori}, for three tDCS epoch pair combinations (*Pre-Stim, Pre-Post)* across experiments with different tDCS current doses (low dose ≤1mA and high dose >1mA).. Comparison between tDCS and Sham experiments were made using independent t-tests. The number of neurons *N* varied from session to session and we discarded any session with *N*<10. Experimental sessions from the two monkeys were merged because several sessions with monkey W needed to be discarded for this reason. The total number of sessions used was *n*=99, with *N* ranging from 10 to 54 with median of 27. The following table further breaks down the number of samples by session type:

	anodal	cathodal	sham
low dose	n=14	n=14	n=40
high dose	n=13	n=18	

Table 2. Number of experiments for each population dynamics analysis

Figure 1.16 shows box plots of all sampled quantities along with these p-values.

For each tDCS modality, the sampled measured quantities are compared to those of sham sessions (control) and the statistical significance of effects is established using the p-value of an independent t-test.

RESULTS

Changes in single-unit firing rate during tDCS

We recorded 2671 putative neurons from sensorimotor cortex (MI, monkey S; SI, monkey W) over 109 experiments (45 Sham, 29 a-tDCS, 35 c-tDCS). Neural data, including single unit activity (SUA) and local field potentials (LFP), were recorded from the gyral crown by 96-channel microelectrode arrays (**Figure 1.3a-b**) before, during, and after tDCS (**Figure 1.3a**, Pre, Stim/Sham, and Post epochs, respectively). We followed strict cell inclusion criteria similar to other studies (*Supplement: Cell inclusion criteria*). tDCS was delivered through saline-soaked cellulose sponge electrodes (**Figure 1.1d**) and ranged from low in human studies (0.027 mA/cm^2, 0.25mA) to about four times the maximal current density currently used in humans (0.44 mA/cm^2; 4mA). Monkeys performed a visuomotor target-tracking task by controlling the position of a cursor via isometric wrist torques registered by a 2-axis manipulandum (**Figure 1.1e**). During each trial, the monkey was cued to move the cursor to one of eight targets by contracting his forearm muscles to produce isometric torques in wrist flexion/extension and radial/ulnar deviation; the monkeys performed the task for the duration of the experiment. The

task was simple and over-trained to maintain tight behavioral control. tDCS had little to no effect on the monkey's ability to perform the task (**Figure 1.2**), thus eliminating any potential confounds from behavioral changes induced by tDCS.

First, we evaluated whether the firing rate of SUA changed during tDCS and Sham experiments. We calculated the relative difference in firing, ΔF, from the Pre epoch to the Stim epochs as $100 \cdot (F_{STIM} - F_{PRE}) / \max(F_{PRE}, F_{STIM})$ for each neuron. **Figure 1.3b** shows that a-tDCS significantly increased firing across the population for both monkeys (red data points, sigmoid dose-response curve, *Eq. 1.14*, **Figure 1.4** shows results by experiment). Increases in firing were dose dependent, and statistically significant for both monkeys at high currents (>1mA). Maximal sensitivity to tDCS intensity was similar for both monkeys (dose-response midpoint; S: 1.2mA; W: 1.14mA). Interestingly, c-tDCS produced no statistically significant changes in firing rate across the population for any dose (**Figure 1.3b**, black data points).

Time course of effects

Figure 1.3c shows the change in mean firing rates for successive minutes of high dose a-tDCS (>1mA, dark red bars; all data presented as median±95% confidence interval unless otherwise stated), low dose a-tDCS (≤1 mA, light red bars), and sham sessions (grey bars). Neuronal firing increased immediately following the onset of both low and high dose a-tDCS (**Figure 1.3c**). Changes persisted for about 15 minutes after tDCS was turned off only for high doses (Wilcoxon rank-sum test $p<0.01$). These changes were continuous for about 15 minutes following offset of tDCS.

Percent of cells modulated by tDCS

Population-wide changes in firing rate depicted in **Figure 1.3b** may mask mixed effects in individual cells, so we examined whether c-tDCS or a-tDCS impacted the likelihood that any individual cell's firing was increased or decreased. **Figure 1.3d,e** show the percent of neurons with a given change in firing across three conditions. During high dose a-tDCS, a higher percentage of neurons exhibited increased firing ($\Delta F > 0$), and a lower percentage showed decreased firing ($\Delta F < 0$) than during Sham or c-tDCS (**Figure 1.3d**), in agreement with population averages. Interestingly, a higher percentage of neurons had increased or decreased firing during c-tDCS as compared with Sham, suggesting that c-tDCS affected firing, but the effects were mixed. To highlight this, **Figure 1.3e** shows the percent of cells with an absolute change in firing greater than or equal to a given $|\Delta F|$. More cells had larger absolute firing rate changes during both a- and c-tDCS, suggesting that the percent of cells affected by c-tDCS is comparable to that affected by a-tDCS. Differences from Sham were more pronounced for larger absolute changes in firing – for instance, neurons were about 1.5x more likely to be undergo a >20% change during a- and c-tDCS (corresponding to about 10-15% of neurons).

We also estimated the percent of neurons affected by tDCS by labeling cells as modulated up or down if their mean firing rate during high dose tDCS or Sham exceeded 3·SD from the baseline during Pre (**Figure 1.5a**). Using these criterion, results were similar to data presented in Figure 2D-E. Neurons were more than twice as likely to change their firing during tDCS as compared with sham (**Figure 1.5b,** "+/-"), a higher percentage were modulated up than down during a-tDCS, while c-tDCS increased the likelihood that cells were modulated either up or down. This mixed effect explains why average population firing rate changes were not obvious during c-tDCS (**Figure 1.3b**).

Direction of modulation depends on cell type

Why might firing rate changes be mixed for a given polarity? Modeling and experiments in-vitro suggest that the effects of tDCS on single neurons will depend on their morphology[65] and orientation[38]: anatomical factors that correlate with cell type. Neurons with a major somato-dendritic axis in parallel with the induced electric field (such as pyramidal cells) should be more susceptible to somatic modulation by tDCS, whereas those without a dominant axis or with a centrally positioned soma (such as interneurons), would not be as directly affected. Cell-type specific optogenetic stimulation has shown that the width of the extracellularly recorded action potential is well correlated with these two broad classes of neurons[66] (although it has limitations[67]) – narrow spike widths correspond with "fast spiking" (FS) putative interneurons and broad spike widths with "regular spiking" (RS) putative pyramidal neurons. As shown in **Figure 1.7a**, the distribution of spike waveform width is bimodal. The average spike shape of each cluster is shown in **Figure 1.7b** (green RS cells: ≥250μs, N=1812, blue FS cells: <250μs, N=859). Consistent with other studies, FS firing rates were higher than that of RS neurons, and exhibited task related dynamics that were similar between monkeys (**Figure 1.6**)

We found that while tDCS affected both RS and FS cells, the changes in RS cell firing rates were greater, and opposite for a- versus c-tDCS (**Figure 1.7c**, green bars, both monkeys: $p<0.001$). **Figure 1.7c** shows the change in firing rate for each cell type during high dose tDCS (low dose effects were not significant, both monkeys: $p>0.05$). Note that a-tDCS increased the firing rates of RS cells, whereas c-tDCS decreased firing rates. In contrast, FS cells tended to increase their firing rates for both a-tDCS and c-tDCS. **Figure 1.7d,e** depict the cell-specific change in firing rate by tDCS intensity. This figure is similar to **Figure 1.3b**, but reveals a dose-dependent

decrease in firing among RS cells (**Figure 1.7d**) in response to c-tDCS. FS cells showed less modulation to both a-tDCS and c-tDCS, but rates generally increased with both (**Figure 1.7e**).

The same neurons are consistently modulated by tDCS

There is some question whether tDCS produces the same physiological effects across sessions[68], so we determined if increases or decreases in individual neuron firing rate were consistent for a given polarity. Neurons were identified across experiments using a combination of previous methods[56–58] (*Supplement: Longitudinal analysis,* **Figure 1.8**) and the algorithm classified 1178 potentially unique neurons, 518 of which were recorded more than once (**Figure 1.9**). **Figure 1.11a-c** show a typical example neuron recorded across four cathodal experiments (**Figure 1.11a**), one sham experiment (**Figure 1.11b**), and two a-tDCS experiments (**Figure 1.11c**). The firing rate of this neuron decreased proportionally with c-tDCS intensity, but the pattern of firing in torque space (firing rate heat maps and directional polar plots) was preserved. For this neuron, firing rates remained constant during the sham and low-dose a-tDCS experiments (there were no high dose a-tDCS experiments with this neuron).

Once cells were identified across experiments, we calculated the percentage of neurons consistently excited or inhibited during each condition **Figure 1.11d**, insert). We tested the null hypothesis that neurons exhibited consistent firing rate changes by chance alone using a shuffling algorithm (*Supplement: Shuffle distributions*), and found that both a- and c-tDCS had significant repeat excitatory and inhibitory effects (z score>5.3 or $p<0.001$) (**Figure 1.11d,e**). Interestingly, about 13% of neurons consistently modulated their firing during Sham ($p<0.05$, **Figure 1.11e**), but neurons were 2.5 and 2.4 times more likely to undergo the same direction of firing rate changes during high dose a- and c-tDCS (**Figure 1.11d,e**). This analysis, distinct from firing rate changes reported above, further supports the finding that high dose tDCS

modulated firing. This analysis also revealed that a-tDCS decreased firing in some neurons (z-score=5.3 or p<0.001, **Figure 1.11e**, *Always decrease*), an effect that was not obvious from changes in firing rate changes alone.

Single neuron tuning

Neuron dynamics in sensorimotor cortex covary with a multitude of movement parameters in complex ways[69–71] – we investigated whether tDCS disrupted relationships between behavior and firing by analyzing neuron tuning to torque direction and torque space maps, which were robustly evident in both monkeys. To analyze a neuron's preference for a given torque direction, we calculated the mean resultant vector (MRV) from the direction tuning function (**Figure 1.12a,b**). The MRV length (R_L, *Eq. 1.15*) and angle (φ_R, *Eq. 1.16*) respectively describe the degree to which a neuron is directionally tuned and its preferred direction, irrespective of firing rate. **Figure 1.12a** shows the peak-normalized torque direction tuning curves for all recorded neurons ordered by R_L and rotated so that φ_R align. **Figure 1.12b** shows directional tuning of example neurons with corresponding R_L with peak firing rate indicated. A sizeable proportion of neurons recorded in both monkeys were directionally tuned (R_L>.1; Monkey S: 33.6%, Monkey W: 35.8%). We found that neither a-tDCS nor c-tDCS at any dose changed the strength of tuning (**Figure 1.12d**) or preferred direction (**Figure 1.12e**).

Many neurons showed phasic activation that was not strongly directionally tuned, such as increased firing during the hold phase, rest phase, early contraction, etc. (see example neuron in **Figure 1.12**). These correlations are reflected in the torque space firing rate map as hot spots, and we used these rate maps to assess cell tuning similarity (Pearson's correlation coefficient, ρ) and specificity (information per spike *Eq. 1.17*, I[72]) across epochs. **Figure 1.12f and h** explain how ρ and I vary with changes in the rate map. We found that cell tuning was relatively stable

during the experiment (**Figure 1.12g,** Sham), and high dose tDCS produced a small but significant drop in ρ that reflected minor shifts in the rate map which exceeded those observed during Sham. Low dose tDCS did not produce this change (**Figure 1.12g**). Rate map shifts did not correspond with decreases in firing specificity (*I*) during tDCS experiments although it did during Sham (**Figure 1.12i**). Overall, these effect sizes were very small, indicating that tDCS had very minor to no effect on single neuron tuning.

Neural population dynamics

Neural activity associated with movement may be best described by activity of the population, not single cells[70,73–75]. To check whether tDCS affected the joint spiking of many neurons, we quantified activity of the recorded ensemble (N>10) in a "neural space" whose dimensions corresponds to the firing of a neuron in the ensemble[52,75,76]. We used a version of demixed principal component analysis (dPCA)[61,62] to extract the most informative linear subspaces (manifolds) within ensemble trajectories during the task. We asked: (1) does tDCS affect the dimensionality of ensemble trajectories? and (2) does tDCS change the dominant pattern in neural ensembles?

Similar to previous studies[52], we analyzed smoothed spike trains from MI (Gaussian filter σ=100ms) from 0 to 500ms after target appearance. This period contained neural activity most relevant to stereotyped contractions during the task. On each trial, the spike trains of every neuron were normalized to zero mean and unit variance (over the time course of that trial) to mitigate the biasing effects of heterogeneous firing rates across neurons and tDCS induced firing rate changes (though results were similar without normalizing for firing rate changes). Normalized spike trains were averaged across trials conditioned on target number (demixing step), and then standard PCA was performed on the concatenated, target-specific, N_{cells}-

dimensional spike rate functions (for experiments where $N_{cells} \geq 10$) for each experiment epoch (*Supplement: population analysis*). Averaged ensemble trajectories projected into epoch-specific 2-D manifolds were well separated for distinct target, and even resembled torque trajectories, indicating that neural population dynamics in the space of the first two principle components reflected motor performance. **Figure 1.14a** shows average torque and ensemble trajectories for each target during Pre, Stim and Post epochs.

We used two measures to test whether the dynamic organization of the ensemble shifted during tDCS (*Supplement*: *Neural population dynamics*). First, we calculated the *dimensionality* (*Eq. 1.18, D*) of the ensemble trajectories[63,64]. If all neuronal firing is highly correlated, points in the neural space approach a line ($D=1$), whereas if all neurons are firing independently, points are dispersed throughout the neural space ($D=N_{cells}$). Population activity is typically restricted to a smaller subspace ($1<D<<N_{cells}$), which is thought to reflect functional connectivity of the network[75]. In our experiments, D was similar across experiments (5.20±0.15). Interestingly, we found that the dimensionality of ensemble trajectories decreased with time under normal conditions (Sham, **Figure 1.14b**), whereas a- and c-tDCS both increased D at high doses (**Figure 1.14b,** independent t-test Sham vs tDCS; a-tDCS p=0.002, c-tDCS p=0.012). This effect persisted after tDCS was turned off (**Figure 1.14**).

We also tested whether new dominant patterns of activity arose during tDCS by measuring the principle angles between the intrinsic manifolds pictured in **Figure 1.14a**. We calculated the mean cosine of principle angles, S_{ori}, which ranges from 0 (orthogonal ensemble activity) to 1 (unchanged) (**Figure 1.14c$_{i}$**, *orientation similarity, S_{ori}*). Manifold orientation changed very little during Sham epochs (S_{ori} = 0.87; **Figure 1.14c$_{ii}$**, Sham), indicating that ensemble activity patterns were stable over time. c-tDCS and low dose a-tDCS did not produce shifts in the

manifold, but there was a significant shift during high dose a-tDCS (**Figure 1.14c$_{ii}$**; a-tDCS thick bars, p=0.02), and this result weakly persisted after a-tDCS was turned off (**Figure 1.16,** p=0.059). These findings indicate that high dose tDCS produced ensemble activity outside of the existing subspace, and that new dominant ensemble patterns were elicited by high dose a-tDCS.

Features in spike-triggered LFP are diminished during tDCS

Finally, we investigated the effects of tDCS on synaptic currents correlated with neuron spiking observed in the LFP using the whitened spike-triggered LFP (wst-LFP)[60]. This method calculates the average spike-triggered LFP at multiple electrode sites and applies a spatial filter to separate the effects of a single neuron from non-specific components of the LFP which are common across the whole array (e.g., beta oscillations). Consistent with previous studies, wst-LFP from our arrays support the notion that resultant features are synaptic currents evoked by spikes of the triggering neuron: they occurred after the spikes (**Figure 1.17a,b**), and were restricted to electrode sites close to the neuron within known limits of axonal projection[77] (**Figure 1.14b,c**).

Figure 1.17 shows that tDCS affected the wst-LFP. wst-LFP features are consistent throughout recordings without stimulation (**Figure 1.17c**). When all cells were considered, there was a significant decrease in wst-LFP features for adjacent channels (0.4 and 0.8mm) to both high dose a- and c-tDCS. Upon further inspection, we found that fields from RS cells were more affected by a-tDCS, while those from FS cells were more affected by c-tDCS. **Figure 1.17**Figure 1.14**d,e** show how high dose tDCS affected RS (**d**, green spike) and FS (**e**, blue spike) neurons. Notably, changes were restricted to neighboring electrode sites. Low dose tDCS did not produce any significant changes (≤1mA, p>0.05). See *Table 1.1* for fit parameters and corresponding N for Figure 1.17d,e.

DISCUSSION

There are many concerns about the widespread adoption of tDCS in clinical research. Human studies typically measure effects of tDCS using secondary outcomes, and those that measure neurophysiological responses are often hard to compare or in disagreement[35]. Except for evoked responses, there is little direct evidence from clinical-type tDCS that informs the design of experiments in humans. Consequently, there is no accepted standard for current intensity, duration, and polarity, and the most common settings are still a best-guess adaptation of early polarization experiments in animals. Despite its obscure action, tDCS may deserve refinement: many trials suggest it holds therapeutic promise, and it is noninvasive and simple to deliver.

Our objectives in this study were twofold. First, considering that basic parameters such as charge dose are not standard across tDCS experiments, we wanted to measure sensitivity of ongoing spiking activity to different current intensities and polarity using a primate model that resembles clinical-tDCS. Second, we wanted to test hypotheses generated by the most recent tDCS theory stemming from modeling and rodent experiments, such as demonstrated effects on single neurons, synaptic transmission, and LTP[16,40,78].

Implications for human tDCS

Our results confirmed that current intensity is an extremely important parameter – differences due to tDCS intensity were evident in every aspect of spiking activity that we measured. We found effects in the primate brain at current densities well within clinical safety limits, but at levels that were higher than that generally used in humans ($0.11 mA \cdot cm^{-2}$). We stress, though, that exact current intensity values from our monkey model cannot be assumed to have the same effects in humans (discussed further in *OSM: Limitations*). The highest current densities in our study are about four times higher than are currently used in tDCS, but are within the safety

guidelines for tDCS and comparable protocols have been used before. Between 1960 and 1998, a few studies[79] delivered tDCS through much smaller scalp electrodes and often delivered current densities of 0.2mA/cm^2, well within the range of effects in our study. One older study successfully applied 2.4 mA/cm^2 to one patient with local anesthetic under the electrode [cite].

We also found differences in the neural response to anodal and cathodal stimulation, and it is reasonable to expect that these effects will extend to humans. These data should be useful for interpreting mixed and often confusing effects related to polarity observed in humans. Early evidence for "opposite" modulation of excitability by a- and c-tDCS has given way to a more complex picture – one in which c-tDCS can be partly excitatory and a-tDCS can be partly inhibitory[cite]. Our data suggests that anodal and cathodal tDCS can both increase or decrease firing in single neurons, an effect that is consistent in the same neuron across experiments.

Another open question following recent review of tDCS literature is the question of inter-subject reliability[68]. Our results indicate that tDCS is a reliable intervention. Despite differences day to day in the composition of neurons sampled, the average response to a given polarity and dose was surprisingly robust across days (**Figure 1.4**). Not only did we find that the average population statistics were similar across days, single neurons that were repeatedly sampled across days were also more likely to be consistently modulated up or down by high dose tDCS.

Applicability to other cortical areas

tDCS had similar effects in neurons recorded in both pre- and post-central gyrus. Recordings from both monkeys were remarkably similar in their basic cell compositions, firing rates, task activation and torque tuning profiles, which likely reflects the analogous structure and overlapping function of the two regions[80–82]. Interestingly, tuning to torque persisted during tDCS in both regions, and these correlations presumably reflect a mixture of both efferent and

afferent cortical signals. Furthermore, waveform shape-based identification of RS and FS cell types is employed across species and brain regions, having been applied areas as far reaching as hippocampus in the rat to throughout neocortex in humans[60,83]. These cell types, each recorded from pre- and post-central gyrus in our experiments, showed a trend of modulation by tDCS and we presume that similar relationships will exist elsewhere in cortex with similar cell organization.

Single cell effects and network amplification

We recorded from a depth of 1.5 mm at the gyral crown, directly under the stimulating electrode where the electric fields are strongest[43] and are expected to be most radial to the cortical surface. Here the effects are be expected to be most pronounced for cortical pyramidal neurons[65], in part because the electric field is aligned with the somato-dendritic axis . Our data supports this notion because putative pyramidal neurons (RS) were more affected by tDCS than FS cells, and they were oppositely modulated by anodal versus cathodal stimulation. FS cells, the putative inhibitory neurons, often lack a major somato-dendritic axis, thus avoiding significant somatic polarization by any field direction. At the same time, firing rates of these neurons were positively correlated with a- and c-tDCS intensity. These effects could be the result of dendritic depolarization, or secondary to network effects following the primary modulation of other cell types.

tDCS currents in our study produced electric fields in the cortex that are far too weak to trigger action potentials in resting neurons (~1mV/mm[43,47] versus 20mV/mm[38] required to trigger action potentials). In our experiments tDCS probably modulated firing rates because many neurons were near threshold and angaged in normal activity. Indeed, it has been reported that the threshold for modulation by electric fields is lower for active neurons than a silent ones[84], and

that ephaptic coupling by extracellular oscillations can entrain neuron spiking[43,85,86]. Subthreshold effects may be collectively amplified because a neuron near to threshold may be activated sooner, or more often, with only a small bias.

Features of the unitary LFP (postsynaptic currents initiated by spiking, wst-LFP[60]) were diminished by tDCS in a dose-dependent matter, which suggests an influence of tDCS on synaptic pathways. Deflections in the wst-LFP are thought to reflect inhibitory currents and may therefore reflect inhibitory postsynaptic potentials in apical dendrites of pyramidal cells[60]. tDCS decreased the amplitude of these currents, an effect most pronounced among RS cells during a-tDCS and that coincided with a global increase in firing. These findings are consistent with direct modulation of RS cells by tDCS with a consequent drop in feedback inhibition[87] and decreased inhibitory driving force while the apical dendrites are predicted to be hyperpolarized. Also, the larger decrease in wst-LFP associated with RS, but not FS, cells could be due to divergent effects of the RS neuron on many inhibitory interneurons consistent with known connectivity patterns[88]. Decreases in RS firing during c-tDCS did not correspond with an increase in wst-LFP, suggesting that c-tDCS directly inhibited RS cells. One puzzling result is the decrease in wst-LFP associated with FS cells during c-tDCS, a condition when the apical dendrites of pyramidal cells are predicted to be relatively depolarized. This change in wst-LFP coincided with decreased firing in RS cells and modestly increased firing in FS cells. Future studies in vitro may elaborate on this interplay between simultaneously polarized synapses and neurons.

"Specificity" of stimulation and single neuron tuning

It appears that tDCS is most effective when paired with training that recruits target brain networks[19,42,89,90], and there is evidence that only synapses active during delivery of tDCS are potentiated[40]. By modulating synapse-specific activity common to learning[91], tDCS may be more

specific than one might naively expect, although this would require that tDCS does not completely disrupt existing representations.

Our data suggests that tDCS immediately modulates firing rates, an effect that is not necessarily beneficial. At the same time, single cell task-related activity during tDCS resembles normal activity, which supports the "specificity" theory of tDCS. The fact that single cell tuning and spike information content stays high during tDCS suggests that extra-field firing is not increased – that is, cells are not becoming noisier. In fact, our data suggests that the network may become less noisy because spike information content is higher during tDCS than Sham, and more neurons are reliably coordinated during stereotyped movements during tDCS (increased D_{var}). These "specific" effects may be the result of specific synaptic modification, or due to the fact that cells are likely to be more affected by tDCS during neural/behavioral states when they are intrinsically excited. Our results indicate that both may play a role, because firing rates increased immediately with the onset of tDCS, (too fast for LTP), but also persist once tDCS was turned off (potentially LTP).

We found that single neurons tuned to a particular torque direction still preferred that direction during tDCS, even if their firing rate was increased or decreased. The strength of tuning, independent of overall firing rate, was also unaffected by tDCS. This may not be consistent with the theory of increased firing by somatic depolarization, in which one might expect the shifted membrane threshold to reflect broad tuning in membrane potential that was previously filtered out by the non-linearity of spike generation (softening tuning curves by "boosting" non-preferred inputs, a phenomenon called the "iceberg effect"[87]). Increases in putative inhibitory (FS) cell firing during both a- and c-tDCS may serve to sharpen the tuning and counteract the iceberg effect. Overall, analysis of single neuron tuning revealed that tDCS did not grossly disrupt SUA

correlations with behavior. At the same time, we found significant changes in the spatiotemporal patterns of simultaneously recorded populations of neurons.

Population dynamics

Population activity is known to be confined to a small part of the total neural space[75] (the manifold); and activity unexpressed by the population (areas outside of the manifold) are thought to reflect intrinsic limitations imposed by functional connectivity patterns in the network[75]. New patterns of activation produce subsequent shifts in the manifold once learned, and tasks associated with points farther from the manifold (neural associations rarely expressed) take longer to learn[75,92]. In our experiments, dimensionality of ensemble trajectories increased during tDCS, although it tended to *decrease* with time otherwise. This finding is consistent with theories underlying the warm-up effect, in which a network refines its activity during practice of a rehearsed task[93]. Conversely, increasing the dimensionality (and therefore dispersion) of firing during tDCS may explain tDCS-associated increases in learning rates: by increasing the size of the working neural subspace, new, successful patterns can be more quickly tried and reinforced[94]. Therefore, it appears that high dose tDCS releases constraints imposed by functional connectivity patterns (by dendritic depolarization, disinhibition, etc) to speed learning from otherwise deeply embedded associations.

Comparison with other studies

Only recently have experiments begun to explore neural effects in the parameter space of clinical tDCS. Computational models predicted that intracranial electric fields are attenuated by extracranial soft tissue when current is applied to the scalp[cite], a finding just confirmed in human cadavers[43]. These researchers further demonstrated that electric field strength recorded in the cadavers was not sufficient to modulate firing rates in anesthetized rats, and concluded that

higher doses are necessary in humans. Although we reached similar conclusions, we note that unanaesthetized states may be more susceptible to modulation by tDCS than anesthetized states.

Two other studies have applied stimulation to the scalps of monkeys and found effects at doses similar to those used in humans for tDCS delivered to prefrontal cortex[44], and for tACS delivered to the middle temporal area[46]. Similar to our study, Kar et al reported that neural firing rates, but not tuning, was affected[46], while Kraus et al did not find changes in neural firing rates[44].

The present data extends this line of research by documenting the basic physiological effects across different doses and polarity, from single neurons to network-level dynamics and coding, in the most common form of tDCS used in humans. These effects were not present in all cells, and to properly detect and quantify them required the analysis of many more neurons than previously recorded. In agreement with new experiments that directly measured intracranial electric fields across species[43], our results in the active primate brain also indicate that human trials are probably not delivering sufficient current.

Limitations

While we tried to match human tDCS as closely as possible, some differences were unavoidable: to record intracortically requires a bone defect where the recording electrode wire bundle passes into the intracranial space, and we used a thin titanium strap to hold the bone flap in place immediately post implantation. Implants and boney defects may distort the electric field or shunt current. On the other hand, we found that the bone flap reintegrated fully, the residual passage for the wire bundle was very small, and extracranial tissue recovered fully. Furthermore, the skull itself is naturally porous due to features like cranial sutures and Haversian canals, and the relatively snug passage for the wire bundle may not be so different.

Another reason these numbers cannot be directly projected to humans is that the monkey and human head and skull are significantly different: human skulls are thicker than monkey skulls, and hair is often left in place during human experiments, whereas we removed it. Future work may compare the predicted intracranial electric field intensity using finite element head models of monkeys and humans. It is worth noting that despite these differences, a recent human trial tested a range of currents outside of normal tDCS, and the lowest current density that produced changes (in EEG alpha oscillations) was similar to that which produced significant single cell effects in our study[43] (0.125mA/cm^2 versus 0.11mA/cm^2). Finally, while the two-pad form of tDCS is still the most common, newer types of tDCS exist that may be more targeted and effective[43,95–97].

Conclusions

Clinical-type tDCS delivered to monkeys modulated task-related spiking in sensorimotor cortex at current densities higher than typically used in humans (but within the safety guidelines). Changes in spiking only weakly persisted in time, but were consistent across animals, trials, and single neurons over multiple days. Anodal and cathodal tDCS had mixed effects at the cellular and synaptic level that depended on cell type. Importantly, we found that modulation by tDCS did not disrupt existing movement representations evident in single cell tuning curves, although effects were evident in network-level activity. Future studies could investigate the potential for these changes to beneficially affect physiological markers of learning and plasticity.

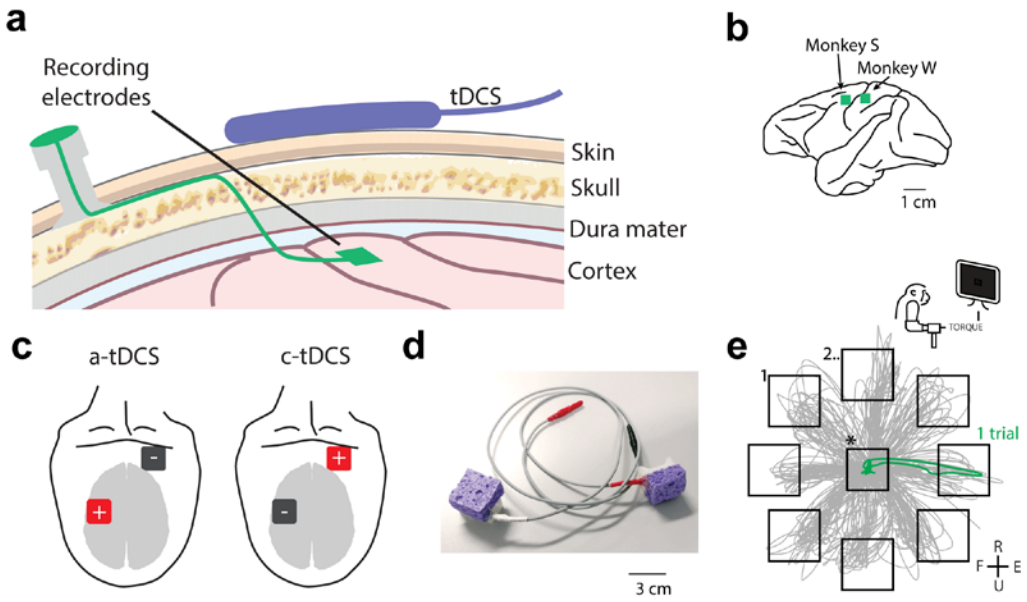

Figure 1.1. Clinical-type tDCS, cortical implants, and task. (a) Relative placements of microelectrode array (green) and tDCS electrode (purple). (b) A microelectrode array was implanted on the gyral crown of left MI (monkey S) and left SI (Monkey W) in the areas corresponding to the right forearm. (c) tDCS electrode montage for anodal (left) or cathodal (right) unilateral stimulation of sensorimotor cortex. (d) 3x3cm cellulose sponge electrodes were designed to match those used in human trials. (e) Torque trajectories (gray traces) during 10 minutes of task performance with target locations indicated by black boxes.

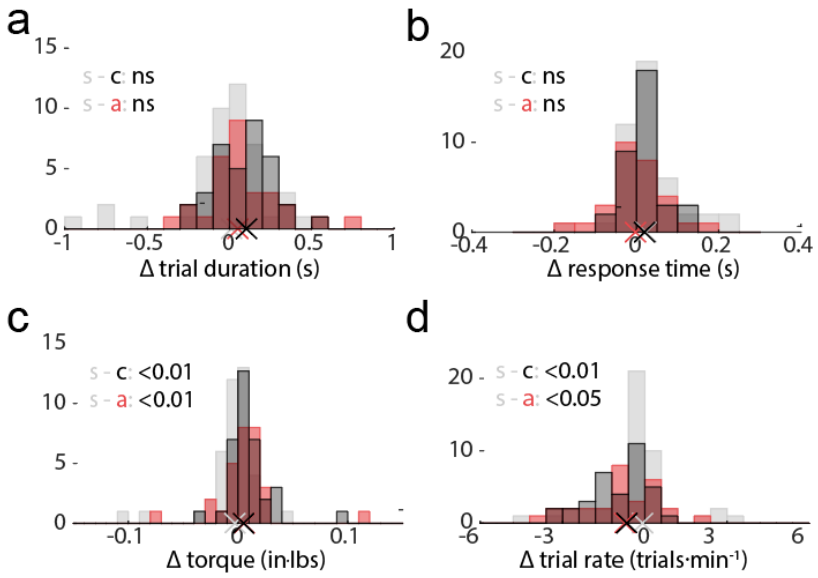

Figure 1.2. Task performance and behavior during tDCS and Sham. Each plot shows histogram of changes for a given performance metric from Pre to Stim/Sham, with the median indicated along the x-axis with an 'X' (Sham: light gray, a-tDCS: red, c-tDCS:black). There was no difference between the time it took monkeys to complete trials (trial duration, $p>0.05$, **a**), or the time it took monkeys to move the cursor to the target following the variable hold period (response time, $p>0.05$, **b**). There was a small but significant difference between the changes observed during tDCS and Sham for the median torque produced during trials (**c,** median Δtorque, Sham=-2.9e-3 in·lbs, a-tDCS = 5.7e-3, c-tDCS = 5.2e-3) and number of successful trials per minute (**d**, trials with duration <6secs, Sham=-0.08 trials/min, a-tDCS =-0.72, c-tDCS =-0.6). Overall, behavior was tightly controlled during tDCS and was similar across experiments, because the monkeys were overtrained and completed the task at peak performance. Regular performance was important to eliminate any potential confounds associated with behavioral changes.

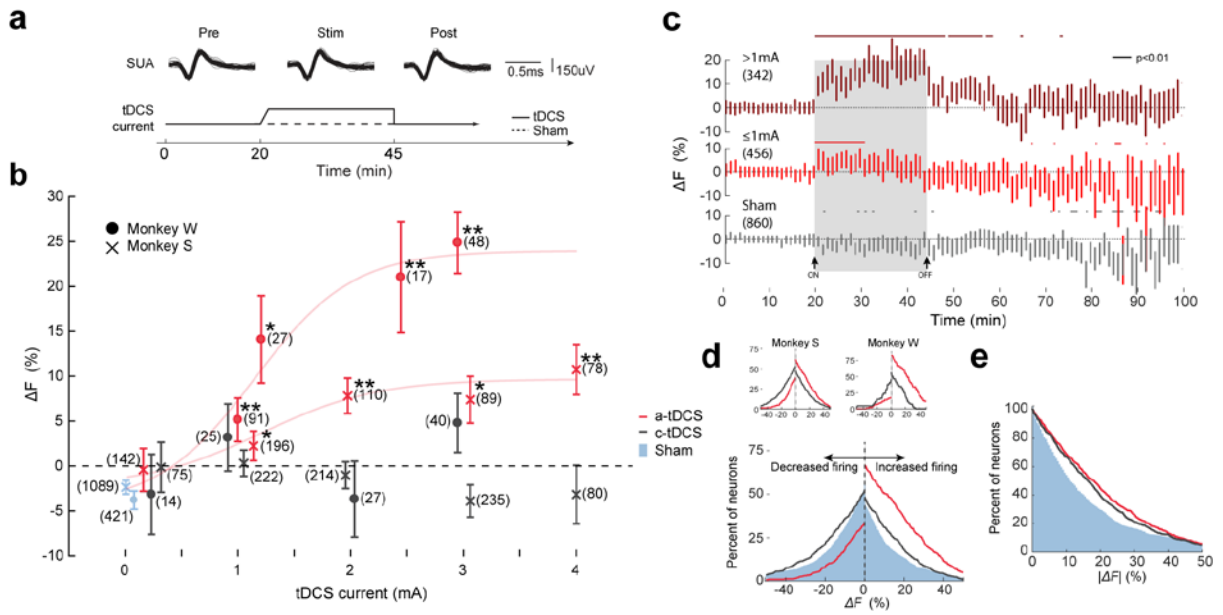

Figure 1.3. Firing rate changes during and after tDCS. (a) Time-course of experiment and with example neural data. Top: sample SUA waveforms recorded during Pre, Stim, and Post epochs. Bottom: experiment time-line. (b) Change in firing rate (ΔF) between Pre/Stim for all recorded neurons. Average change in firing rate increased with dose during a-tDCS (red data points); the data is fitted with a sigmoidal dose-response curve Supplementary Eq. 4 (a-tDCS: Monkey S: x50=1.20mA, b=0.85 percent·mA-1; Monkey W: x50=1.14mA, b=1.0 percent·mA-1). No significant change in firing rate was observed for any dose of c-tDCS (black data points; Sham: blue data points). Two-sided Wilcoxon rank sum test tDCS vs. Sham, *p<0.01, **p<0.001 (c) Time-course of ΔF (relative to average firing in Pre) during high and low dose a-tDCS and Sham. Vertical bars: median ± 95% confidence interval, horizontal bars: p<0.01, Wilcoxon sign-rank test. The Stim/Sham epoch is indicated by two arrows and light gray background. (d) Percent of cells with altered firing during tDCS or Sham. The percent of neurons with increased firing was greater during a-tDCS (red line) relative to sham (blue area), but the percent of neurons with decreased firing dropped. The percent of neurons with changed firing (both increased or decreased rates) was higher during c-tDCS (black lines) relative to sham. (e) Percent of neurons with absolute change in firing greater than or equal to |ΔF|.

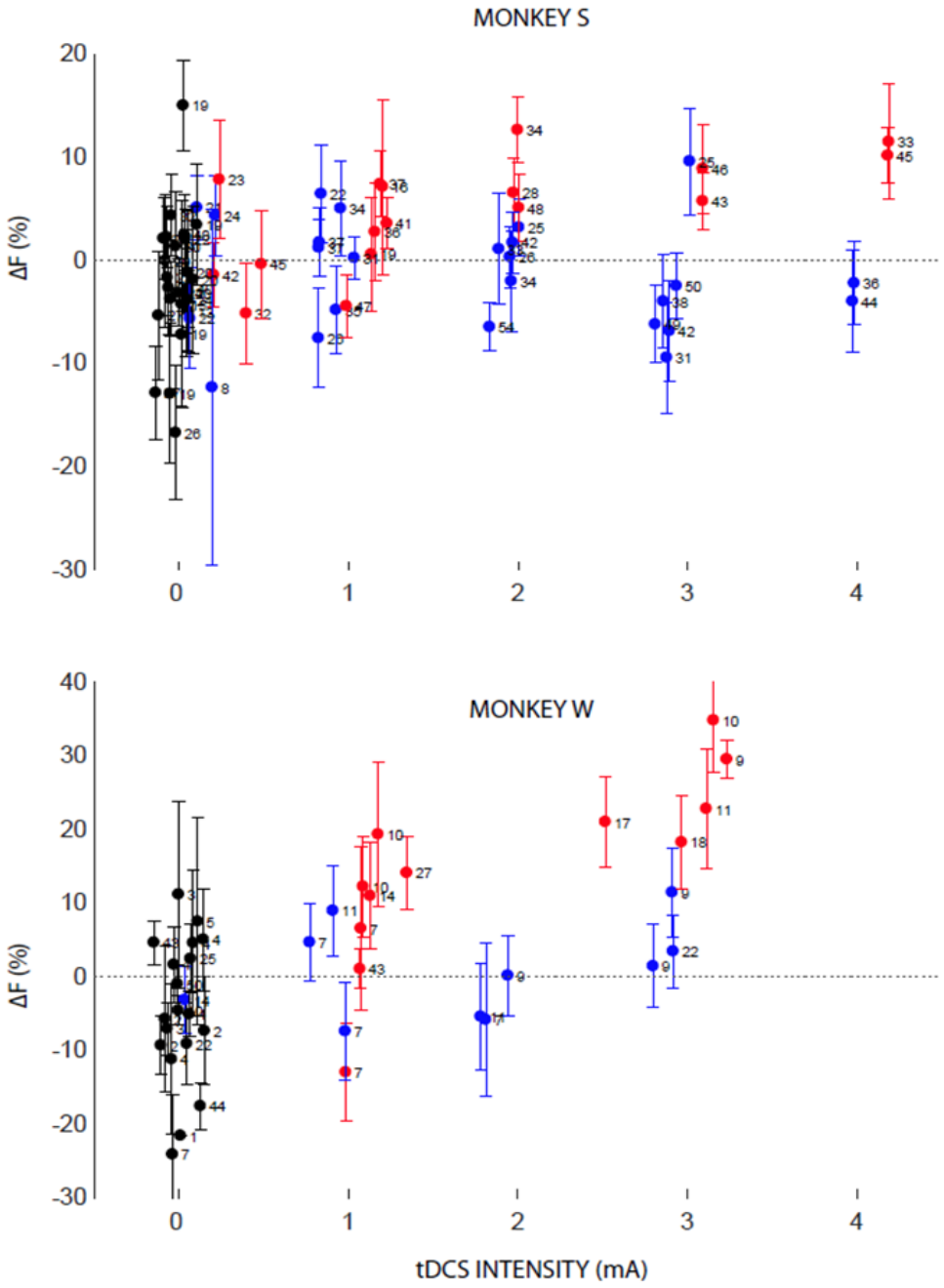

Figure 1.4 Average change in spiking for every experiment. Data plotted is mean ± standard error, and the number of neurons recorded is indicated in parentheses.

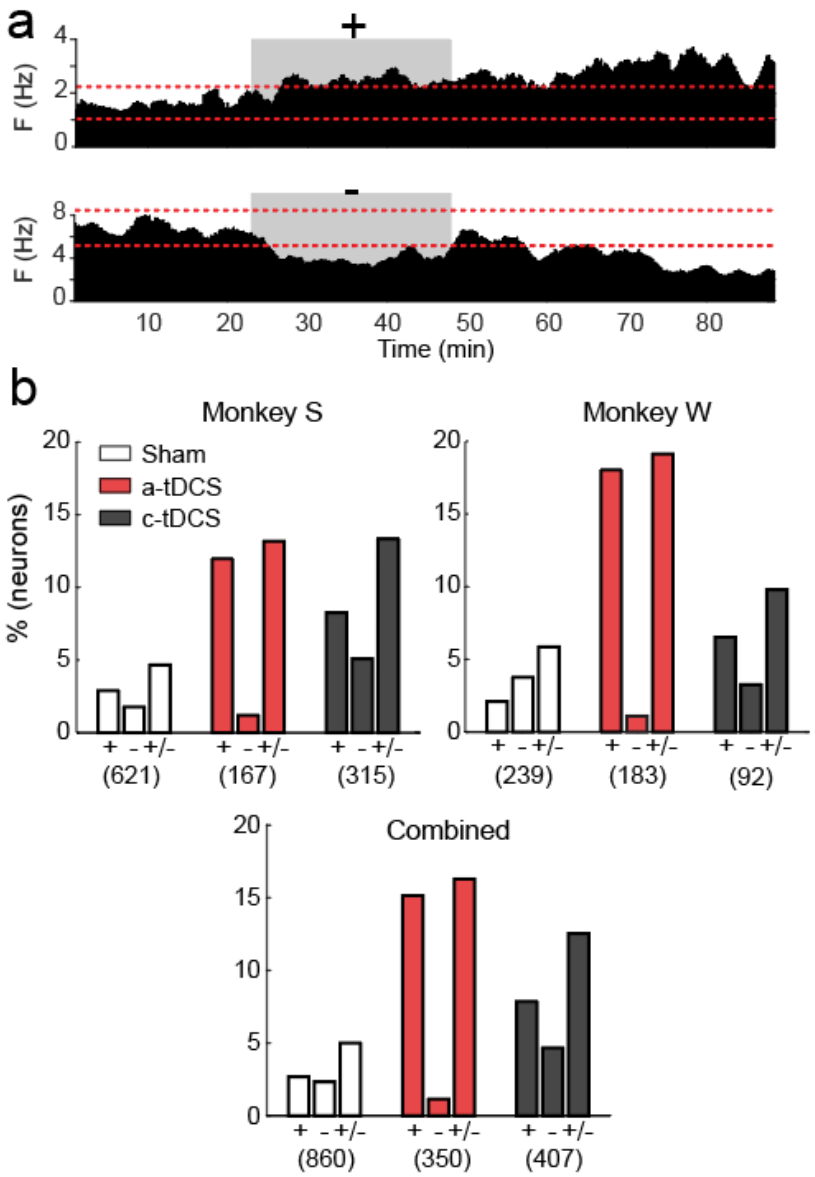

Figure 1.5 Percent of cells that increase or decrease their firing during tDCS. (a) We labeled neurons as increasing (+) or decreasing (-) if the mean firing rate during the Stim epoch was greater or less than 3 SD from the baseline during PRE (b) Percent of cells with increased (+), decreased (-) or changed (+/-) firing from Pre to Stim. Neurons were generally more than twice as likely to have significant changes in their firing rates during either a- or c-tDCS as compared with sham (+/-, Monkey S, Monkey W, and Combined). A higher percentage of neurons were modulated up (+) during both a-tDCS and c-tDCS than during sham. However, the percent of cells with decreased firing dropped below sham levels during a-tDCS and was higher during c-tDCS. Interestingly, the total number of modulated cells was comparable for a-tDCS and c-tDCS, although modulation by c-tDCS was mixed, explaining the absence of an effect in the population firing rates in Figure 1.3B.

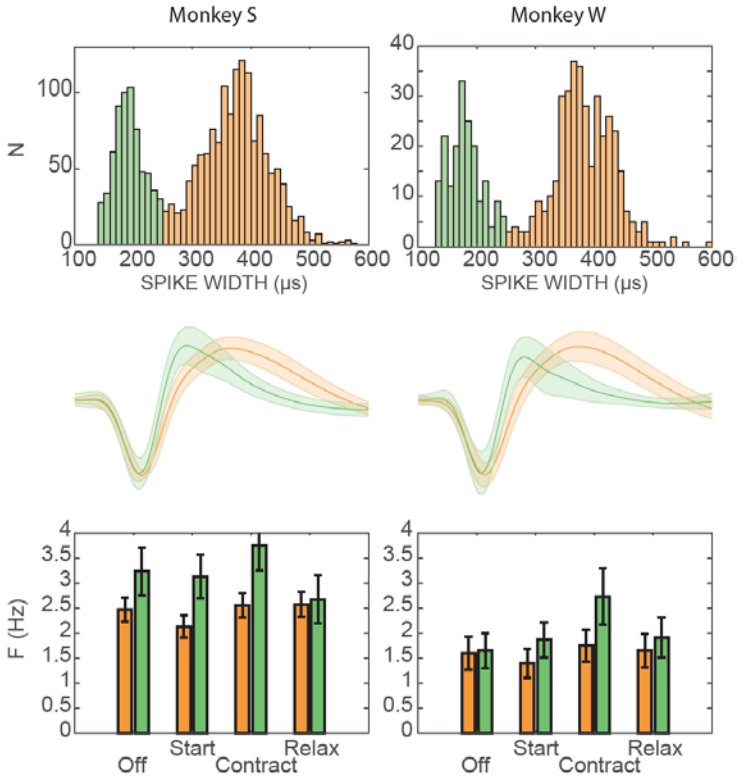

Figure 1.6. Population composition of FS and RS cells. Both monkeys had comparable ratios of RS:FS cells. Top: distribution of waveform width across all cells recorded in each monkey. Middle: average waveform and standard error for FS (green) and RS (orange) cells. Bottom: Median firing rates ± 95% confidence interval for RS and FS cells during four task periods. Consistent with other studies, RS cells fired less than FS cells overall. Modulation of firing by cell type was consistent in both monkeys.

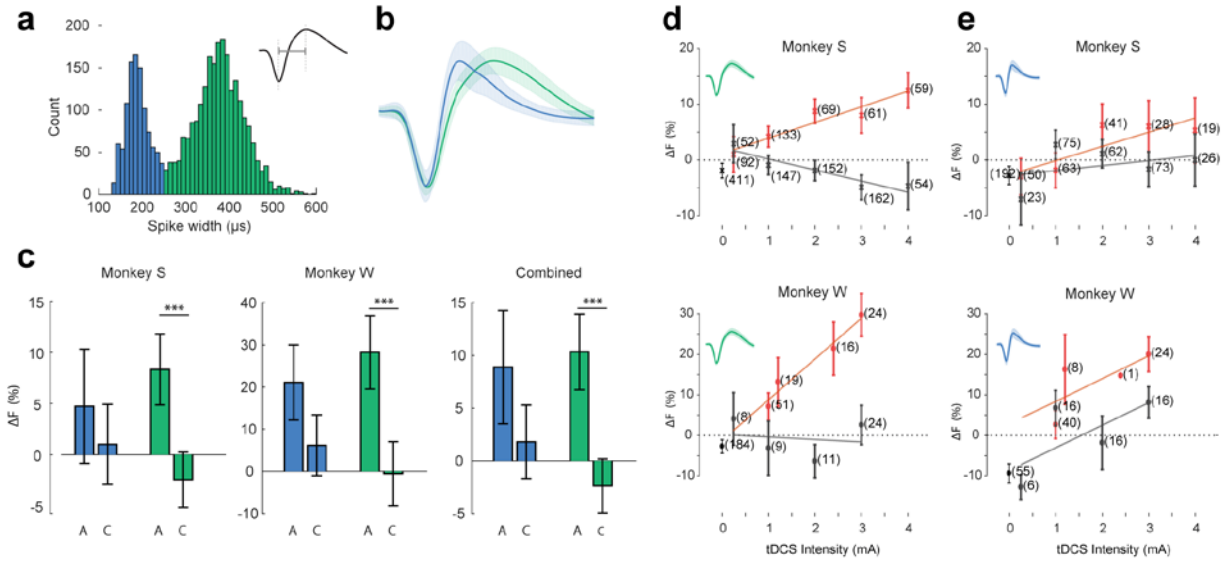

Figure 1.7. Regular spiking (RS) and fast spiking (FS) neurons are differently affected by tDCS **(a)** Histogram of spike width (trough – peak distance) for all neurons is bimodal and used to delineate two clusters (RS: ≥250μs, N=1812 and FS: <250μs, N=859). **(b)** Average waveform of FS (blue) and RS (green) neurons (peak normalized for clarity). **(c)** Change in firing by cell type during high dose (>1mA) tDCS. Changes in firing rate from Pre to Stim are significantly different during a- and c-tDCS for RS neurons but not FS neurons ($p<0.001$, Wilcoxon sign-rank test), and RS cells are more robustly affected by a-tDCS than c-tDCS. **(d)** Firing rates of RS cells are positivity correlated with dose during a-tDCS and negatively correlated with dose during c-tDCS (linear interpolation, $y=bx+c$. a-tDCS: Monkey S: b=2.8, $R^2=0.91$; Monkey W: b=10, $R^2=0.96$; c-tDCS: Monkey S: b=-2.0, $R^2=0.87$; Monkey W: b=-0.6, $R^2=0.02$). **(e)** Firing rates of FS cells tend to increase with a- and c-tDCS. Modulation is weaker than for RS cells (a-tDCS: Monkey S: b=2.5, $R^2=0.71$; Monkey W: b=0.9, $R^2=0.13$; c-tDCS: Monkey S: b=5.6, $R^2=0.52$; Monkey W: b=5.5, $R^2=0.48$).

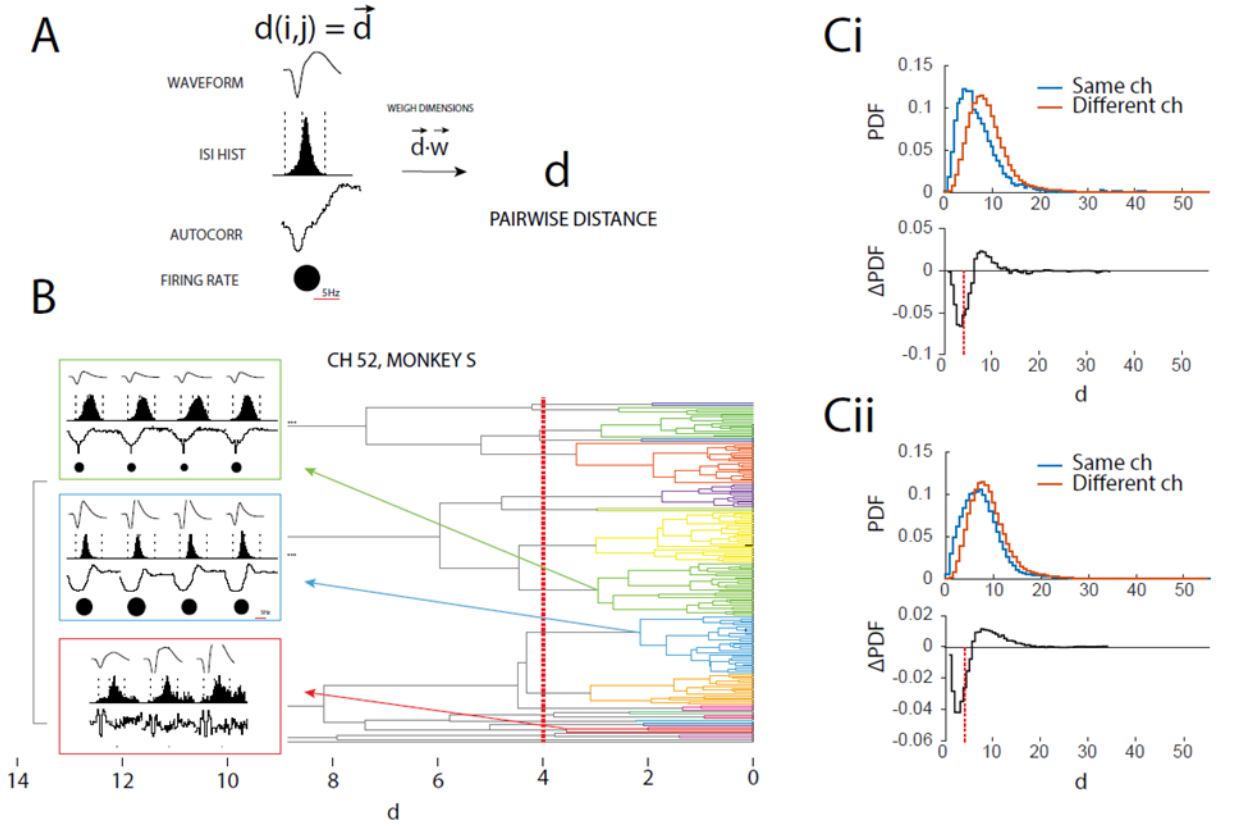

Figure 1.8. Algorithm for longitudinal cell identification. **(a)** Five statistics of firing were calculated for each neuron during Pre, including average waveform shape, inter-spike interval histogram, spike-time autocorrelogram at two timescales, and average firing rate. We calculated pairwise differences for each metric across all recorded neurons, z-scored difference measure, and weighted the combined difference vector **d** by **w** to weight certain factors, such as autocorrelation, more heavily. **(b)** Example clustering results for a single recording channel over many experiments. We performed complete-linkage hierarchical clustering on the weighted set of *d* for each channel, using a distance threshold criteria of 4 derived from distributions shown in **(c)**. **(c)** Distribution of *d* between neurons recorded on the same channel (blue line) and neurons recorded on different channels (red line) in Monkey S **(i)** and Monkey W **(ii)**. There is a higher frequency of low *d* between neurons recorded on the same channel, reflecting the fact that some neurons are repeatedly recorded during separate experiments. We derived the cluster threshold cutoff using these two distributions, selecting a value (4) that corresponded to the *d* most likely to be observed between neurons on the same channel as compared with neurons on different channels.

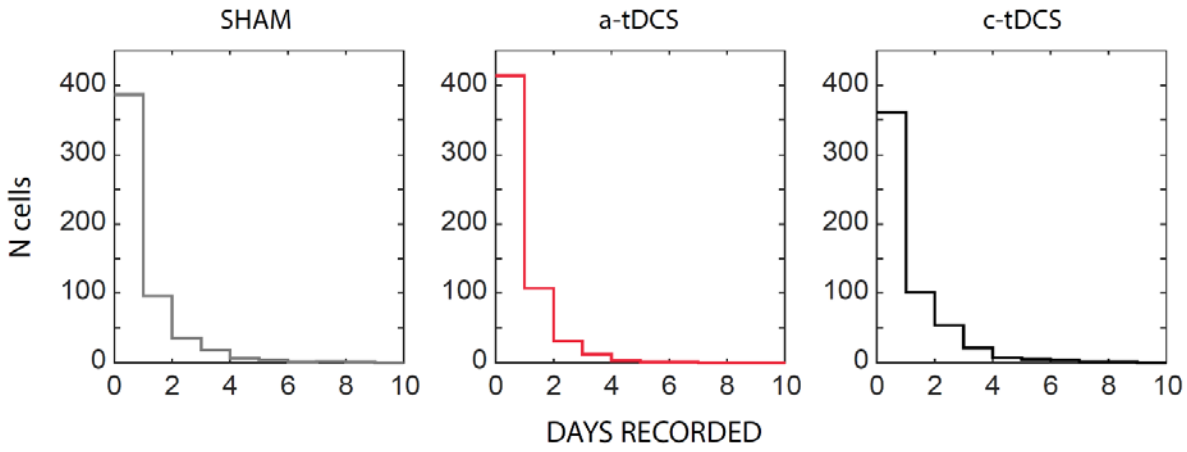

Figure 1.9. The number of cells recorded across sessions was similar for all conditions as detected by longitudinal cell tracking algorithm. Most neurons were recorded only once for a given condition (N=1162), but each condition (a-tDCS, c-tDCS, Sham) had a sizable number of neurons recorded more than once. These neurons permitted estimation of the reliability of tDCS effects in single neurons across sessions.

Figure 1.10 Results of longitudinal cell identification algorithm. Exemplary channels with unusually high repeat neurons are shown. Each neuron is represented by four statistics (Scale bars in top left. From top to bottom: average waveform, average firing rate (grey circle), inter-spike interval histogram, spike time autocorrelation.) Neurons identified across sessions are plotted together in boxes.

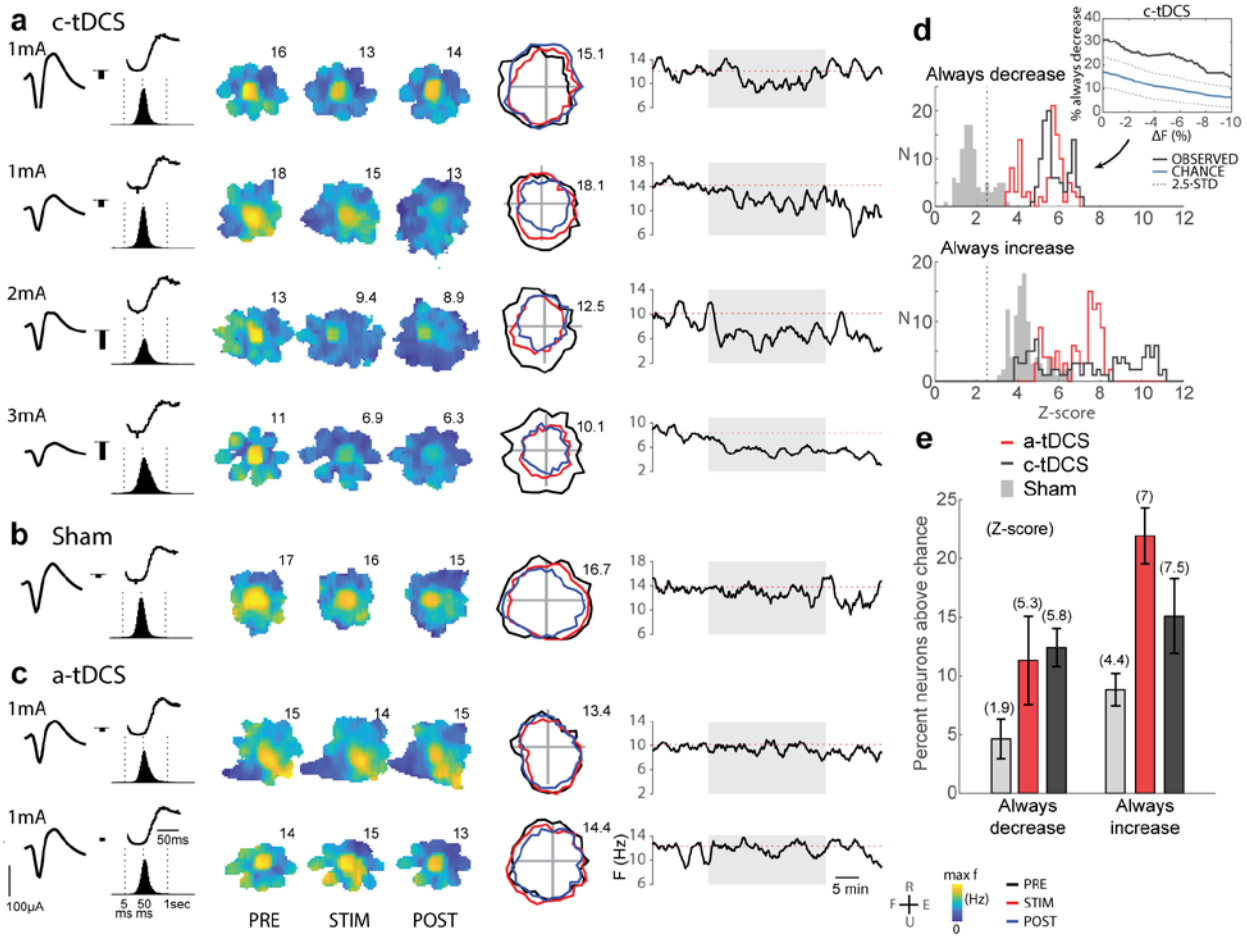

Figure 1.11 tDCS affects the same cells consistently across experiments (a-c). A neuron recorded across 4 c-tDCS experiments (a), 1 sham experiment (b) and 2 a-tDCS experiments (c). From left to right: average spike waveform, percent change in spiking (black bar), spike time autocorrelogram with lag [-20,100] ms (black trace), ISI distribution (black histogram), firing rate maps in torque space for Pre, Stim, and Post epochs, directional tuning function (polar plots), firing rate in time (window: 1 min, step-size 10 sec). Cell firing rate drops with increasing c-tDCS intensity but is unaffected during sham or a-tDCS. (d) Distribution of z-scored probability that neurons are reliably excited or inhibited by tDCS. Dashed line indicates p=0.01 relative to data shuffled within each condition (10,000 iterations). Inset: Example observed probability of consistent decreased firing during c-tDCS by at least ΔF from -10 to 0% (black trace). Chance probability ± 2.58·SD blue and dashed blue traces. (e) Percent of cells that always increased or decreased firing for a-tDCS, c-tDCS, or Sham experiments. Z-score relative to shuffled data indicated in parenthesis. Both a-tDCs and c-tDCS significantly increased the percent of cells that reliably increased or decreased their firing, suggesting that both polarities produce reliable, mixed effects in single neurons across sessions (z-scores>5.3, or p<0.001).

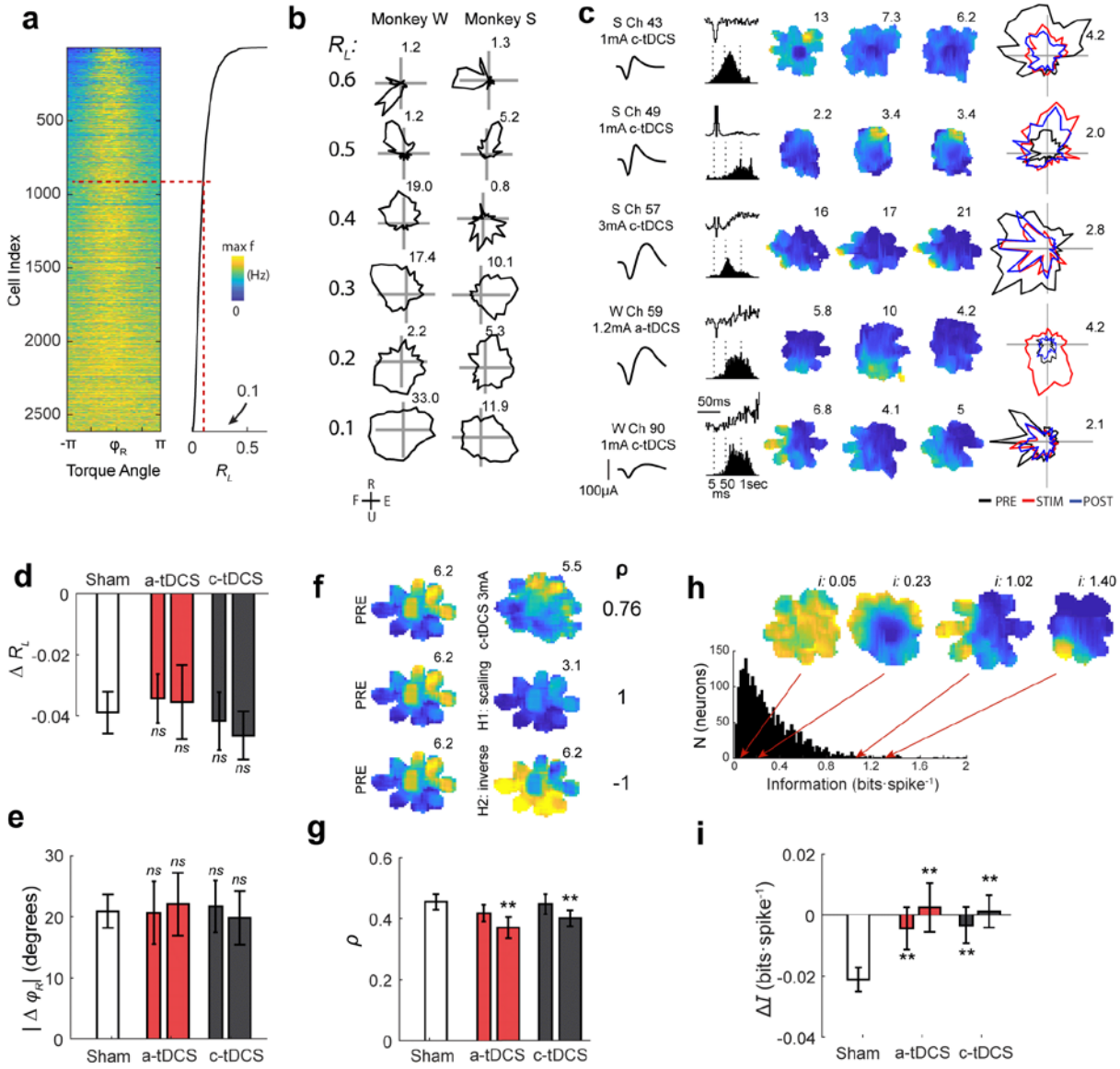
a
Cell Index
500
1000
1500
2000
2500
max f
(Hz)
0
-π
φR
π
Torque Angle
0
0.5
0.1
RL
b
Monkey W
Monkey S
RL:
0.6
0.5
0.4
0.3
0.2
0.1
1.2
1.3
1.2
5.2
19.0
0.8
17.4
10.1
2.2
5.3
33.0
11.9
R
F
E
U
c
S Ch 43
1mA c-tDCS
S Ch 49
1mA c-tDCS
S Ch 57
3mA c-tDCS
W Ch 59
1.2mA a-tDCS
W Ch 90
1mA c-tDCS
100μA
50ms
5 50 1sec
ms
13
7.3
6.2
4.2
2.2
3.4
3.4
2.0
16
17
21
2.8
5.8
10
4.2
4.2
6.8
4.1
5
2.1
PRE
STIM
POST
d
Sham
a-tDCS
c-tDCS
Δ RL
0
-0.02
-0.04
ns
ns
ns
ns
e
| Δ φRel | (degrees)
30
20
10
0
ns
ns
ns
ns
Sham
a-tDCS
c-tDCS
f
PRE
PRE
PRE
6.2
6.2
6.2
c-tDCS 3mA
H1: scaling
H2: inverse
5.5
3.1
6.2
ρ
0.76
1
-1
g
ρ
0.6
0.4
0.2
0
**
**
Sham
a-tDCS
c-tDCS
h
i: 0.05
i: 0.23
i: 1.02
i: 1.40
N (neurons)
150
100
50
0
0
0.4
0.8
1.2
1.6
2
Information (bits·spike-1)
i
ΔI (bits·spike-1)
0.02
0
-0.02
-0.04
**
**
**
**
Sham
a-tDCS
c-tDCS

Figure 1.12 Single neuron coding during tDCS. (a-e) Directional tuning is unaffected by tDCS. (a) Directional tuning functions of all neurons (peak normalized and rotated by their preferred direction) are ordered by RL. (b) Polar plots of raw directional tuning functions for neurons from both monkeys with varying RL. Numbers give peak firing rate. (c) Five directionally tuned neurons (RL>0.1) during a- and c-tDCS. Spiking features and rate maps as in Figure 4. While the amplitude of tuning is modulated by tDCS, directionally is preserved. (d) tDCS did not significantly change the strength of directional tuning as compared with sham ($p>0.05$; Wilcoxon rank-sum test). There was a small but statistically significant decrease in RL for all conditions ($p<0.001$; paired Wilcoxon sign-rank test). (e) Absolute change in preferred angle from PRE-STIM/SHAM for directionally tuned neurons (RL>0.01). tDCS did not significantly change the direction of tuning relative to sham ($|\Delta\varphi R|$ $p>0.05$), and there was no bias in the population-wide changes in preferred direction for any condition ($\Delta\varphi R$, not shown; $p>0.05$, Wilcoxon sign-rank test). (f-i) There were small changes in torque space tuning during high dose tDCS. (f) Three rate map comparisons and their associated correlation coefficient (ρ) for illustrative purposes. ρ is high for a cell with tuning during 3mA c-tDCS (top), maximal (1) in the hypothetical case of pure rate scaling (middle), and minimal (-1) in the hypothetical case of inverted peaks/troughs (bottom). (g) There were small shifts in tuning shape between Pre and Stim/Sham epochs ($\rho\approx0.45$), and this effect was more pronounced during high dose tDCS. (h) Histogram of all torque vector spike information content (i) for all neurons. Four example rate maps with corresponding i values above demonstrate how “peaky” neurons carry more information than do neurons with dispersed spikes. (i) Shifts in tuning were not associated with drops in spike information during tDCS, but they were during Sham. (**$p<0.001$, Wilcoxon rank-sum test)

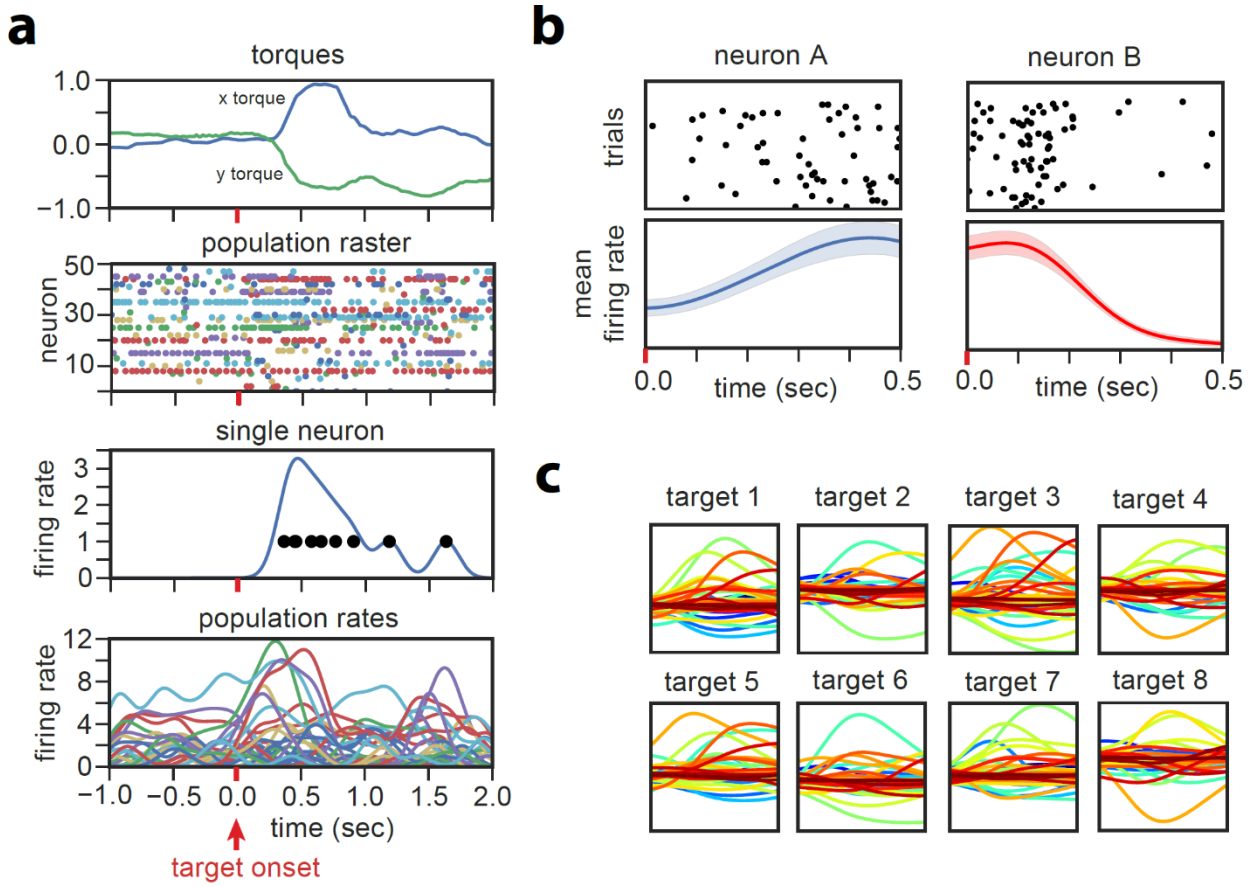

Figure 1.13. Task-specific population dynamics. **(a)** Example dynamic quantities for a target tracking task (N=49 neurons). Target onset occurs at t=0 (red bar on time axis). Top panel: manipulandum x- and y-torque trajectories. Second panel: population raster plot, each dot represents a spike time. Third panel: spike times of single neuron (black dots) and Gaussian-filtered rate (σ=100 milliseconds). Bottom panel: population firing rate curves as in third panel, colors match those of second panel (not normalized for illustration). **(b)** Target-specific, cross-trial spiking for two example neurons. Top: cross-trial raster plot. Bottom: mean firing rate curve. Shaded area shows one standard error of the mean. **(c)** Population mean firing rate curves (each color indicates a specific neuron) separated by target number for same time interval as (b).

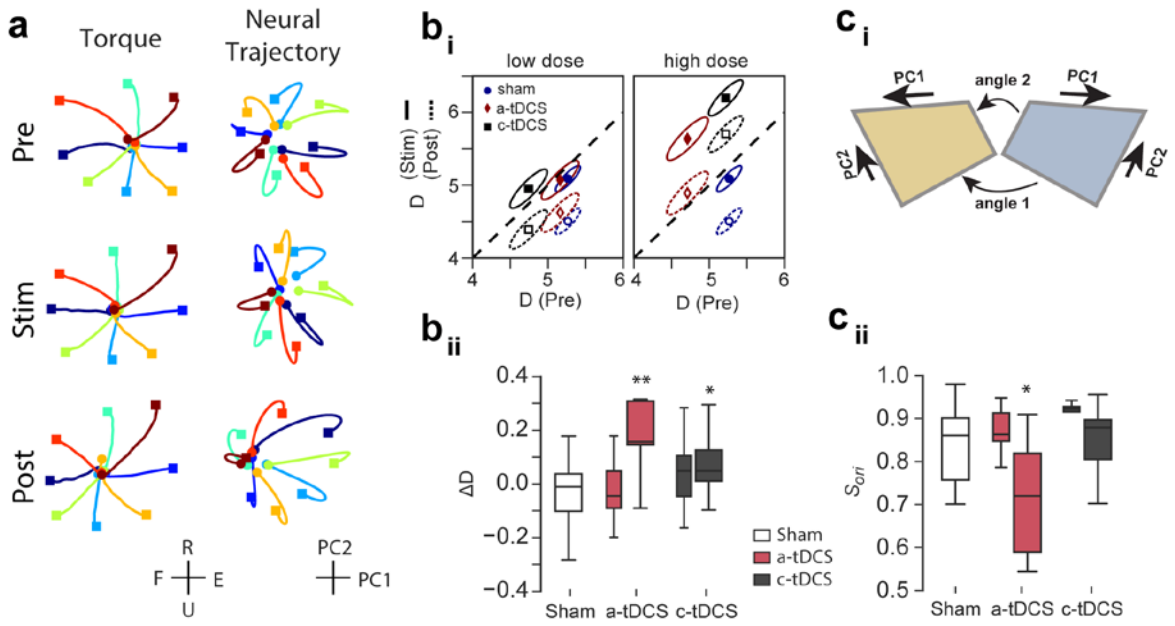

Figure 1.14. Population dynamics during the task and tDCS. **(a)** Target-specific, averaged manipulandum torques (left) and population firing rates projected in first two PCs (right) for an example session, not normalized for illustration (3 mA c-tDCS, N_{cells}=49). Colors indicate target identity, circle markers: t=0 seconds (target onset), square markers: t=0.5 seconds. **(bi)** Mean dimensionality between Pre-Stim epochs (solid) and Pre-Post epochs (dashed). Points show mean of bivariate sample and ellipses show one standard error. Data points above the line (high dose tDCS during Stim and Post) indicate an increase in ensemble trajectory dimensionality, whereas points below the diagonal indicate a drop in dimensionality. Low dimensional ensemble trajectories utilize a smaller subspace of possible population patterns as compared with high dimensional trajectories. **(bii)** Box plots showing statistics of Pre-normalized dimensionality change for neural trajectories during Pre and Stim. Box edges show first and third quartiles, internal bar shows mean, whiskers show extremal values. Data plotted for tDCS low (≤ 1, thin bars) and high (>1mA, thick bars) doses. **(ci)** Illustration of principal angles between two linear PC manifolds. **(cii)** Change in *orientation similarity* (S_{ori}) of manifolds (PC1 & PC2 as depicted in **a**) from Pre to Stim. S_{ori} remains high during Sham epochs, indicating that ensemble patterns are stable over time. High dose a-tDCS evoked new dominant patterns of activity in the ensemble, indicated by a decrease in S_{ori}. (*p<0.05, **p<.01, Sham vs. tDCS, independent t-test)

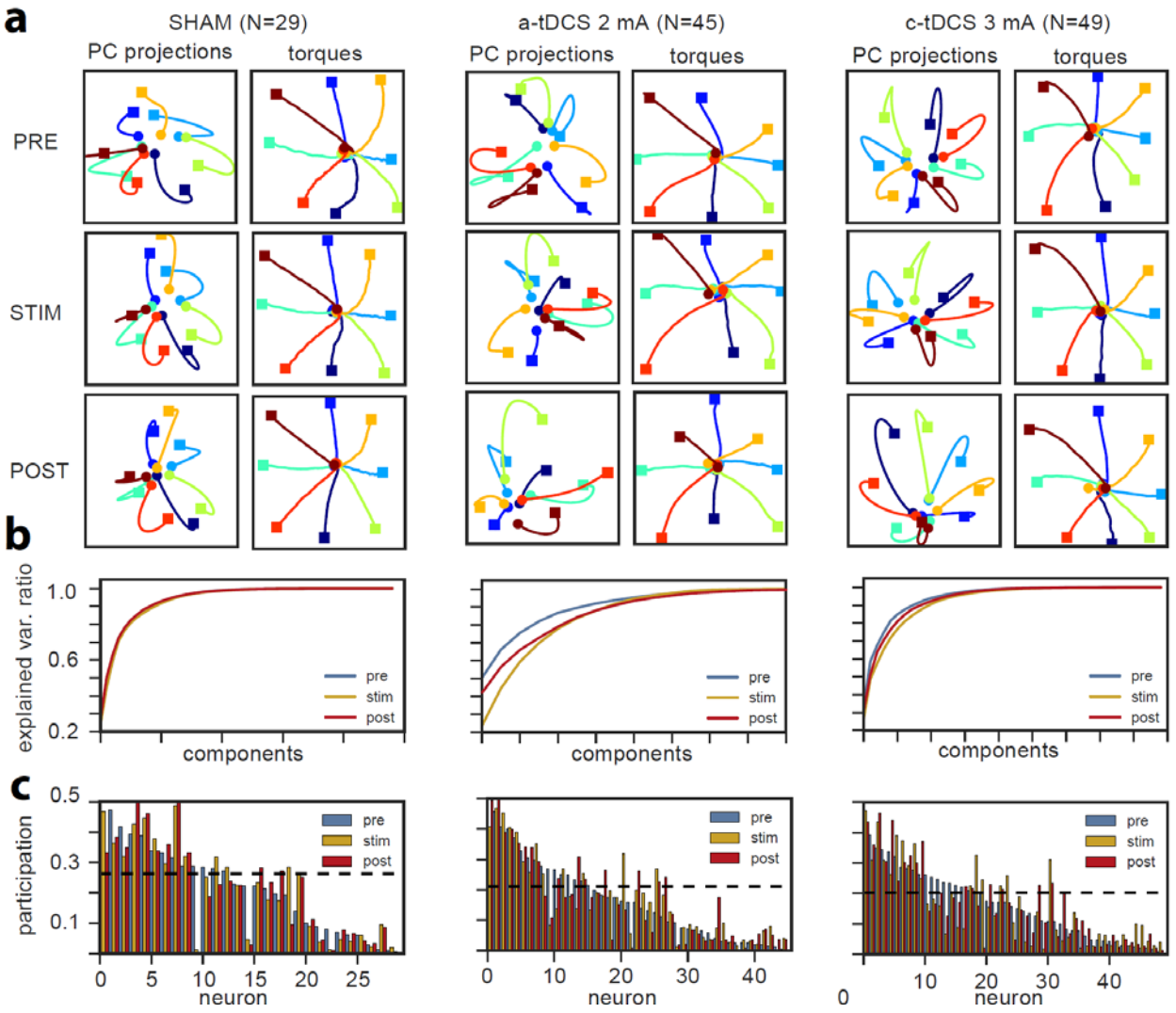

Figure 1.15 Examples of ensemble trajectories in 2D manifold. PCA–related quantities for three representative sessions. **(a)** Sham, N=29. **(b)** A-tDCS (2 mA), N=45. **(c)** C-tDCS (3 mA), N=49. Top three rows (for all panels): Target-specific, averaged population firing rates projected in first two PCs (left) and averaged manipulandum torques (right). Each row indicates tDCS epoch (Pre, Stim, Post). Colors indicate target identity, circle markers indicate t=0 seconds (target onset), square markers indicate t=0.5 seconds. **(b)** Explained variance ratio curves from PCA. **(c)** *Participation scores* of all neurons, for subspaces spanned by first two PCs (d=2) of PCA models PRE, STIM and POST, respectively. Neurons are ordered in decreasing order of score in model PRE. Dotted line indicates score that equally participating neurons would hold.

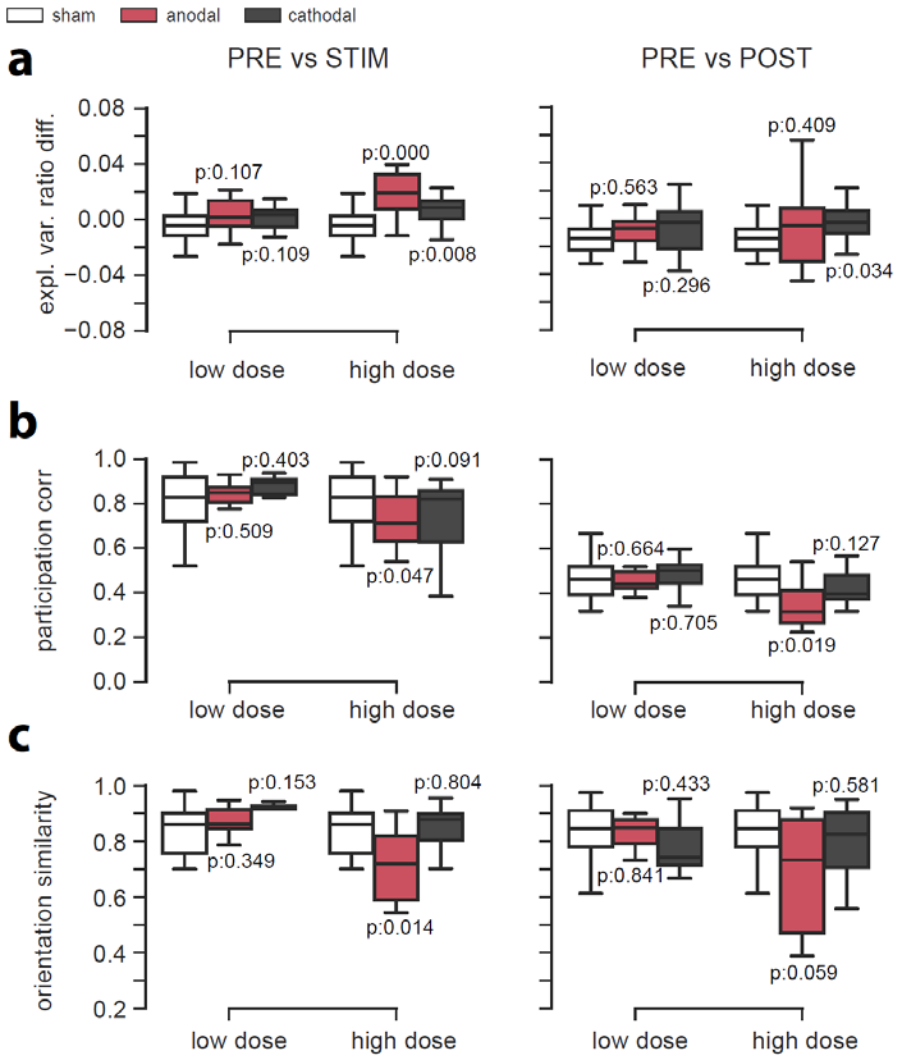

Figure 1.16. Statistics of population coding metrics. **(a)** Change in dimensionality of ensemble trajectories. Dimensionality is normalized by Pre to account for differences across experiments. Main Figure 6 shows pre-normalization values. **(b)** Correlation coefficient for participation score of neurons to the subspace spanned by the first two (d=2) PCs of PCA models. **(c)** Orientation similarity measure between subspace spanned by first two PCs (d=2) of PCA models. For all panels: Box edges show first and third quartiles, internal bar shows mean, whiskers show extremal values. Comparative quantities are plotted for model pairs. From left to right: Stim-Pre, Post-Pre. In each plot, quantities are shown for tDCS low (≤ 1mA, left) and high (>1mA, right) doses, for three conditions: sham (white), a-tDCS (red), c-tDCS (black). Sham box is repeated for low and high doses. P-values are computed from comparison with sham samples with an independent t-test. Effects during Post reflect activity for 30 minutes after tDCS was turned off.

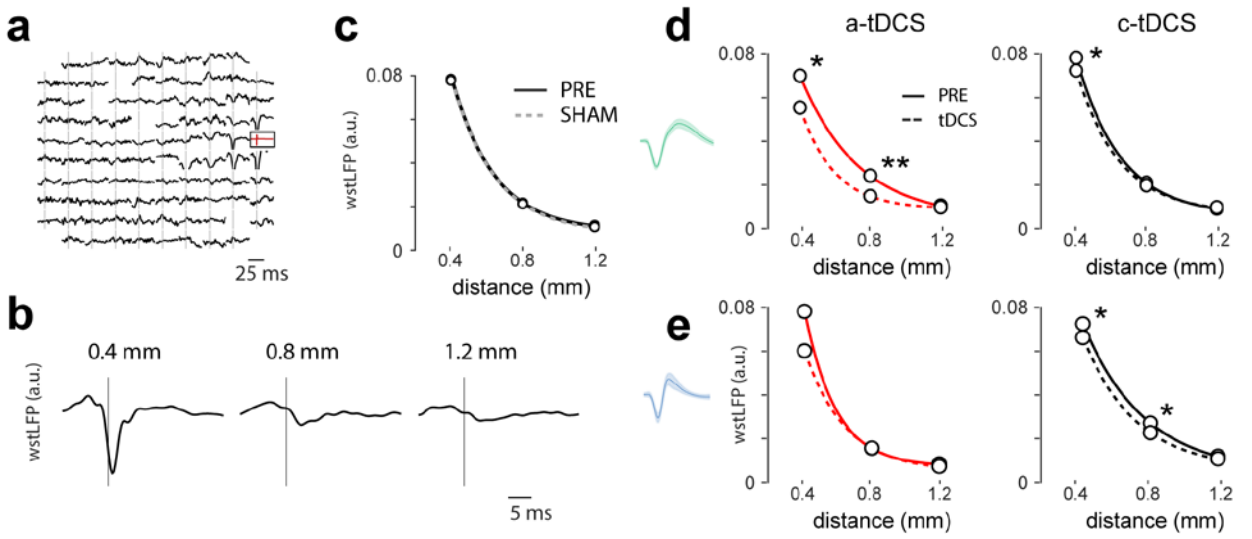

Figure 1.17. tDCS diminishes the amplitude of RS neuron spike-triggered LFP **(a).** Whitened spike triggered LFP (wst-LFP) across the microelectrode array shows significant post-spike features at channels close to the neuron. **(b)** Example wst-LFP at three distances from triggering neuron (Manhattan distance). **(c)** Trough amplitude of wst-LFP (global minimum between 0 and 6ms lag) are stable from Pre to Sham epochs. The data is fitted with an exponential $A\ exp(-x/\lambda)+C$, where x is the distance and λ (0.24mm) is the space constant. **(d-e)**. Effects of high dose tDCS on RS and FS cells. (*N*, *A* and *λ* reported in *Supplemental table 1*). (**d)** Amplitude of wst-LFP at channels adjacent to RS cells is diminished by high dose a-tDCS (distance 0.4mm: $p<0.01$; 0.8mm: $p<0.001$; paired Wilcoxon sign-rank test). Effect is small, but significant for 0.4mm distance during c-tDCS ($p<0.01$). (**e)** Amplitude of wst-LFP at channels adjacent to FS cells is diminished by c-tDCS (distance 0.4mm and 0.8mm $p<0.001$) but not a-tDCS. **$p<0.001$, *$p<0.01$, paired Wilcoxon sign-rank test

Chapter 2. EPIDURAL CORTICAL STIMULATION TRIGGERED BY EMG ACTIVITY

We tested a novel paradigm for directing reorganization of primary motor cortex using CS that was spatiotemporally defined by muscle activity (activity dependent CS). Previously, the Fetz lab demonstrated that activity-dependent CS triggered from cell or muscle activity produced predictable plastic changes between cortical sites. In the present study, EMG signals triggered epidural stimulation to unrelated cortical sites (crossed myo-cortical feedback) with the goal of shifting motor maps in a targeted fashion. Epidural conditioning stimulation resulted in broad changes across the array that were difficult to interpret. Epidurally-evoked motor maps were unstable and reflected the coactivation of multiple muscle groups, which made it difficult to identify independent cortical sites for targeted reorganization. Over the course of five months, muscle outputs became uniform across the epidural electrode array and we attempted a different paradigm (direct myo-cortical feedback). During these experiments, we delivered EMG-triggered epidural stimulation to a single cortical site known to evoke activity at the triggering EMG channel. In contrast to “crossed” conditioning, effects of “direct” conditioning were repeatable across the array. These results suggest that epidural CS may provide a less-invasive alternative to activity-dependent intracortical CS, but motor mapping by epidural stimulation is not an appropriate measure of plasticity.

BACKGROUND

Experimental CS-based treatments for brain injury claim to boost the brain's ability to find a more functional motor cortex representation by modulating excitability and/or inhibition with tonic or preprogrammed stimulation[3,4,6,98]. The predominant interventions include tonic stimuli delivered via transcranial direct current stimulation (tDCS, described in *Chapter one*), transcranial magnetic stimulation (TMS), or epiduraltorrque cortical stimulation (ECS)[2,6]. In the following chapter, we study a less common form of CS that is conditioned on brain activity, called "activity dependent stimulation". This technique is different from existing stimulation protocols because it is temporally correlated with brain activity and may hold potential for more effective and targeted recovery.

Two recent studies from the Fetz lab demonstrated that the activity-dependent CS paradigm is effective in producing predictable plastic changes. The first study used action potentials detected from an intracortical electrode to trigger conditioning CS (intracortical microstimulation) at a separate electrode site via an implantable computer[7,99]. This pattern of closed-loop stimulation mimics the pre- to post-synaptic neuron activation underlying spike-timing dependent plasticity[100], a form of Hebbian plasticity[101]. After overnight conditioning, targeted changes were documented in the motor output lasting as long as 10 days. This result was intriguing for many reasons, including 1) the novel technology for inducing profound functional and electrophysiological effects and 2) it provided strong evidence in support of Hebb's theory in-vivo by using natural spike patterns to drive plasticity.

The second study asked, can EMG activity be used as a less invasive surrogate for cortical activity[33]? For these experiments, EMG signals triggered intracortical microstimulation in an unrelated cortical site ("crossed" myo-cortical feedback), which subsequently shifted the

isometric torques elicited from stimulation at cortical sites associated with the EMG trigger. The following experiments extend this line of work by removing all invasive intracortical electrodes with the aim of developing a safer intervention for clinical trials.

In the following experiments, we measured motor maps of isometric wrist torques evoked from an array of epidural electrodes. Once the mapping was complete, a forearm EMG channel was selected as a trigger signal to time subthreshold stimulation to an unrelated epidural cortical site. After hours of conditioning, we checked for specific changes in the motor map that were indicative of targeted plasticity. Unfortunately, epidural stimulation was not specific enough to produce motor maps of isometric torques that were distinct across different electrodes. Furthermore, daily changes in the motor map within 4 months of implantation of the array made it difficult to determine whether changes were related to cortical conditioning. Future attempts at non-invasive myo-cortical feedback should explore alternative outcome measures.

SPECIFIC METHODS

Subjects and behavioral tasks

One monkey (K) was trained to perform two tasks using the manipulandum for smoothie reward in the primate booth: 1) a center-hold task in which no torques are exerted by the animal and the cursor is held steady, and 2) a center-out task in which the animal must control the manipulandum in 4 dimensions including pronation/supination (p/s), flexion/extension (f/e), radial/ulnar (r/u) and grip.

Surgical procedures

Nine epidural electrodes made of 9mm cut platinum rods with insulated, crimped gold pins were lowered and fixed in 0.5mm craniotomy holes over the forelimb area of M1 (**Figure 2.4**).

Localization of burrholes was measured stereotactically with respect to ear-bar-zero, and a titanium chamber was placed over the implant site and fixed to the skull using dental acrylic. EMG wires were subcutaneously tunneled and led directly into the head chamber along the posterior midline via a port between the scapulae. Percutaneous EMG electrodes were inserted into the muscle belly of forearm muscles and remained in place for one week. Proper location was confirmed by stimulation and by observing wire movement during passive joint articulation. A primate jacket was used to prevent the animal from disrupting the percutaneous EMG wires.

Experiment timeline

The experiments consisted of 1) a preconditioning epoch, in which forearm activity is mapped by stimulating epidural electrode sites in M1, 2) a conditioning epoch, in which activity-dependent stimulation was delivered during free behavior in the home cage or during a torque-driven task in the booth, and 3) one or more post-conditioning epochs to measure effects of conditioning or sham stimulation (**Figure 2.1**). During the preconditioning epoch, the animal remained still in a primate booth by performing a center-hold task with a manipulandum while trains of cortical stimulation pulses (17 biphasic pulses, 0.2ms width, 333Hz, 0.5-2mA depending upon motor threshold) elicited forearm motor outputs measured by EMG and isometric torque via the manipulandum.

During the **conditioning epoch**, motor units known to be correlated with CS were used to trigger sub-threshold CS (**Figure 2.2**). Conditioning was conducted in two ways: 1) using the NeuroChip[53] to autonomously deliver EMG-triggered stimulation during prolonged periods of free behavior (**Figure 2.1**, top) or 2) in the primate booth during the center-out target-tracking task requiring four dimensions of movement (**Figure 2.1**, bottom). The advantages to free behavior included the ability to conduct very long conditioning periods with natural movement, not isometric torques. The advantages to the booth included the ability to deliver a higher number of stimuli under more

controlled conditions in a shorter amount of time, which could better document onset time of effects. During the post-conditioning epochs, forearm activity is mapped once again during the center-hold task and compared with the preconditioning map.

Selection of neural sites for conditioning and control

Data collected during the preconditioning mapping epoch was used to determine three neural sites for the experiment: N_{rec}, N_{stim}, and $N_{control}$ (**Figure 2.3**). These three sites represent the presynaptic, postsynaptic, and unconditioned targets in the activity-dependent stimulation paradigm described in earlier studies[7,8]. During crossed myo-cortical feedback experiments, we tried to follow the same inclusion criteria for N_{rec}, N_{stim}, and $N_{control}$ as reported in these experiments. This included: motor effects that were non-overlapping, were in muscles that we could record by EMG, and were stable. Our preparation provided less flexibility in located sites than that of Jackson and Lucas and colleagues because the array of nine epidural electrodes was not movable.

Measuring plastic changes

We checked for specific changes in isometric torques elicited by cortical stimulation after conditioning. In previous studies, our group used a torque vector analysis (TVA) in which the angle between torque vectors was calculated from a joint space[7,8]. This analysis is potentially misleading because the angular distance is arbitrary (ulnar deviation is 180 degrees from radial deviation, but extension is only 90 degrees), therefore, changes in the motor field angle may be spuriously interpreted as approximating a target torque vector. For this analysis, we used a true distance measure, the Mahalanobis Distance, between torque vectors defined across four joint dimensions and 6 time points encompassing the duration of twitch responses (**Figure 2.7a**).

Data analysis

Online analysis of EMG signals during experiments utilized oscilloscopes (booth conditioning) and the NeuroChip (free behavior conditioning) to discriminate motor unit spikes to trigger stimulation. Offline analysis of isometric torque was conducted using MATLAB.

RESULTS

Motor maps of isometric torque elicited by epidural stimulation

We performed a total of 47 conditioning experiments over the course of five months. There were motor effects from 4-6 epidural electrode sites (9 possible) at the start of every experiment, and each evoked complex twitches suggesting that multiple muscle group were recruited (**Figure 2.4**). In the months immediately following implantation, the motor maps at various electrodes were somewhat unique (**Figure 2.4a**), although they often overlapped and made it impossible to identify a single N_{Rec} site. Five months following initial implantation, effects were similar across all electrodes (**Figure 2.4b**), at which point we could not continue experiments using this conditioning paradigm.

Evoked twitches were complex in shape, and sometimes involved antagonist movements or differing temporal profiles. **Figure 2.5** shows two example channels with evoked twitches towards flexion and then extension. The speed of twitches was also variable from site to site (**Figure 2.5 a vs. b**). Motor maps measured at the beginning of **Figure 2.6** shows that motor thresholds were often >1mA; thresholds increased considerably (≃150%) over the course of five months.

Crossed myo-cortical feedback

In the first set of experiments (N=37), we delivered free behavior conditioning to an epidural cortical site (N_{Stim}) triggered by EMG activity (M_{Rec}) known to be associated with a different epicortical site (N_{Rec}, "crossed myo-cortical feedback"). **Figure 2.3** depicts the conditioning paradigm and expected effects at N_{Rec}.

We observed changes in twitch shape and direction following conditioning. There was some evidence that conditioning produced predicted effects: the motor map at N_{Rec} approached that of N_{Stim}. **Figure 2.8** depicts a sample experiment in which N_{Rec} acquired pronation from N_{Stim}, thereby diminishing the predominant supination observed before conditioning. At the same time, changes were also noted in N_{Stim}, which was not expected. Post conditioning changes were often observed in other electrode sites as well, perhaps because motor maps of two or more electrode sites overlapped.

We measured how twitches changed before and after conditioning using the Mahalanobis distance (D_M) between data points at six time points across all four torque dimensions (**Figure 2.7a**). We expected twitches in N_{Rec} to approach that of N_{Stim} measured before conditioning, but we found that twitches diverged from N_{Stim} in all conditions. **Figure 2.7b** shows D_M to N_{Stim} before conditioning for N_{Rec} and $N_{Control}$ (other sites with motor effects unrelated to N_{Rec}). $N_{Control}$ sites tended to drift away from N_{Stim} more so than N_{Rec} sites.

Direct myo-cortical feedback

Five months after implantation, there were no longer distinct motor effects across electrode sites in the array (**Figure 2.4)** so we could not perform conditioning experiments as described above. Instead, we tested whether effects at a single cortical site could be enhanced or diminished by "direct feedback" stimulation.

We conducted 10 experiments (6 conditioning, 4 control) to test the effects of delivering stimulation triggered by EMG activity (M_{Rec}) to a cortical site (N_{Rec}) previously mapped to the same EMG channel. **Figure 2.9a** illustrates this conditioning paradigm. Conditioning was conducted in the primate booth during some experiments (conditioning = 3, control = 3) because subcutaneously tunneled EMG wires were explanted secondary to infection. Control experiments using the Neurochip applied randomly timed stimulation trains generated by drawing stimulus-intervals from a uniform distribution such that the number of pulses delivered over the duration of control experiments was the same as during conditioning experiments. In the booth, control experiments used stimulation trains saved from previous experiments. The method of control used in the booth was preferred over that used with the Neurochip because it matches all conditioning stimulus-train statistics without activity-dependence. Unfortunately, the Neurochip was not capable of this type of stimulation timing.

Direct feedback conditioning in the booth and the cage both produced specific elimination of evoked twitches associated with M_{Rec} at N_{stim}. **Figure 2.9** shows supination torques evoked by N_{Stim} before and after three conditioning experiments and one control experiment ordered chronologically. Supination torques were eliminated for about 3 hours following positive feedback conditioning triggered by a motor unit recorded from the supinator muscle, after which they began to recover. We reproduced this effect with 2 other electrode sites (channel 16, N experiments=3; channel 6, N experiments=1). Control stimulation, which was unrelated to supinator activity, did not produce this change. Furthermore, supination effects at other cortical sites were not eliminated – in fact, these sites were associated with an increased activity of M_{rec} evoked responses after conditionings (**Figure 2.10a**). This pattern of decreased/increased evoked

response following conditioning may be interpreted as an induced inhibition at N_{Stim} and a compensatory boosting at other cortical sites (**Figure 2.10b**).

DISCUSSION

Motor maps evoked by epidural stimulation were overlapping and non-specific

Suprathreshold epidural CS currents corresponded with complex motor fields during pre- and post-conditioning mapping epochs that reflected the activation of multiple muscle groups, including antagonist muscle groups. Since motor effects overlapped significantly across different cortical sites, it was often impossible to identify a single N_{Rec} site for which we expected changes. Indeed, we often found that multiple electrode sites had remapped during conditioning. While Lucas et al reported that multiple responses were rarely evoked by intracortical microstimulation[102], every epidural electrode in our study produced multiple responses, even at barely suprathreshold current levels. This is likely due to the fact that motor thresholds are much higher for epidural stimulation than for intracortical stimulation (~1mA as compared with <0.1mA), resulting in greater current spread.

Implications for epidural conditioning

Poor spatial specificity reflected in torque maps also suggests that spatial specificity of conditioning was compromised, which means that the present paradigm had neither the spatial nor temporal precision of successful experiments reported by Jackson at al[7]. Loss of temporal precision introduced by EMG, rather than SUA, activity-dependent CS was likely the difference underlying relatively weaker and briefer effects reported by Lucas et al[8], and we believe that further distancing the preparation from ideal single neuron-to-single neuron activation precluded targeted, repeatable changes.

Effects of open-loop stimulation

We also found that motor effects changed over the course of mapping epochs, even in the absence of conditioning. In fact, it has been shown that prolonged durations of repetitive CS can shift representations in motor cortex[103]. In our experiments, motor maps shifted across days (and even over the course of a mapping epoch), thus we cannot rule out that open-loop epidural CS induced plastic changes itself.

Methods of induced plasticity in-vivo and in-vitro

Differences between the present experiments and others attempted in-vivo are significant, but the differences between our preparation and those used to demonstrate spike-timing dependent plasticity in-vitro are even greater[100,104–107]. Perhaps most significantly, artificial potentiation of horizontal connections in motor cortex is known to require disinhibition[106,108]. Future experiments (microstimulation included) may therefore benefit from pharmacological dis-inhibitors such as the systemic administration of dextromethorphan[109].

Implications of spatially specific effects following direct myo-cortical feedback

Interestingly, we found that *direct* myo-cortical feedback produced changes in N_{Stim} evoked twitches that were distinct from changes in $N_{Control}$ evoked twitches. Similar to crossed feedback, effects following direct feedback were present across the entire array, but they were repeatable and more easily interpreted. While this is somewhat encouraging, motor effects across the array were uniform and unchanging in the absence of stimulation by the time these experiments were underway. As mentioned above, motor effects during crossed-feedback experiments were instead quite variable day to day (and even during mapping epochs in the booth), which made it difficult to determine whether changes were related to conditioning or not. Thus, the age of the implant

array is a major confound when comparing crossed feedback experiments with direct feedback experiments.

Conclusions

We aimed to induce plasticity in motor cortex by following previously developed methods for conditioning stimulation[7,8], but with less invasive implants. In contract with these earlier studies, which used intracortical microwires to deliver CS, we used epidural electrodes that do not require penetration of the dura mater and are safer and more viable for clinical adoption. Unfortunately, these data suggest that crossed myo-cortical conditioning by epidural stimulation does not produce reliable effects. This was likely because currents required to evoke movements using epidural CS are much greater than those required during intracortical microstimulation, resulting in poor spatial specificity.

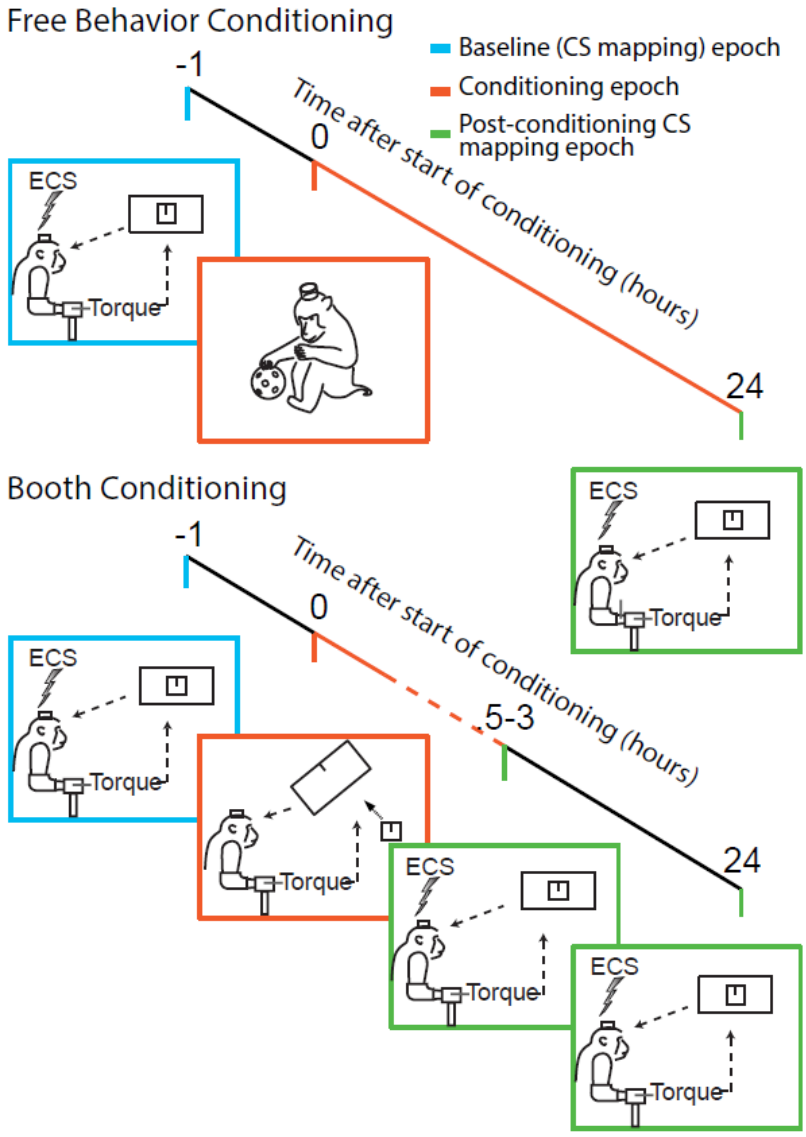

Figure 2.1 Two conditioning paradigms**.** Blue: mapping epoch, orange: conditioning epoch, and green: post conditioning mapping. Top panel. Conditioning during free behavior using the Neurochip2. Bottom panel. Conditioning in the primate booth.

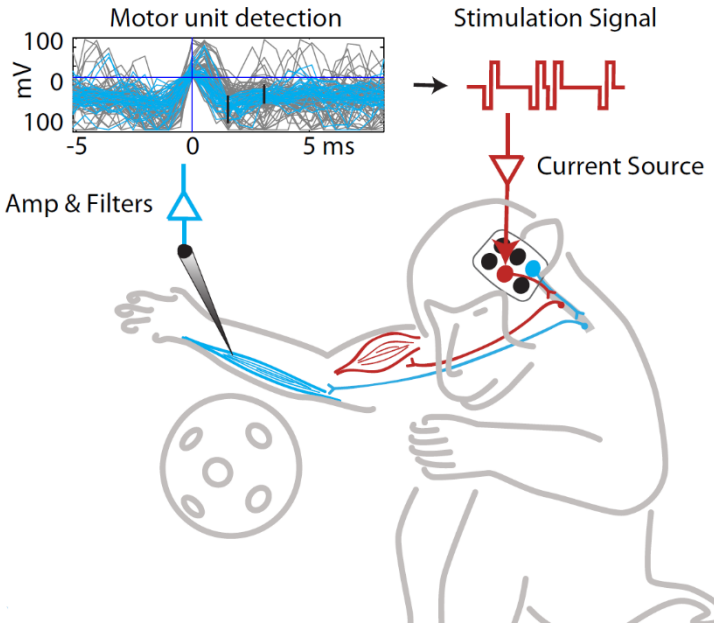

Figure 2.2. Cartoon of activity-dependent stimulation. In this example, EMG activity during free behavior is recorded from flexor carpi ulnaris (blue muscle). Motor unit spiking activity is converted into a train of biphasic current pulses (red "stimulation signal"), delivered to cortical site (red ECS electrode) previously mapped to biceps brachii (red muscle). Post-conditioning ECS mapping would show remapping of blue ECS electrode to include activation of both muscles.

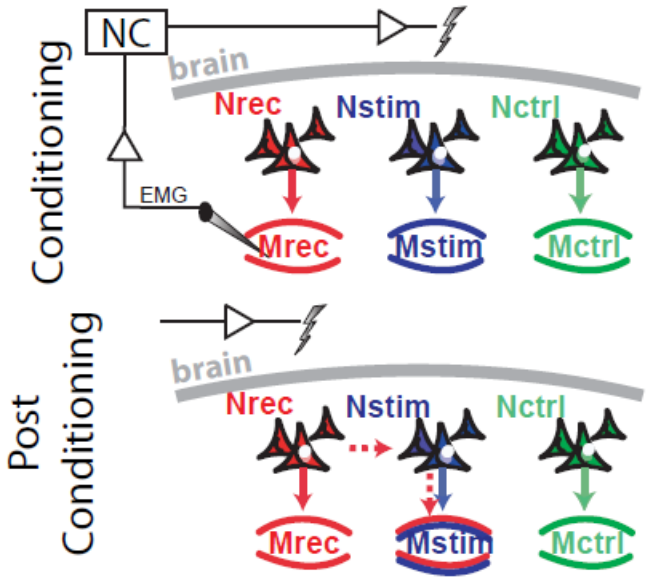

Figure 2.3 Hypothetical effects of crossed myo-cortical feedback. Top: during conditioning, EMG activity at a muscle triggers stimulation to an unrelated cortical site. Bottom: after conditioning, motor maps reflect plastic changes directed from sites associated with the triggering muscle to the CS electrode.

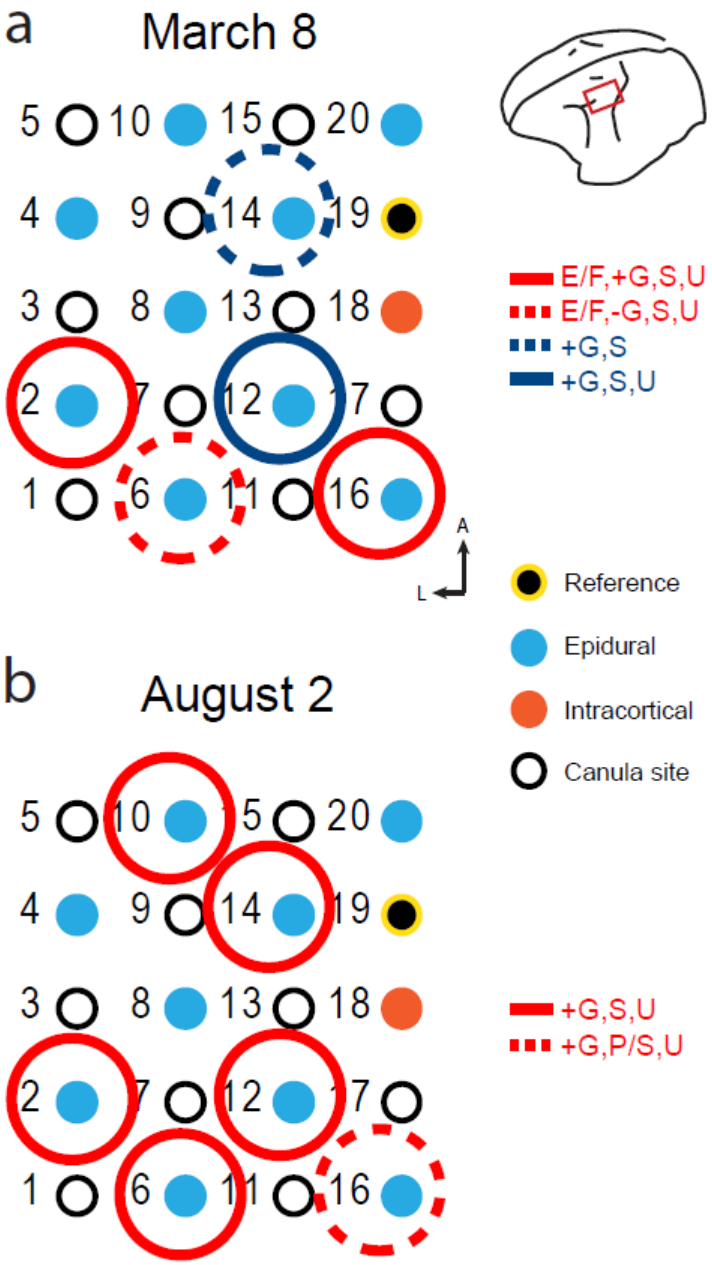

Figure 2.4. Implant array and motor effects early (**a**) and late (**b**) after implantation. -G/+G: grip flexion/grip extension; P/S: pronation/supination; F/E: flexion/extension; R/U: radial/ulnar

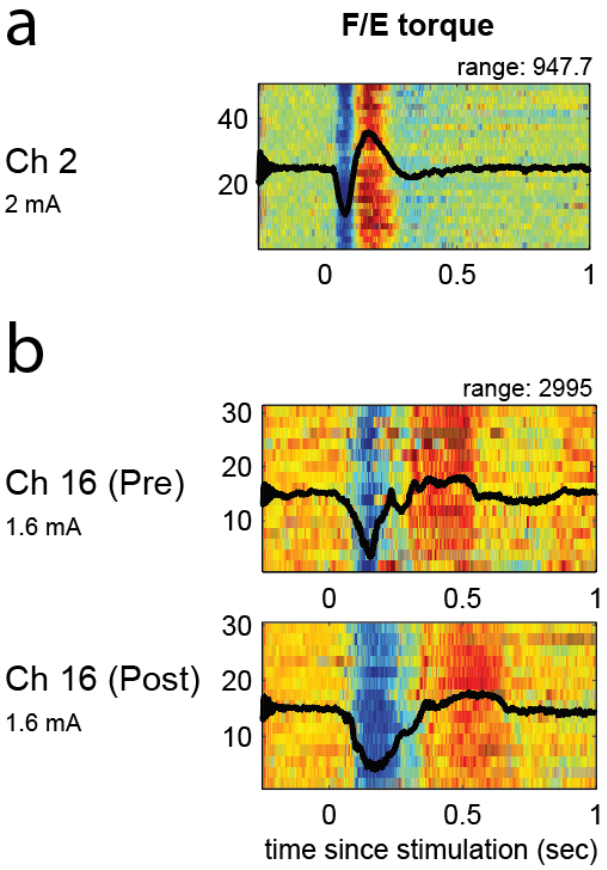

Figure 2.5. Complex evoked twitches during a single mapping epoch. Color indicates torque magnitude, y-axis represents trial number, and x-axis represents time relative to suprathreshold stimulation. **a.** Torques evoked from epidural electrode channel 2 reflected activation of antagonist muscle groups (extension followed by flexion). **b.** Similar to (a), torques evoked from channel 16 produced both extension/flexion, but the twitch speed was much slower. Mapping stimulation train was identical in both cases except for amplitude.

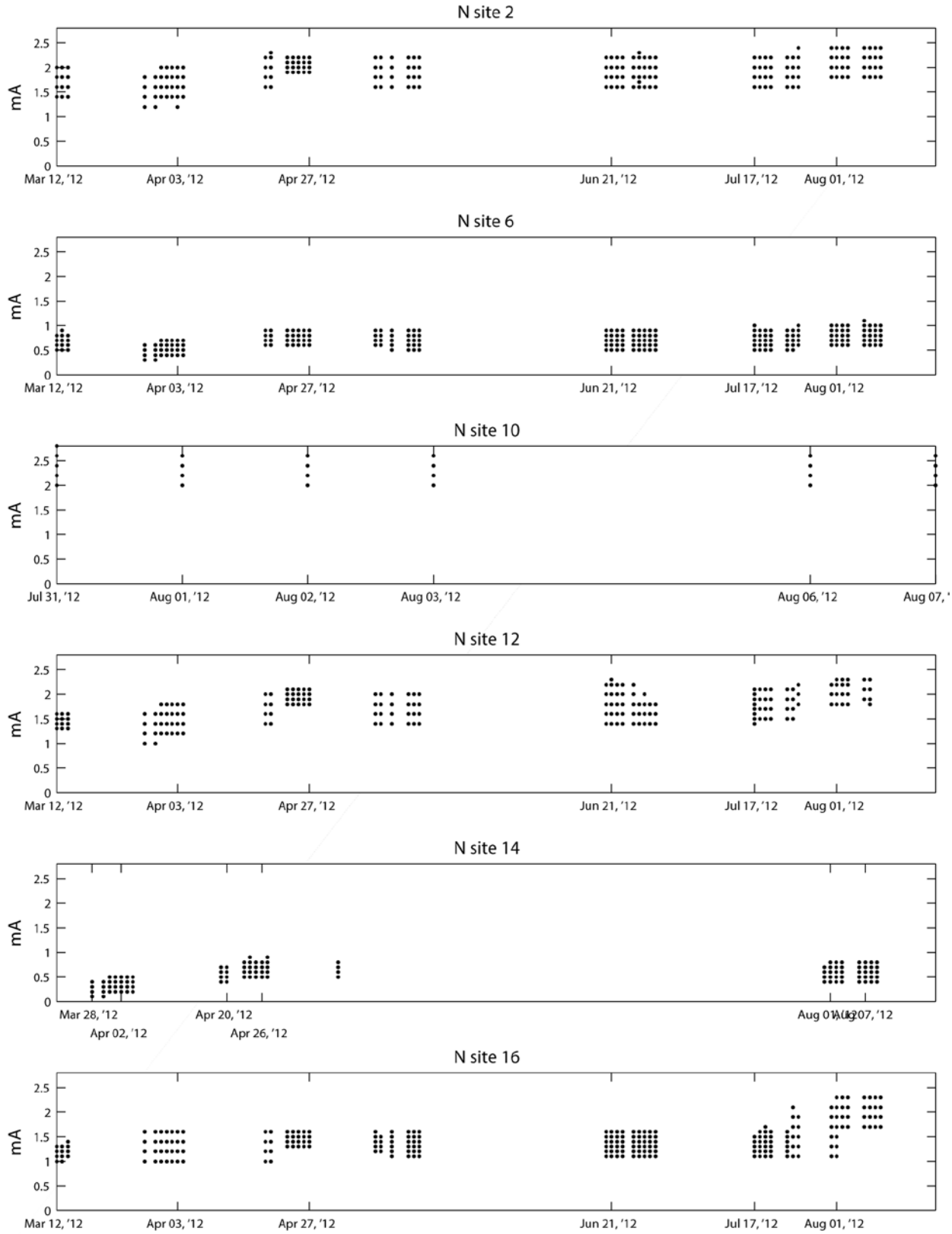

Figure 2.6. Stimulation intensity during torque mapping epochs for each epidural electrode site. Dots indicate a current range from subthreshold to suprathreshold. Thresholds increased considerably over the course of five months.

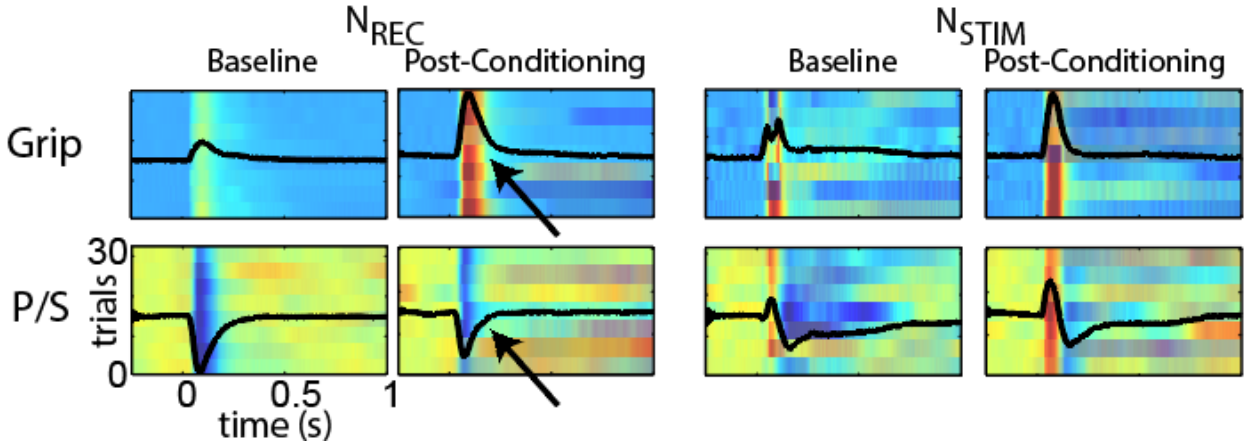

Figure 2.8 Evidence of targeted changes in motor maps after crossed myo-cortical feedback. After conditioning, twitches evoked from N_{rec} included more grip and less supination, which reflect activity at N_{stim}. Direction of torques evoked from N_{stim} are unchanged, but there is a small change in amplitude.

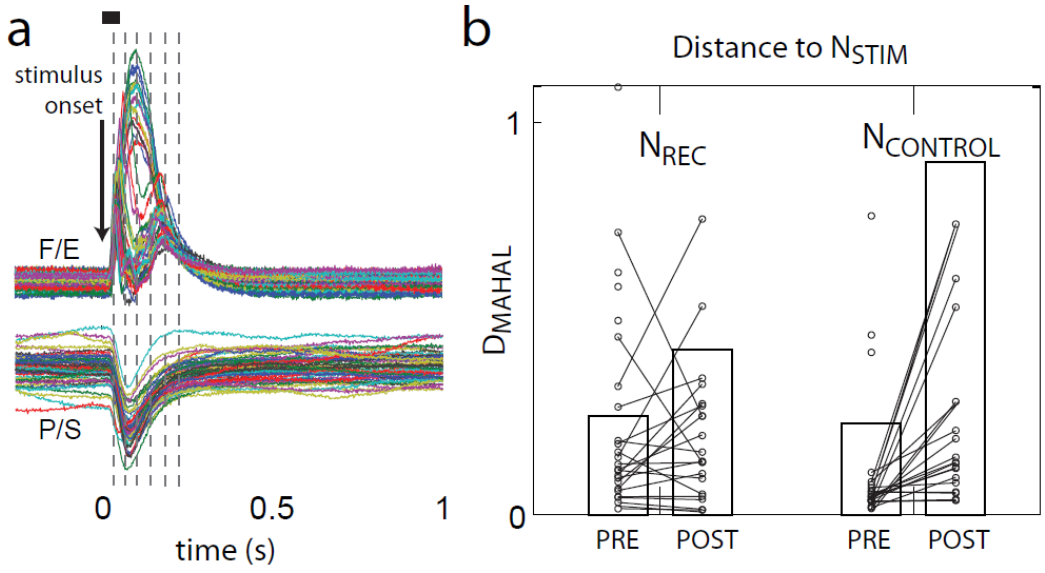

Figure 2.7 Quantifying similarity between motor maps. **a.** We used the Mahalonobis distance to measure the difference between motor maps with respect to torque direction and temporal profile. Each torque signal (F/E, R/U, P/S, G) was sampled at six timepoints during the response period (dashed vertical lines) following mapping CS (black bar above). In this example, it is clear that the shape of flexion/extension (F/E) torques are variable. **b.** Results across all experiments. We found that motor maps drifted farther away from N_{stim} in all cases, although N_{rec} remained more similar to N_{stim} than other electrode sites (N_{contol}).

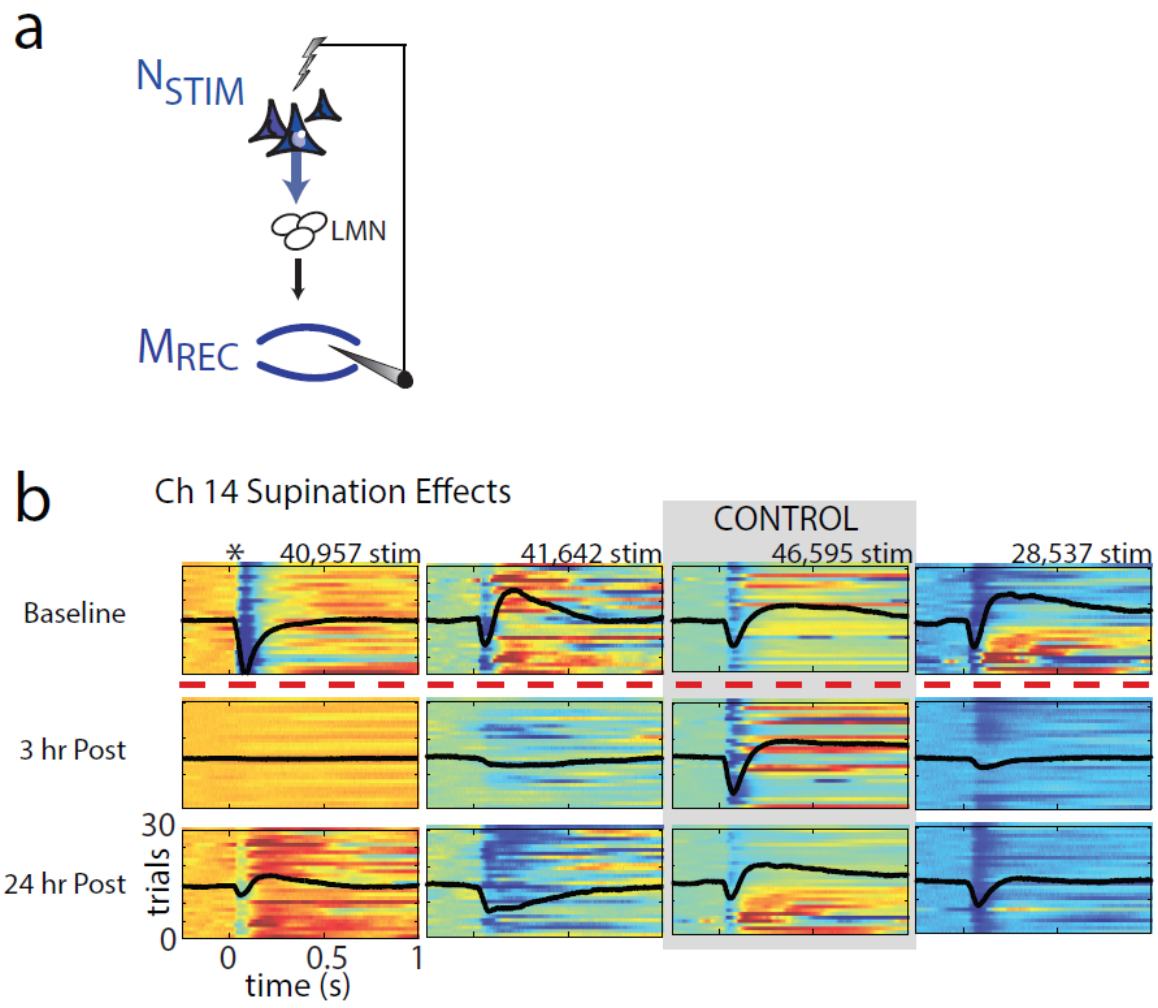

Figure 2.9 Direct myo-cortical feedback conditioning. **a.** Cartoon of experimental paradigm. **b.** Isometric torque effects (supination) before and after four conditioning experiments ordered chronologically. During three experiments, EMG from the supinator muscle was used to trigger stimulation of a cortical site known to evoke supinator activity (Nstim=Nrec). The supination effects are gone 3 hours after conditioning, and have partially recovered 24 hours later. Sham stimulation (gray box) has no effect. Supination effects on other electrodes were enhanced (**Figure 2.10**).

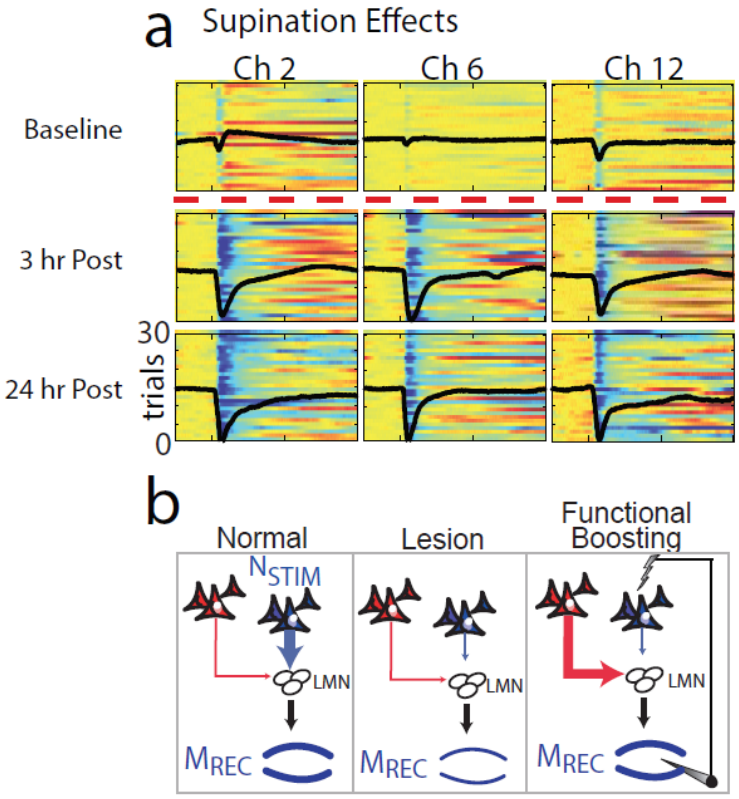

Figure 2.10 Increased responses from unconditioned cortical sites during direct myo-cortical feedback. **a.** Three unconditioned cortical sites from experiment 1 (*) shown in **Figure 2.9**. Each site evoked supinating twitches before conditioning, but, unlike Nstim, these effects intensified after conditioning, and persisted for over 24 hours. **b.** Cartoon depicting a potential clinical application of this effect, which we call “functional boosting”.

Chapter 3. CORTICAL STIMULATION PAIRED WITH VOLITIONAL MOVEMENT PRODUCES LASTING INTRA- AND INTER-HEMISPHERIC EFFECTS

Electrical cortical stimulation (CS) was delivered to primary motor cortex (M1) of one hemisphere during a simple reaction time (RT) task requiring monkeys to perform unimanual movements with either hand. Stimulation was brief and synchronized with phases of the response period corresponding to movement preparation, execution, and post-movement. In line with previous reports, responses were faster when stimulation was delivered before contralateral and ipsilateral movements. Interestingly, CS delivered after contralateral movements slowed subsequent RT for contralateral responses but sped up RT for ipsilateral responses. CS also produced specific changes in beta oscillation dynamics during the task that reflected the timing of stimulation. These experiments provide evidence that interhemispheric signaling and the post-movement beta rebound plays a role in lateralized bimanual coordination, and that CS can modify these pathways to produce a gain of function.

BACKGROUND

In humans, activity dependent stimulation of primary motor cortex (M1) by transcranial magnetic stimulation (TMS) can modulate, and even decrease, onset latencies in reaction time (RT) tasks if delivered early in the reaction period[110–112]. RT is shortened if cortical stimulation (CS) is delivered to the active part of cortex contralateral to movement ($M1_{contra}$) during the preparatory response phase, and is increased if CS is delivered right before the movement is about to be initiated. There is also evidence that stimulation to the ipsilateral cortex ($M1_{ipsi}$) shortens RT[110]. The precise neurophysiological mechanism underlying this effect is not known, but there is reason to believe that transcallosal inhibition may play a role.

Effects of brief stimulation to M1 ipsilateral to movement are, for the most part, inhibitory. This was demonstrated in the evoked activity of the opposite M1[113], and in evoked and volitional electromyographic (EMG) activity[114]. For instance, the motor evoked potential from one hemisphere can be diminished by first delivering conditioning pulses to the opposite M1 (interhemispheric inhibition, IHI), an effect which is sensitive to conditioning stimulus timing and intensity. Alternatively, volitional EMG activity during tonic contraction is briefly inhibited by single pulses delivered to the ipsilateral M1 (ipsilateral silent period, ISP). Finally, direct recording from neurons in target regions of M1 revealed that simulation of callosal fibers or motor cortex produces a predominantly inhibitory response about small area of excitation. Although IHI and ISP are well documented in the MEP, it is unclear whether these interactions play a role in natural movements.

We can gather hints about the neural dynamics underlying movement planning and execution by quantifying features of the local field potential (LFP). Beta oscillations, which are especially prevalent in sensorimotor cortex, are predictably modulated during rest (sustained oscillations),

action initiation (transient decrease, or “event desynchronization”), tonic contraction (sustained oscillations), and end of movement (post movement beta rebound, PMBR). The neural processing that these phasic bouts of beta represent remains under debate. Perturbations induced by CS may shed light on the functional role of these oscillations as they are modulated throughout coordination of bimanual movement.

The purpose of this study was to investigate the behavioral and neural impact of perturbations to neural processing at various phases of movement planning and execution during a bimanual reaction time (RT) task. We trained three monkeys to respond to a cue to the left or right hand with a quick, unilateral hand extension. Suprathreshold cortical stimulation (CS) was repeatedly delivered to the hand area of one M1 at a fixed period relative to anticipated movement time, and we recorded acceleration from both hands and local field potential (LFP) from multiple sites bilaterally over M1.

SPECIFIC METHODS

Subjects and behavioral task

Experiments were conducted with three male Macaca nemestrina monkeys (I, K and U). During each experiment, monkeys were seated in a primate chair and accelerometers were affixed to the dorsum of each hand. Visual cues on the computer monitor prompted quick, unilateral hand extensions to drive a cursor into a target box for a smoothie reward. Trials were randomly selected to be left or right, and a trial was successful if the proper cursor entered the target box within a timeout period (600ms), while the other cursor stayed in the start box (**Figure 3.1A**).

Behavioral/neural recordings and data processing

Behavioral data, including cursor position, target presentation time, and raw accelerometer signal was recorded at 1 kHz. The behavioral task and all offline analyses were conducted using custom scripts (MATLAB R2017a). During the behavioral task, cursor height was driven by the rectified, smoothed (50ms boxcar) accelerometer signal generated by each hand. RT was measured offline using the accelerometer signal processed in three steps: 1) band-pass filtered (10-150 Hz) 2) rectified, and 3) low pass filtered (5 Hz). We calculated a movement threshold as 1/6 the peak of the median response over the last 600ms of correct trials, and RT was defined as the time between the target presentation and the onset of the processed accelerometer response (the time of threshold crossing, **Figure 3.1c**).

Neural local field potential (LFP) data was recorded at 9600Hz for monkey U, 2400Hz for monkey I, and 9600Hz for monkey K (g.USBamp, Guger Technologies) and stored to disk. The beta band was determined by obtaining a range of 6Hz around the peak in power spectral density within the beta range (15-25Hz) (Monkey U: 19-25Hz, Monkey I: 15-21Hz, Monkey K:17-23Hz), and the beta filtered signal was extracted using a third order bandpass Butterworth filter. Instantaneous beta power was calculated offline as the absolute value of the Hilbert transform of the beta filtered signal.

Surgery and implants

Both monkeys underwent implantation of a custom electrode array over left and right motor cortex (I: 8 epidural electrodes bilaterally, U: 7 intracortical electrodes bilaterally, K: 2 intracortical electrodes bilaterally; **Figure 3.2**).

Experiment timeline and conditioning stimulation

The experiment timeline is depicted in **Figure 3.1b**. At the beginning of each experiment, we collected about 500 trials to characterize RT in the absence of CS ("Pre" epoch). We discarded the first 50 trials to avoid warm-up effects as the monkey settled into the task. After the Pre epoch, CS was initiated and continued for about 1000 trials ("Cond" epoch). Suprathreshold CS (negative leading, 10 pulses, 0.2ms width, 333Hz) was delivered between electrodes at sites that elicited a twitch registered by the contralateral accelerometer and current amplitude was determined daily as the lowest suprathreshold intensity. For each experiment, stimulation was delivered to either the movement generating hemisphere (*contralateral* CS), or to the non-movement generating hemisphere (*ipsilateral* CS). Timing of CS was determined randomly before each experiment and was fixed relative to the Go signal, and stimuli were labeled according to the response phase during which they were delivered (preparatory phase, "prep": -100-200ms, CS_{prep}; during the movement, "move": 200-500ms, CS_{move}; and post movement "relax": 500-800ms, CS_{relax}). The timing of CS_{prep}, CS_{move} and CS_{relax} relative to RT is shown in **Figure 3.8**.

RESULTS

We recorded a total of 140 sessions from three monkeys (I: 59; U: 50; K: 31; see Table 3.1 for N by experiment type). CS thresholds for evoking motor responses were higher for epidural stimulation than for intracortical stimulation. Table 3.2 shows the motor thresholds used for electrodes in all monkeys.

Figure 3.3 shows that our movement-detection algorithm successfully detected RT in single trials. Variability in the trial-by-trial response is evident in the accelerometer snippets aligned with the

Go signal (**Figure 3.3a**, top: raw acceleration, bottom: processed acceleration). The onset of the earliest responses is evident around 200ms from Go signal. Aligning the accelerometer snippets by RT (**Figure 3.3b**) demonstrates that our algorithm correctly identified the response times. Monkeys performed the task regularly (~250ms RT, **Figure 3.4**), which allowed us to approximate the timing of CS relative to movement. Over the course of experiments, we observed statistically significant changes in RT of ~10ms (slower over time: monkey I and K; faster over time: monkey U). Therefore, statistical tests compare presented data with distributions of RT during control experiments without stimulation (Wilcoxon rank-sum test).

Monkey	Ipsi CS	Contra CS	Ipsi CS 50%	Contra CS 50%	No stim	Asynch
I	2	41	0	0	10	6 (periodic)
K	14	14	0	0	3	0
U	0	5	19	17	3	3 (random)

Table 3.1. Number of experiments by type. We delivered 50% stimulation during some experiments with Monkey U so that we could analyze the LFP without stimulation artifact.

CS delivered to the movement generating hemisphere (Contralateral CS)

We conducted *Contralateral CS* experiments in all three monkeys. **Figure 3.5a** depicts a diagram of the stimulation/response relationship during the task if CS was delivered to the left hemisphere. **Figure 3.5b** shows effects of CS on RT in the following trial. In line with previous reports[115], we found that early stimulation (CS_{prep}) decreased RT_{contra} in all monkeys (†, **Figure 3.5b**). Surprisingly, stimulation during the relax phase (CS_{relax}, after movements had concluded) had pronounced effects in subsequent movements associated with both hemispheres. CS_{relax} slowed subsequent contralateral trials, but sped up ipsilateral trials (‡, **Figure 3.5b**).

Some changes in RT persisted during unstimulated trials, and during the Post epoch

Previous studies suggested that CS paired with quick, unilateral movements can induce lasting directed plasticity[112,116]. Therefore, we analyzed RT of trials that occurred long after stimulation to determine whether effects of CS were limited to trials that were close in time to CS. During the CS_{relax} *Stim* epoch, we focused on responses that arrived at least two trials after CS to determine whether bilateral changes in RT persisted. There were no such trials for RT_{contra} during CS_{prep} and CS_{move} because these trials were always stimulated before the response. **Figure 3.6** shows that effects of CS_{relax} were just as evident in trials that arrived 2, 3, and even 4 trials after the most recent stimulation. Experiments with Monkey U focused on CS_{prep} and CS_{move}, and therefore did not have sufficient data for this analysis.

We also analyzed whether changes in RT persisted after stimulation was turned off. **Figure 3.7a** shows ΔRT for contra- and ipsilateral trials during the Post epoch for CS_{relax} experiments. We found that increases in RT_{cont} did not strongly persist during the Post epoch, but RT_{ipsi} remained faster (white boxes "Post-Pre", **Figure 3.7a**). We found no systematic changes in left or right handed trials over time in the absence of stimulation (**Figure 3.7b**).

Neural dynamics during bilateral movements

Beta oscillations fluctuate predictably during movements, but the significance of its various phases (such as the post-movement beta rebound) is under debate[117]. We analyzed the LFP from M1 during ipsilateral and contralateral movements to determine how the timing of CS coincided with neural dynamics. We identified well-known features in the LFP during contralateral movements, including the readiness potential (RP), a transient increase in gamma power

immediately preceding movement, and a slower, larger, decrease in beta power throughout the movement (**Figure 3.8**). There was also a potential associated with ipsilateral movements – compared with contralateral RP, the ipsilateral feature was opposite in polarity and occurred during and after movements, suggestive of sensory feedback (avLFP, dashed line; **Figure 3.8**). There was also a pronounced dip in beta power before and during ipsilateral movements (β, **Figure 3.8**) that was similar to that observed during contralateral trials. On the other hand, gamma power was not as modulated during ipsilateral trials (γ, **Figure 3.8**).

The three stimulation periods corresponded with the baseline beta amplitude during rest (*prepare*), beta suppression during the movement (*move*), and the post-movement beta rebound (PMBR, *relax*)[117]. With respect to gamma oscillations, the *move* window most obviously correlated with the transient increase before and during movement.

Changes in LFP reflected the timing of CS

We tested for changes in the LFP by measuring average gamma and beta power using the same three time periods used to classify CS: *prepare, move,* and *relax*. Since we found that effects of CS on RT persisted during unstimulated trials, we delivered stimulation to a subset of trials (50%

Monkey	**Channel**	**MT (μA)**	**Type**
I	ML1B/gnd	2000	Epidural
I	ML1C/gnd	2000	Epidural
I	ML3B/ML3C	4600	Epidural
I	MR1B/gnd	2000	Epidural
I	MR2C/gnd	750	Epidural
I	MR3B/gnd	1000	Epidural
I	MR3B/MR3C	4250	Epidural
K	In1a/In1b	350	Intracortical
K	In4a/In4b	350	Intracortical
U	LMC 3/3.5	100	Intracortical
U	LMC 4/4.5	125	Intracortical

Table 3.2. CS intensity by electrode for all monkeys (MT: motor threshold)

probability) with Monkey U so that we could analyze the LFP without complications introduced by stimulation artifact. **Figure 3.9** shows how beta and gamma power changed following CS_{relax}. During contralateral trials (which were slower after CS_{relax}), there was a specific increase in both bands during the relax phase in the stimulated hemisphere which corresponded to the timing of CS during these experiments (**Figure 3.9** arrows 1 and 2). At the same time, beta power in the unstimulated hemisphere specifically dropped during this period (arrow 3). During ipsilateral trials (which were faster after CS_{relax}), the stimulated hemisphere did not show substantial changes, however, there was a drop in beta power during the *prepare* and *relax* periods in the unstimulated hemisphere (arrow 4).

We found evidence that CS induced changes in the LFP of the stimulated hemisphere that were specific to the timing of stimulation, even in the absence of overt behavioral differences. **Figure 3.10** shows how LFP was affected during $CS_{prepare}$, CS_{move} and CS_{relax} experiments. Although CS_{prep} and CS_{move} did not produce lasting changes in RT, there were specific increases in beta power during the response phase coinciding with stimulating timing (just as in CS_{relax}). **Figure 3.10a** shows the change in beta power for each experiment type. From this plot it is clear that the changes in beta power correspond to the trial type and timing of CS (indicated by arrows). Changes in gamma power were equally as specific, but effects were limited to CS_{move} and CS_{relax} experiments (**Figure 3.10b)**.

CS delivered to the non-movement generating hemisphere (Ipsilateral CS)

To further probe interhemispheric interactions, we also tested whether CS delivered to the non-movement generating hemisphere could generate changes in RT (*ipsilateral* CS). **Figure 3.11a** illustrates the pattern of stimulation/response in the example case of right hemispheric CS.

Experiments were conducted in monkeys K and U. We found that CS_{prep} significantly sped up RT for trials ipsilateral to the stimulated hemisphere, whereas CS_{relax} slowed RT in both hands (**Figure 3.11b).**

We calculated changes in the LFP in the same manner as for *contralateral* CS experiments (Monkey U, 50% stimulation). Decreased RT during CS_{prep} coincided with a drop in pre-movement beta amplitude (**Figure 3.11c**) in the stimulated hemisphere. Similar to effects during *contralateral* CS, changes in LFP were limited to the task period corresponding to CS delivery. It should be noted, however, that the direction of change was opposite for ipsilateral CS (beta amplitude decreased).

Asynchronous stimulation only affected stimulated trials

We performed control experiments to test whether it was necessary that CS was delivered synchronous with movements. **Figure 3.12a** shows results from contralateral and ipsilateral CS experiments where the timing of stimulation for each trial was randomly delivered between -100 and 800 ms relative to Go cue (Monkey U). Boxes show RT for responses immediately following stimulation for each condition. These controls showed a similar trend in contralateral RT as observed during consistently-timed CS experiments above (increasing RT with late CS), but the effects were far more variable, and were not significant. On the other hand, ipsilateral trials did not get faster under any conditions. Similarly, randomly timed ipsilateral CS did not produce significant changes in RT. **Figure 3.12b** shows that periodic stimulation delivered to one M1 during the course of the Stim epoch did not produce differential changes in ipsilateral or contralateral RT during the Stim or Post epochs. Notably, we did not observe a decrease in RT during any experiments with randomly timed stimulation. Overall, these results suggest that

changes in RT reflect plastic changes that required movement-related stimulation during the Stim epoch.

DISCUSSION

Summary of findings

The main finding of this study was that stimulation delivered to one motor cortex affected reaction time for movements associated with both hemispheres. The most surprising and robust effect resulted from stimulation consistently delivered after contralateral movements. In this case, subsequent contralateral responses were slower and ipsilateral movements were faster. Another striking effect was the decrease in RT when CS was delivered to M1 ipsilateral to movement during movement preparation. In both of these conditions, CS did not directly target cortical spatiotemporal activity most commonly associated with movement production (contralateral M1 before the response period). This suggests that coordination between homologous areas of M1 is ongoing through the bimanual reaction time task, even after movements.

Some changes in RT persisted long after stimulation was turned off. We found comparable changes in RT that occurred 4 trials after the previous stimulation (~10 seconds) as compared with those immediately following stimulation (~ 1 second). There were also changes in beta and gamma oscillations that persisted during unstimulated trials which were specific to the trial type and timing of CS (e.g. CS_{move} during *contralateral* experiments produced an increase in beta during the movement phase of contralateral trials alone). Not all changes in the LFP corresponded to differences in RT.

The most durable change was the decrease in ipsilateral reaction time following contralateral $CS_{relax,}$ which remained significant during the ~20 minute Post epoch. This finding highlights an interesting point: CS was more likely to decrease RT for ipsilateral movements than for contralateral movements. This effect may be mediated by the disruption of IHI originating from the stimulated M1.

Links with interhemispheric inhibition

Homologous hand areas of primary motor cortex (M1) in both hemispheres likely interact during the coordination of unimanual movements. A connection between the two has been repeatedly demonstrated using a paired-pulse transcranial magnetic stimulation (TMS) paradigm which revealed predominantly inhibitory effects of ipsilateral M1 activation by TMS on motor evoked potentials called IHI. When this protocol is paired with volitional movements, IHI of the movement generating hemisphere is highest just before movements, but is released at the time of movements. On the other hand, IHI of the non-movement generating hemisphere remains strong throughout movement preparation and action. This hypothetical interaction is illustrated in **Figure 3.13a**.

Besides IHI demonstrated by TMS, homotopic projections of the corpus callosum (CC) have been demonstrated by direct electrical cortical stimulation[113,118]. Orthodromic stimulation of callosal fibers results in uniform inhibition of neurons in M1, while single-pulse intracortical microstimulation of homologous areas in opposite cortex reveals wide areas of inhibitory projections surrounding a small excitatory area (indicated by PT cell firing in the contralateral hemisphere). Excitatory effects were not present during callosal stimulation, and higher intensity stimulation of the homologous excitatory area in contralateral M1 did not induce PT cell firing, so it is believed that transcallosal connections produce predominantly inhibitory effects between

homologous regions in both M1 (and that these effects are increasingly recruited as current spread increases with stimulation type or location, such as at the CC). Our stimulation protocols most likely result in a predominantly inhibitory response in the contralateral cortex similar to that observed during high intensity stimulation because we used stimulus trains (10 pulses over 30ms) that are known to recruit more neurons through temporal summation[119].

It seems that existing hand motor representations in one hemisphere imply corresponding inhibitory projections to the other hemisphere. It is known that IHI varies with handedness[120] and is imbalanced in stroke patients[121,122]; in both cases, inhibition from the dominant (or uninjured) hemisphere to the nondominant hemisphere is greater. Also, patients with defects of the corpus collosum suffer from pathological mirror movements[123]. Thus, IHI probably plays an important role during strictly unilateral movements such as those in our experiment.

Although CS probably activated inhibitory projections to the unstimulated hemisphere, decreases in RT were more common in trials ipsilateral to CS. One possible interpretation for this effect is that CS interrupted natural, ongoing interhemispheric inhibition, thereby disinhibiting the unstimulated hemisphere on average. CS is disruptive, not facilitatory, of natural activity[36], so it follows that delivering stimulation to the movement generating cortex is not likely to produce performance gains. In fact, previously studies found that only subthreshold stimuli delivered before contralateral movements would decrease RT – suprathreshold currents produced delays.

Our results, however, suggest that early suprathreshold contralateral stimulation does decrease reaction times. This effect is difficult to reconcile with the related finding that early *ipsilateral* stimulation also decreased reaction times (which has also been demonstrated in humans[115]). One possibility is that monkeys learned to recognize CS and the correlated trial type, and were able to use this information to respond more quickly than to visual cues alone. This is a confounding

issue with human TMS studies as well, because it was shown the RT in response to TMS was faster than all other sensory cues[115]. It must be stressed, however, that this trivial interpretation for effects of CS_{prep} does not explain the modulation of RT by CS_{relax}, in which the stimulation carries no information about the following trial.

Perturbations to neural processing

The role of phasic beta oscillations during movement is under debate[124]. Opposing theories generally label high beta as either an "idling" rhythm to sustain existing motor states (such as non-movement or tonic contraction), or as a marker of top-down control during heightening visuomotor processing of afferent feedback[125,126]. Periods of beta depression are often described as an 'activation' of motor cortex, but this is inconsistent with bilateral depression of M1 beta during unilateral movements. To complicate matters, bouts of high beta after movements (PMBR) might represent different processes than high beta before movements[127].

Our data does not support the theory that beta oscillations reflect a balance between two simple neural states (i.e. idling versus active). We found that perturbing the network during states of high beta had different effects depending upon the phase of movement: CS during post-movement high beta slowed subsequent responses, whereas CS delivered during pre-movement beta sped them up. Thus, it seems that high beta does not reflect a singular mode of activity, but rather that the PMBR periods reflects a specific process preparing the motor system for subsequent movement. Other studies also provide reason to believe this may be the case: in one case, PMBR was prominent in the hand motor area after sensory stimulation of the lip. Our finding that perturbation of the PMBR negatively impacts contralateral movements and disinhibits ipsilateral movements suggests the PMBR is indeed important for preparing future movements, including the orchestration of IHI as mentioned above.

A recent recently demonstrated that monkeys were faster to perform reaches when they were instructed to decrease beta power before the move cue[128]. Interestingly, we noted a decrease in beta before movements during conditions where RT dropped. In one instance, beta of the movement generating hemisphere decreased (contralateral CS_{relax}), whereas in another, beta of the nonmovement generating hemisphere decreased (ipsilateral CS_{prep}). This raises the possibility that pre-movement beta reflects active IHI at the expense of a shift away from movement onset state.

Plastic changes and insights from LFP

TMS-M1 paradigms demonstrated potential for inducing plasticity by movement-related stimulation[112,116], and effects lasted from 20 minutes to over an hour. In one study, TMS delivered 50ms before RT of the target muscle increased the size of the MEP, and decreased RT, for 20 minutes[112]. In another study, TMS delivered after activity of the antagonist muscle (relative to the TMS target muscle) produced shifts in the TMS-evoked twitch direction that lasted over an hour[116]. This study also included ipsilateral and asynchronous conditions, and found that asynchronous stimulation was not effective at inducing plasticity. Interestingly, synchronous, ipsilateral TMS blocked learning effects from training alone.

Results from our experiments support the finding that movement-related CS can induce plasticity. Similar to Butefisch et al[116], post-movement stimulation was effective at producing changes that long outlasted CS. Beyond changes in RT, we observed differences in the oscillatory fluctuations of the LFP at periods which corresponded to the timing of previous CS. This raises the exciting possibility that movement-related CS can induce plasticity in specific circuits that are active during different phases of unilateral movement. These changes were evident in the absence of behavioral effects, and were sometimes different when the behavioral

result was the same (e.g. decreased RT during decreases in either ipsilateral or contralateral beta, depending on CS type). Thus, the LFP can help identify different neural mechanisms underlying similar behavioral effects.

Conclusions

We measured the neural and behavioral impact of CS delivered to one hemisphere, timed relative to ipsilateral or contralateral movements. The most novel and robust finding was that post-movement stimulation repetitively delivered to the movement generating hemisphere produced subsequent changes in RT of both hands. Following CS, responses of the unstimulated hemisphere were faster, and responses of the stimulated hemisphere were slower. This finding suggests that bimanual coordination involves ongoing interhemispheric communication that persists after movements are completed. It appears that CS interrupts important preparation for subsequent movements that occur during the post-movement phase, marked by beta rebound. Lasting decreases in ipsilateral reaction time suggest that symmetric inhibitory networks originating from the stimulated hemisphere were altered by CS. Post movement stimulation might therefore be useful in cases of malignant inter-hemispheric inhibition, such as stroke.

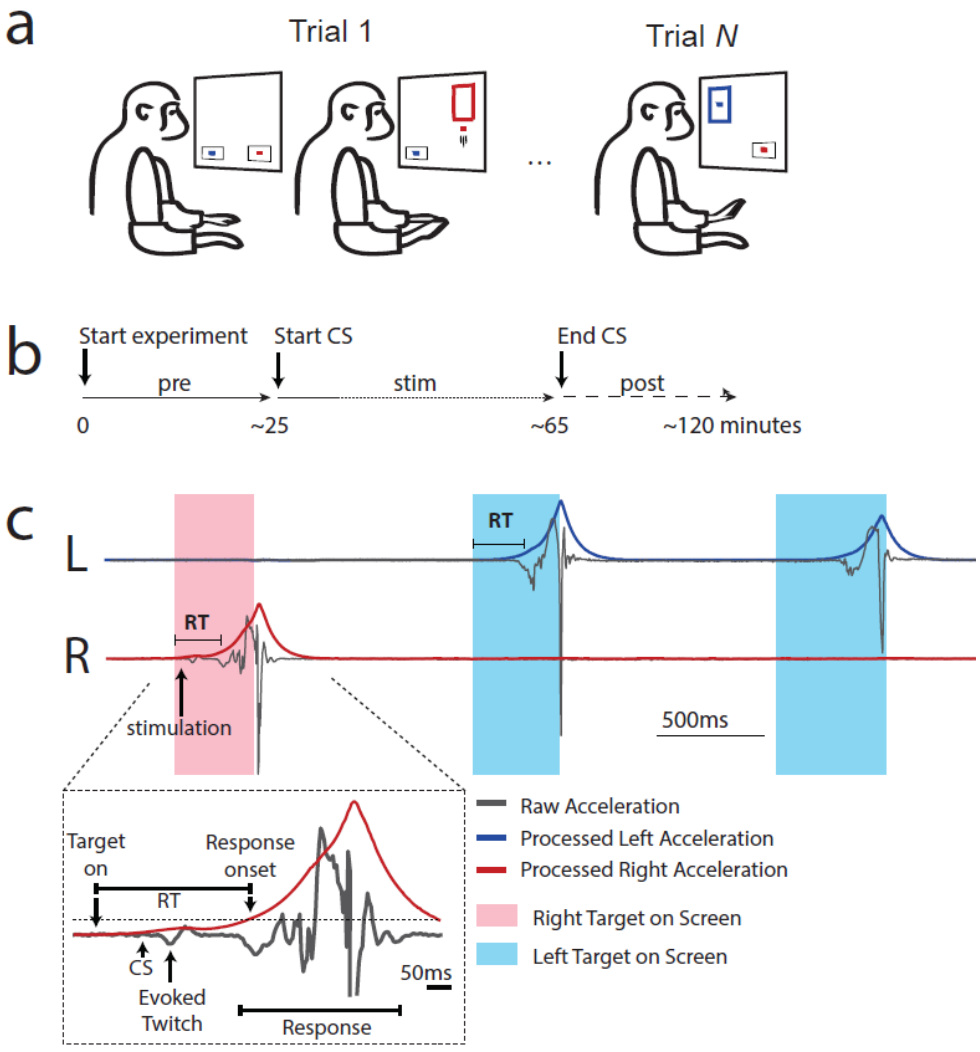

Figure 3.1 Behavior, experiment time-line, and reaction time estimation. **a.** Monkeys were cued to move a cursor into a target box by rapid wrist extension. Trials were randomly selected to be left or right. **b.** Experiment timeline. The task was performed continuously during the experiment. **c.** Three example trials. Colored bars indicate when the monkey was cued to move left (blue) or right (red). Responses were required to be unilateral. Inset: estimation of reaction time. Raw accelerometer signal (gray) is transformed into a processed signal (red) for RT estimation. There is an evoked twitch evident in the raw trace (experitment type: contralateral CS_{prep}, right M1 electrode).

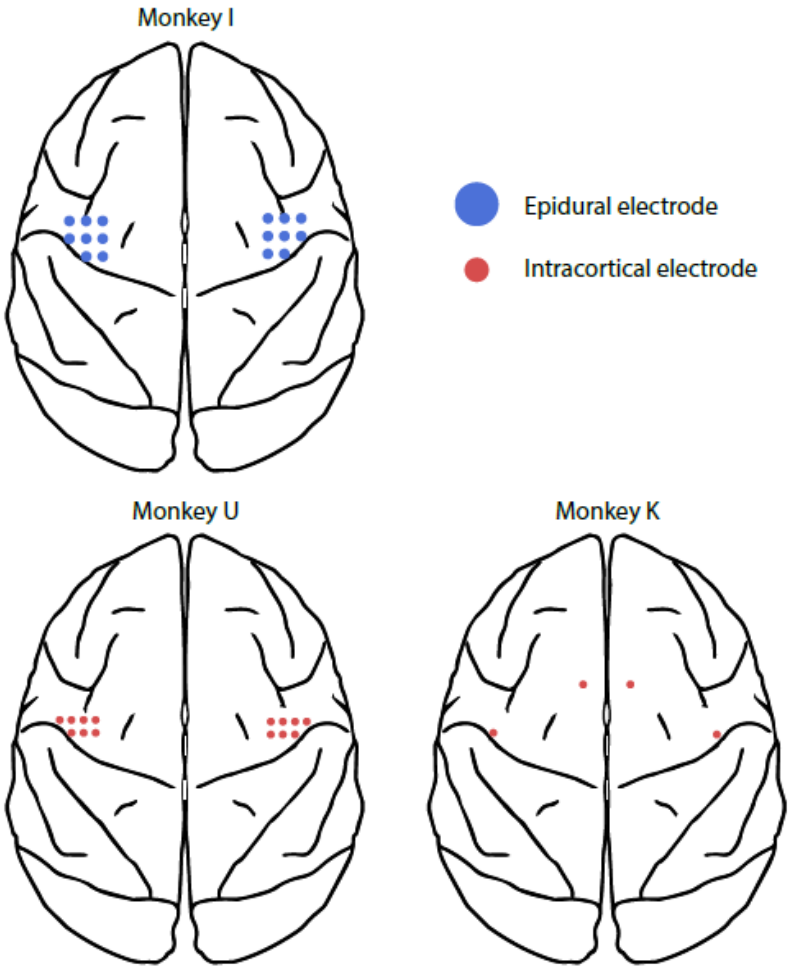

Figure 3.2 Implant diagrams Electrodes were implanted bilaterally over primary motor cortex using epidural (blue) or intracortical (orange) electrodes. Electrode locations reflect inferred positions determined by stereotactic coordinates (3mm spaced grids). Sites in monkey U were verified as pre/post central by sensory evoked potential.

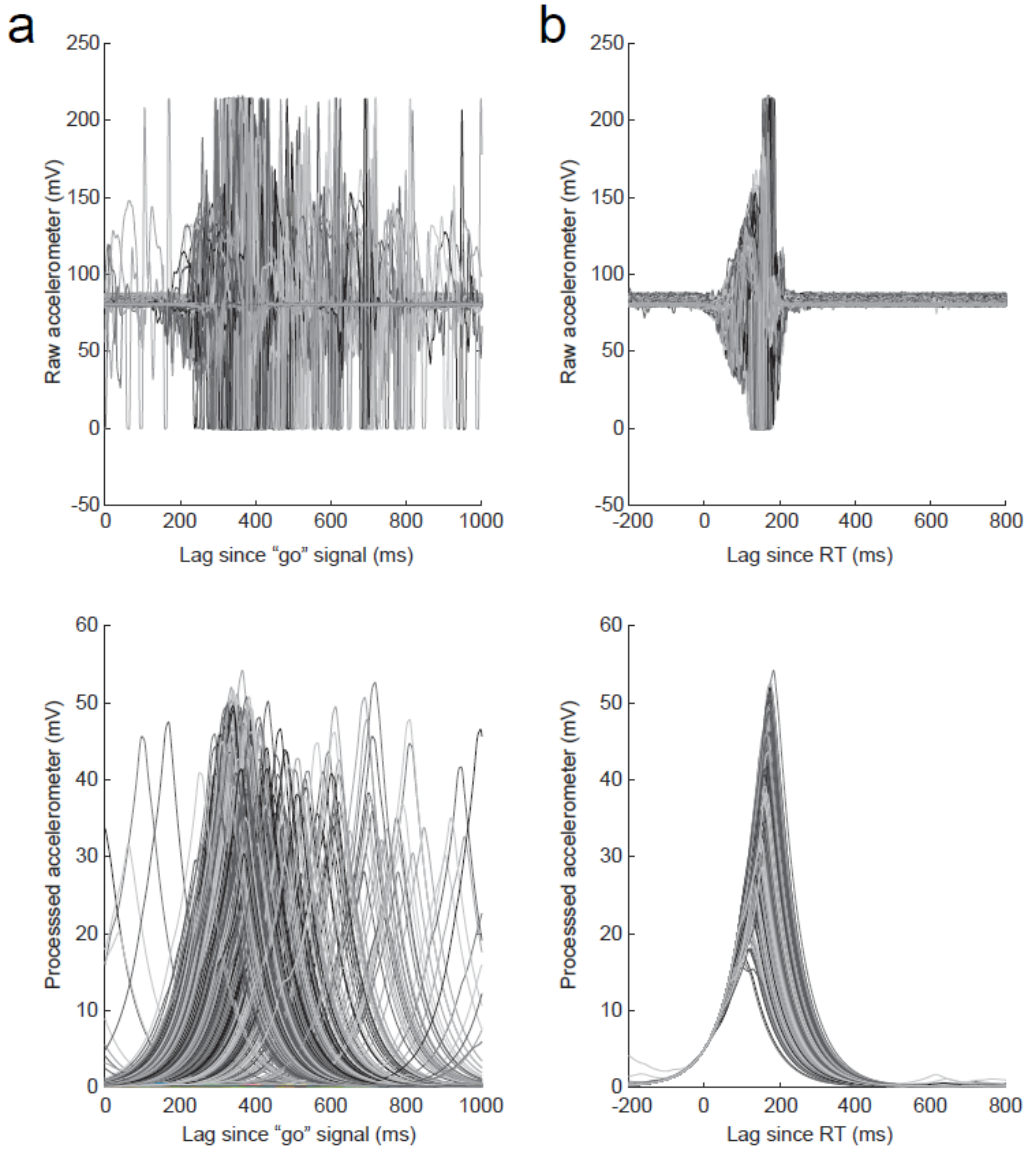

Figure 3.3 RT detection Top: raw accelerometer signals aligned by "Go" signal and by RT. Bottom: processed accelerometer signals aligned by "Go" signal and by RT.

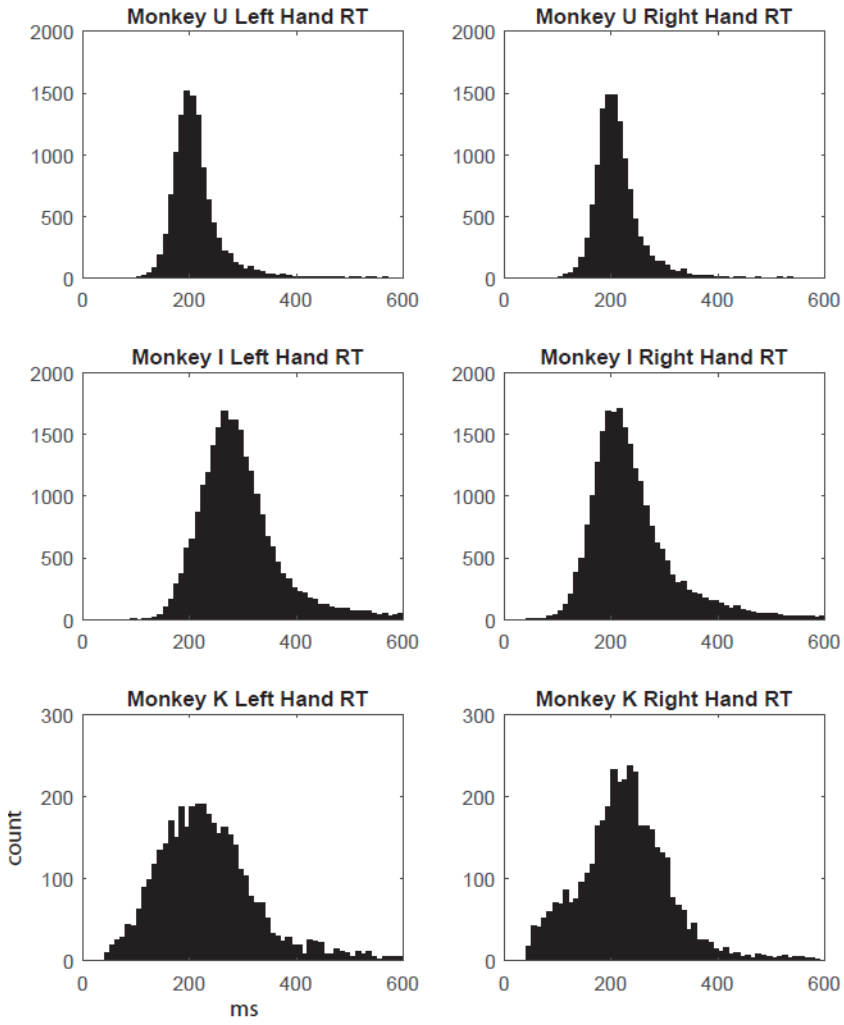

Figure 3.4 Distribution of RT for all monkeys mean ± ste, Monkey I, left: 277.1±29.2 ms, right: 223.4±26.9. Monkey U, left: 210.9±14 ms, right: 212±13.6; Monkey K, left: 219.3±53.2ms , right: 212.2±55.1ms

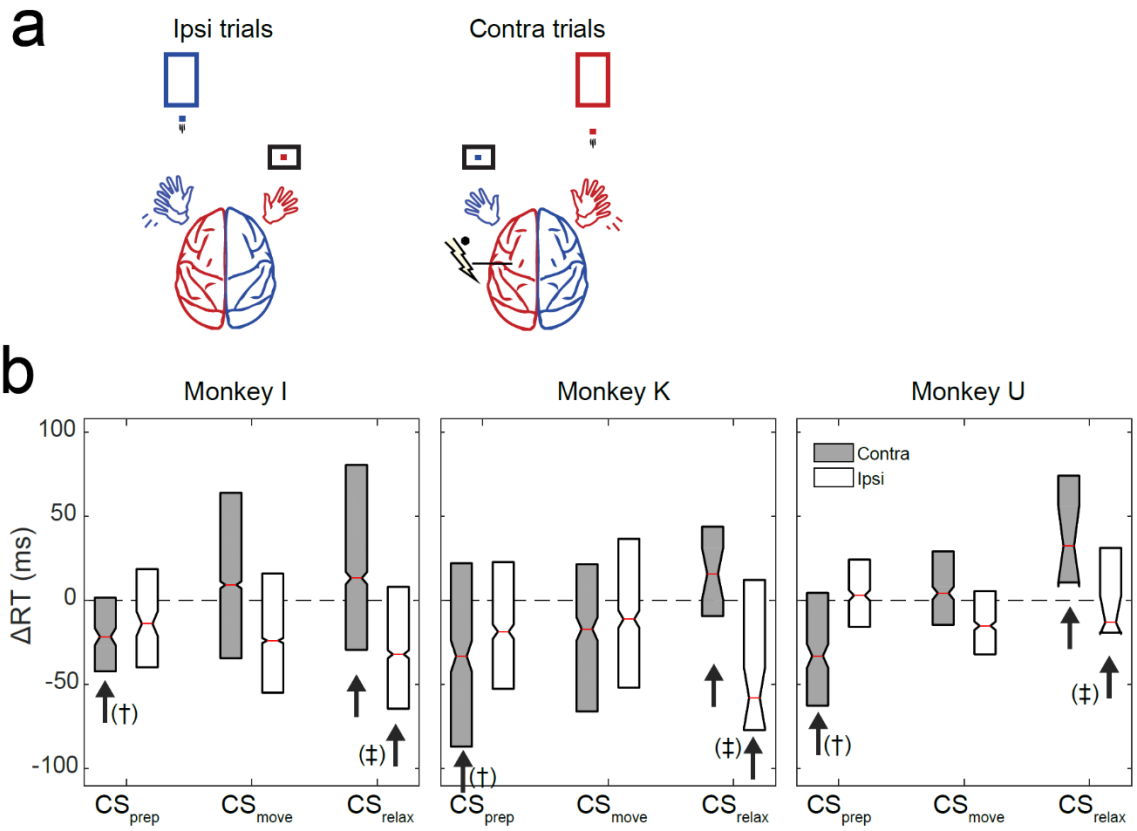

Figure 3.5 Effects of CS to the movement generating hemisphere (*contralateral* CS). **a.** Illustration of CS and task relationship for left hemispheric CS. **b.** RT for trials immediately following stimulated trials. CS_{prep} decreased RT for contralateral trials in all monkeys (†). CS_{relax} experiments produced bilateral effects: speeding up RT ipsilateral to CS and slowing down RT contralateral to CS (‡).

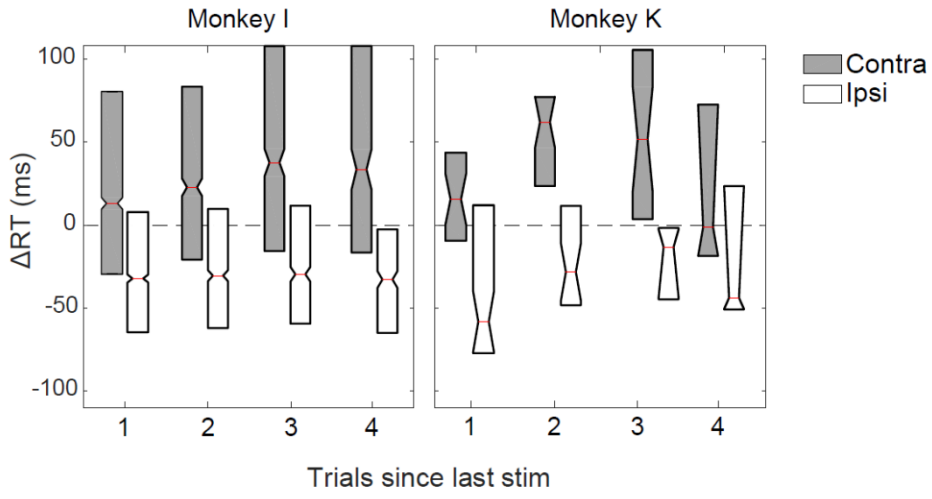

Figure 3.6 Persistent changes in RT during Stim epoch. Each box plot shows ΔRT for subsequent trials following stimulation during *contralateral* CS_{relax} experiments. Effects were obvious in trials arriving long after CS was delivered during experiments with consistently timed CS. Randomly timed CS did not produce effects beyond the immediately stimulated trial (Figure 3.12). Monkey U did not have sufficient data for this analysis.

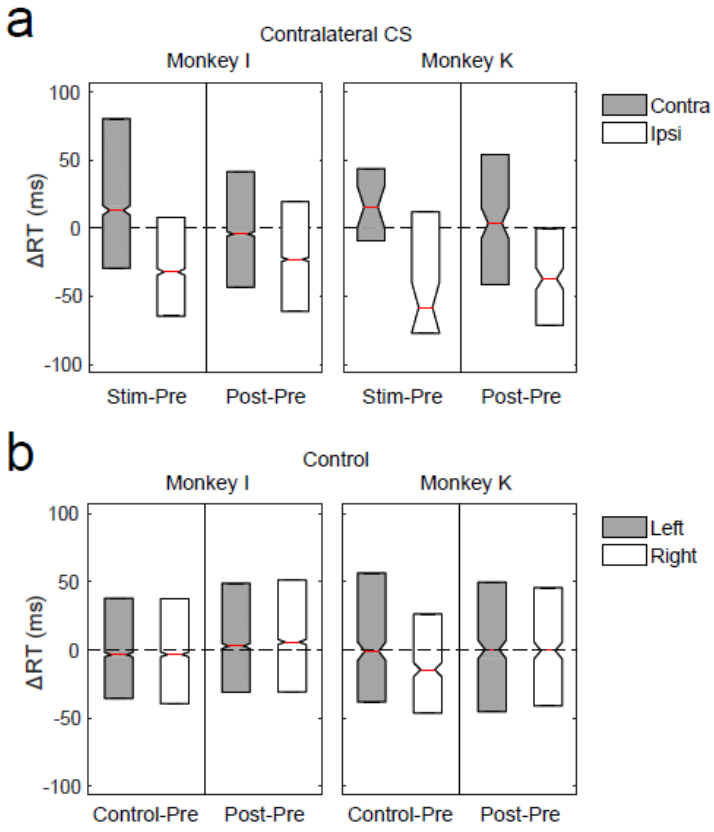

Figure 3.7 Persistent changes in RT during Post epoch. **a.** RT of trials ipsilateral to the stimulated hemisphere stayed faster during Post epoch of CS_{relax} experiments. Increases in in contralateral RT did not persist, however (not shown: decreases in contralateral RT following CS_{prep} did not persist during Post). Monkey U did not have sufficient data. **b.** Control experiments without stimulation did not result in substantial changes in RT.

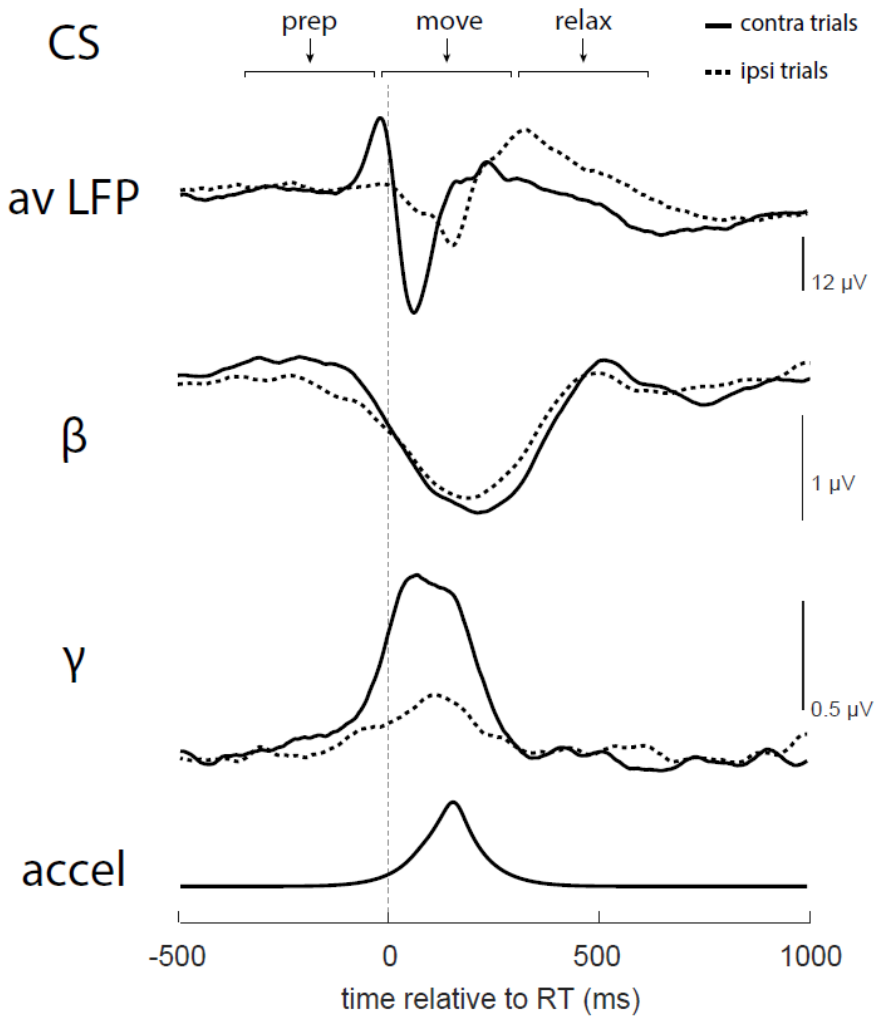

Figure 3.8 CS, LFP and wrist acceleration aligned to RT. Trial-averaged raw LFP, beta power (β), and gamma power (γ) relative to the processed accelerometer signal used for RT estimation (accel). Dashed lines depict the ipsilateral trial-triggered averages, and solid lines depict the contralateral trial triggered averages. During any experiment, CS was delivered with a fixed delay and we grouped experiments (prep, move, or relax) by their CS timing.

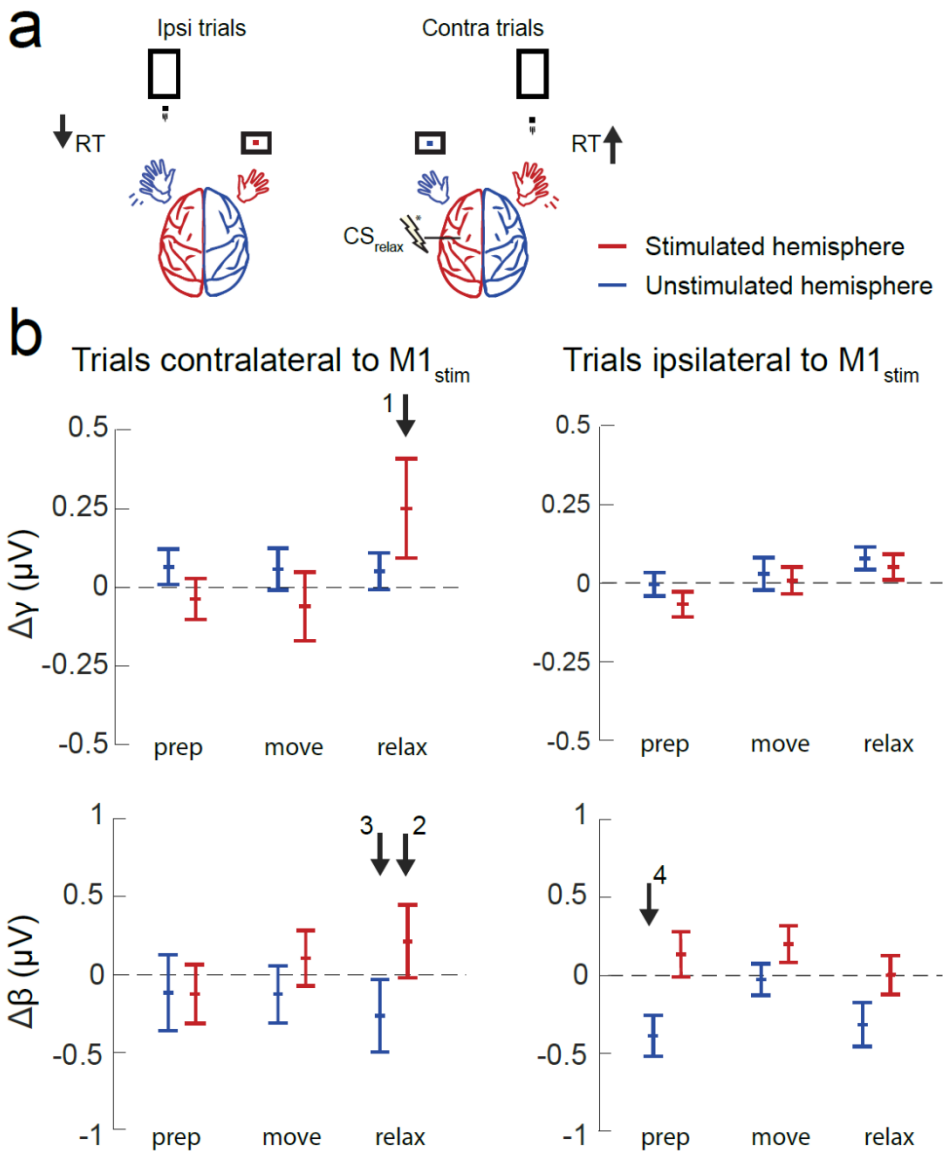

Figure 3.9 Changes in LFP during post-movement stimulation of the movement-generating hemisphere. **a.** Summary of RT changes following contralateral CS_{relax}. Consistent CS post-movement delivered to $M1_{move}$ produced a subsequent decrease in RT ipsilateral to CS, and an increase in RT contralateral to CS. **b.** Change in oscillatory power during prep, move, and relax response phases. Only unstimulated trials are shown to avoid stimulation artifact. There was a specific increase in gamma and beta power in the stimulated hemisphere during the same response phase when CS was delivered (arrows 1 and 2), and a decrease in beta of the unstimulated hemisphere (arrow 3). Beta power also decreased before movements generated by the unstimulated hemisphere (arrow 4).

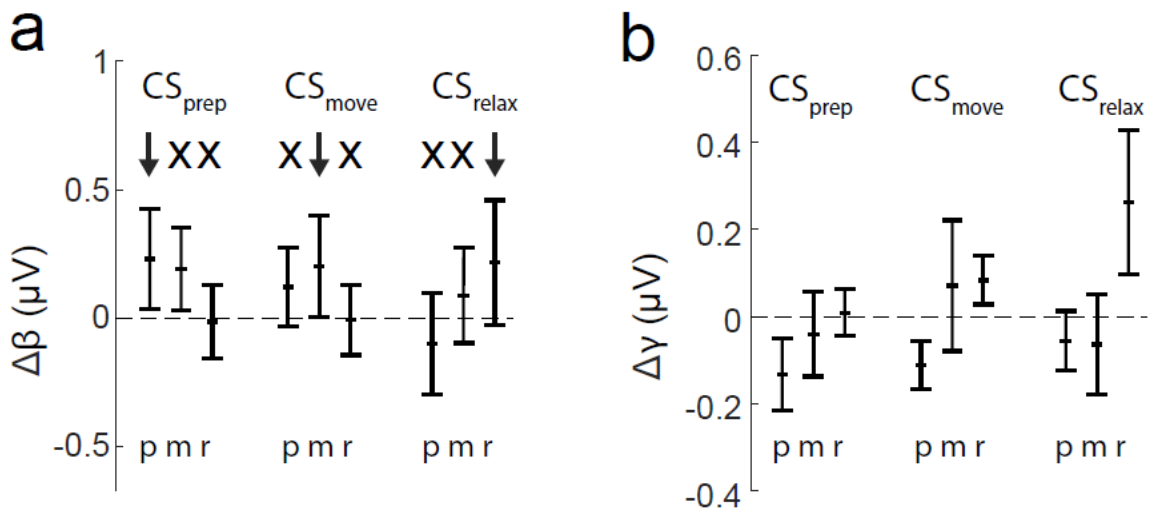

Figure 3.10 Persistent changes in $M1_{stim}$ LFP reflected stimulation timing. Bars shows median ± 95% conf. int. **a.** Average beta power during preparatory (p), movement (m), and relax (r) response phases during unstimulated trials. Increases in beta were most pronounced during the response phase corresponding to CS timing (prep, move, or relax; arrow indicated stimulated phase for each experiment type). **b.** Average gamma power as in (**a**). Unlike changes in beta power, only CS_{relax} experiments produced increased gamma power. Interestingly, this increase was specific to the relax phase. Stimulation during the prep phase specifically decreased gamma power in that phase.

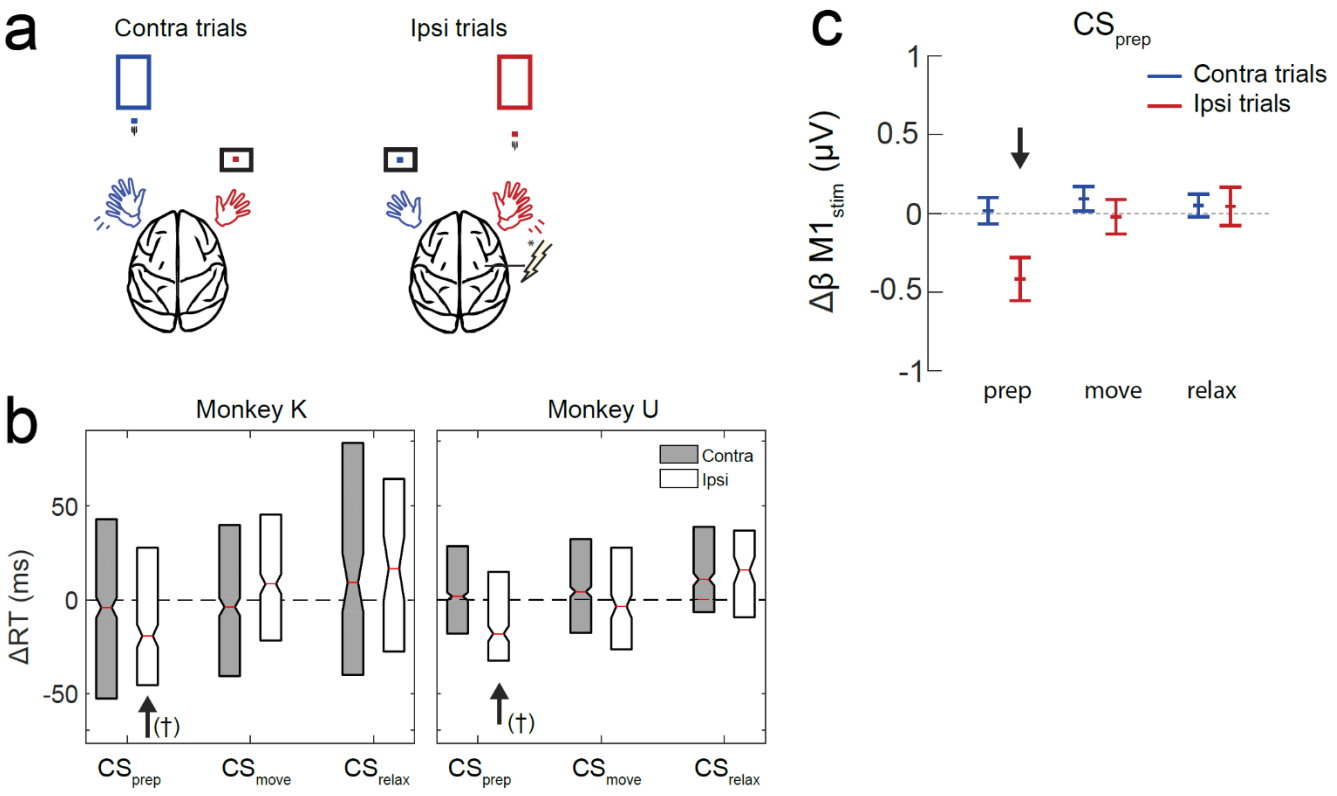

Figure 3.11 Effects of CS to the non-movement generating hemisphere (*ipsilateral* CS) **a.** Illustration of CS and task relationship for right hemispheric CS. **b.** RT for trials immediately following stimulated trials. CS_{prep} decreased RT for ipsilateral trials in both monkeys (†, $p<0.001$). CS_{relax} increased RT for ipsilateral trials and, to a lesser extent, contralateral trials. **C.** Faster responses associated with CS_{prep} coincided with a decrease in beta power in the stimulated hemisphere during the preparation phase (arrow).

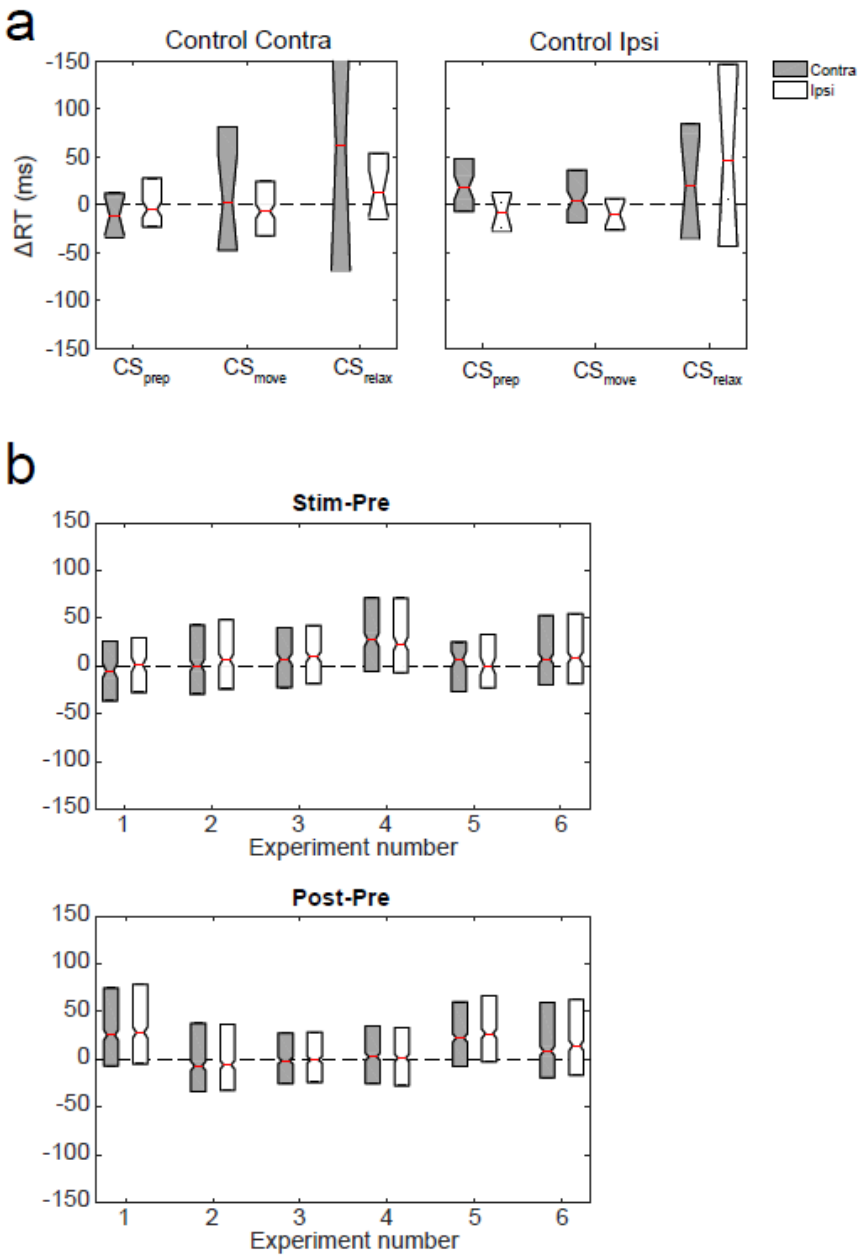

Figure 3.12 Inconsistently timed stimulation did not produce lasting changes. **a.** RT during randomly timed contralateral (left) or ipsilateral (right) CS with monkey U. Boxes show RT for responses occurring after single CS pulses that occurred during prep, move, or relax phases. Left: RT of contralateral trials shows a similar, but weaker, trend as during consistently timed CS experiments, but ipsilateral trials do not speed up with CS_{relax}. Right: There is no significant decrease in ipsilateral RT during CS_{prep}. **b.** Periodic stimulation delivered to one hemisphere did not produce differential effects in RT associated with both hands. Plots show six different experiments with Monkey I and corresponding change in RT (Stim vs. Pre, top; and Post vs. Pre, bottom).

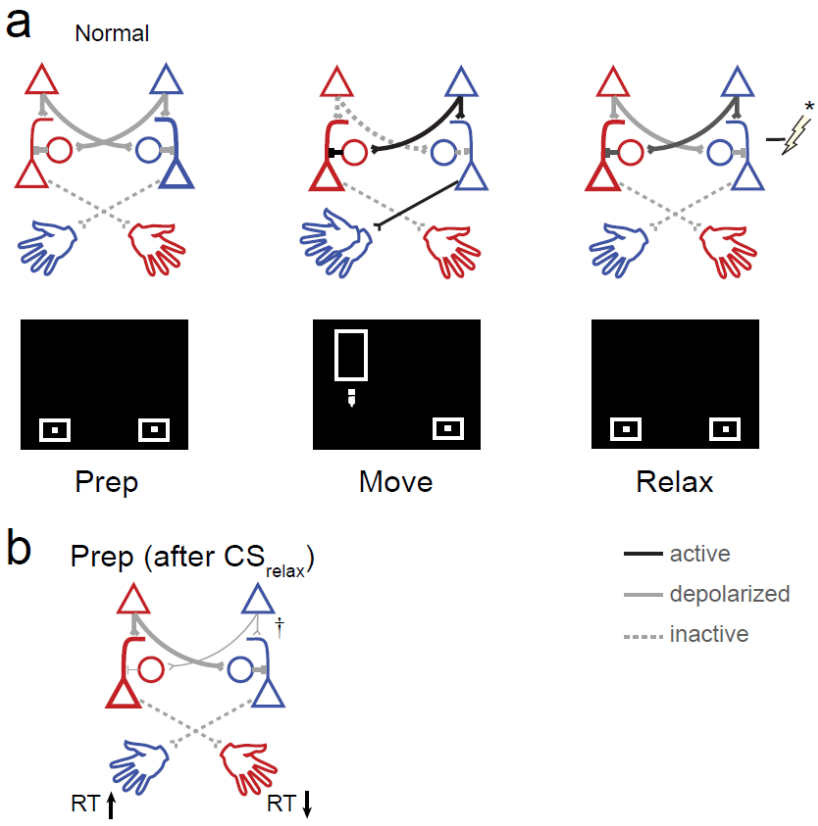

Figure 3.13 Potential mechanism of post-movement CS induced changes. **a.** Studies demonstrating interhemispheric inhibition (IHI) by TMS show that IHI from non-movement to movement generating hemisphere is released just before the onset of movement, while IHI in the other direction stays strong. Lightning bolt (*) indicates timing and location of post-movement contralateral stimulation (contra CS_{relax}). **b.** Proposed synaptic changes during CS_{relax}. The post-movement beta rebound is thought to reflect important preparatory processes for future trials (e.g. contralateral movements and inhibition of contralateral M1). CS delivered during this activity selectively impairs these networks (†, thinner connections), thereby disinhibiting the mirror movement and impairing the planned movement.

BIBLIOGRAPHY

1. Cramer, S. C. Repairing the human brain after stroke: I. Mechanisms of spontaneous recovery. *Ann Neurol* **63,** 272–287 (2008).
2. Cramer, S. C. Repairing the human brain after stroke. II. Restorative therapies. *Ann Neurol* **63,** 549–560 (2008).
3. Elsner, B., Kugler, J., Pohl, M. & Mehrholz, J. Transcranial direct current stimulation (tDCS) for improving function and activities of daily living in patients after stroke. *Cochrane Database Syst. Rev.* **2013,** Cd009645 (2013).
4. Hsu, W. Y., Cheng, C. H., Liao, K. K., Lee, I. H. & Lin, Y. Y. Effects of repetitive transcranial magnetic stimulation on motor functions in patients with stroke: A meta-analysis. *Stroke* **43,** 1849–1857 (2012).
5. Lindenberg, R., Renga, V., Zhu, L. L., Nair, D. & Schlaug, G. Bihemispheric brain stimulation facilitates motor recovery in chronic stroke patients. *Neurology* **75,** 2176–2184 (2010).
6. Edwardson, M. A., Lucas, T. H., Carey, J. R. & Fetz, E. E. New modalities of brain stimulation for stroke rehabilitation. *Exp. Brain Res.* **224,** 335–358 (2013).
7. Jackson, A., Mavoori, J. & Fetz, E. E. Long-term motor cortex plasticity induced by an electronic neural implant. *Nature* **444,** 56–60 (2006).
8. Lucas, T. H. & Fetz, E. E. Myo-cortical crossed feedback reorganizes primate motor cortex output. *Ann. Intern. Med.* **158,** 5261–5274 (2013).
9. Morrell, F. Effect of anodal polarization on the firing pattern of single cortical cells. *Ann N Y Acad Sci* **92,** 860–876 (1961).
10. Bindman, L. J., Lippold, O. C. J. & Redfearn, J. W. T. Long-lasting Changes in the Level of the Electrical Activity of the Cerebral Cortex produced by Polarizing Currents. *Nature* **196,** 584–585 (1962).
11. Gartside, I. B. Mechanisms of sustained increases of firing rate of neurones in the rat cerebral cortex after polarization: role of protein synthesis. *Nature* **220,** 383–384 (1968).
12. Bindman, L. J., Lippold, O. C. & Redfearn, J. W. The Action Of Brief Polarizing Currents On The Cerebral Cortex Of The Rat (1) During Current Flow And (2) In The Production Of Long-Lasting After-Effects. *J Physiol* **172,** 369–382 (1964).
13. Creutzfeldt, O. D., Fromm, G. H. & Kapp, H. Influence of transcortical d-c currents on cortical neuronal activity. *Exp. Neurol.* **5,** 436–452 (1962).
14. Priori, A., Berardelli, A., Rona, S., Accornero, N. & Manfredi, M. Polarization of the human motor cortex through the scalp. *Neuroreport* **9,** 2257–2260 (1998).
15. Nitsche, M. A. & Paulus, W. Excitability changes induced in the human motor cortex by weak transcranial direct current stimulation. *J. Physiol.* **527,** 633–639 (2000).

16. Jackson, M. P. *et al.* Animal models of transcranial direct current stimulation: Methods and mechanisms. *Clinical Neurophysiology* **127,** 3425–3454 (2016).

17. Bikson, M. *et al.* Safety of Transcranial Direct Current Stimulation: Evidence Based Update 2016. *Brain Stimulation* **9,** 641–661 (2016).

18. Marshall, L. Transcranial Direct Current Stimulation during Sleep Improves Declarative Memory. *J. Neurosci.* **24,** 9985–9992 (2004).

19. Reis, J. *et al.* Noninvasive cortical stimulation enhances motor skill acquisition over multiple days through an effect on consolidation. *Proc. Natl. Acad. Sci. U. S. A.* **106,** 1590–1595 (2009).

20. Elsner, B., Kugler, J., Pohl, M. & Mehrholz, J. Transcranial direct current stimulation (tDCS) for improving activities of daily living, and physical and cognitive functioning, in people after stroke. *Cochrane Database of Systematic Reviews* **2016,** (2016).

21. Frank, E. *et al.* Treatment of chronic tinnitus with repeated sessions of prefrontal transcranial direct current stimulation: Outcomes from an open-label pilot study. *J. Neurol.* **259,** 327–333 (2012).

22. Fregni, F. *et al.* A sham-controlled, phase II trial of transcranial direct current stimulation for the treatment of central pain in traumatic spinal cord injury. *Pain* **122,** 197–209 (2006).

23. Kekic, M., Boysen, E., Campbell, I. C. & Schmidt, U. A systematic review of the clinical efficacy of transcranial direct current stimulation (tDCS) in psychiatric disorders. *Journal of Psychiatric Research* **74,** 70–86 (2016).

24. Hummel, F. *et al.* Effects of non-invasive cortical stimulation on skilled motor function in chronic stroke. *Brain* **128,** 490–499 (2005).

25. Ferrucci, R., Mameli, F. & Guidi, I. Transcranial direct current stimulation improves recognition memory in Alzheimer disease. *Neurology* **71,** 493–498 (2008).

26. Flöel, A. *et al.* Non-invasive brain stimulation improves object-location learning in the elderly. *Neurobiol. Aging* **33,** 1682–1689 (2012).

27. Hummel, F. C. *et al.* Effects of brain polarization on reaction times and pinch force in chronic stroke. *BMC Neurosci.* **7,** (2006).

28. Külzow, N. *et al.* No effects of non-invasive brain stimulation on multiple sessions of object-location-memory training in healthy older adults. *Front. Neurosci.* **11,** (2018).

29. Horvath, J. C., Forte, J. D. & Carter, O. Quantitative review finds no evidence of cognitive effects in healthy populations from single-session transcranial direct current stimulation (tDCS). *Brain Stimul.* **8,** 535–550 (2015).

30. Hill, A. T., Fitzgerald, P. B. & Hoy, K. E. Effects of Anodal Transcranial Direct Current Stimulation on Working Memory: A Systematic Review and Meta-Analysis of Findings from Healthy and Neuropsychiatric Populations. *Brain Stimulation* **9,** 197–208 (2016).

31. Accornero, N., Li Voti, P., La Riccia, M. & Gregori, B. Visual evoked potentials modulation during direct current cortical polarization. *Exp. Brain Res.* **178,** 261–266 (2007).

32. Lindenberg, R., Sieg, M. M., Meinzer, M., Nachtigall, L. & Flöel, A. Neural correlates of unihemispheric and bihemispheric motor cortex stimulation in healthy young adults. *Neuroimage* **140,** 141–149 (2016).

33. Kirimoto, H. *et al.* Transcranial direct current stimulation over the motor association cortex induces plastic changes in ipsilateral primary motor and somatosensory cortices. *Clin. Neurophysiol.* **122,** 777–783 (2011).

34. Wirth, M. *et al.* Effects of transcranial direct current stimulation (tDCS) on behaviour and electrophysiology of language production. *Neuropsychologia* **49,** 3989–3998 (2011).

35. Horvath, J. C., Forte, J. D. & Carter, O. Evidence that transcranial direct current stimulation (tDCS) generates little-to-no reliable neurophysiologic effect beyond MEP amplitude modulation in healthy human subjects: A systematic review. *Neuropsychologia* **66,** 213–236 (2015).

36. Griffin, D. M., Hudson, H. M., Belhaj-Saïf, A. & Cheney, P. D. Hijacking cortical motor output with repetitive microstimulation. *J. Neurosci.* **31,** 13088–13096 (2011).

37. Wiethoff, S., Hamada, M. & Rothwell, J. C. Variability in response to transcranial direct current stimulation of the motor cortex. *Brain Stimul.* **7,** 468–475 (2014).

38. Bikson, M. *et al.* Effects of uniform extracellular DC electric fields on excitability in rat hippocampal slices in vitro. *J Physiol* **557,** 175–190 (2004).

39. Rahman, A. *et al.* Cellular effects of acute direct current stimulation: Somatic and synaptic terminal effects. *J. Physiol.* **591,** 2563–2578 (2013).

40. Kronberg, G., Bridi, M., Abel, T., Bikson, M. & Parra, L. C. Direct Current Stimulation Modulates LTP and LTD: Activity Dependence and Dendritic Effects. *Brain Stimul.* **10,** 51–58 (2017).

41. Rahman, A., Lafon, B., Parra, L. C. & Bikson, M. Direct current stimulation boosts synaptic gain and cooperativity in vitro. *J. Physiol.* **595,** 3535–3547 (2017).

42. Fritsch, B. *et al.* Direct current stimulation promotes BDNF-dependent synaptic plasticity: potential implications for motor learning. *Neuron* **66,** 198–204 (2010).

43. Vöröslakos, M. *et al.* Direct effects of transcranial electric stimulation on brain circuits in rats and humans. *Nat. Commun.* **9,** (2018).

44. Krause, M. R. *et al.* Transcranial Direct Current Stimulation Facilitates Associative Learning and Alters Functional Connectivity in the Primate Brain. *Curr. Biol.* **27,** 3086–3096.e3 (2017).

45. Huang, Y. *et al.* Measurements and models of electric fields in the in vivo human brain during transcranial electric stimulation. *Elife* **6,** (2017).

46. Kar, K., Duijnhouwer, J. & Krekelberg, B. Transcranial Alternating Current Stimulation Attenuates Neuronal Adaptation. *J. Neurosci.* **37,** 2325–2335 (2017).

47. Datta, A. *et al.* Gyri-precise head model of transcranial direct current stimulation: Improved spatial focality using a ring electrode versus conventional rectangular pad. *Brain Stimul.* **2,** (2009).

48. Bikson, M., Rahman, A. & Datta, A. Computational models of transcranial direct current

stimulation. *Clin. EEG Neurosci.* **43,** 176–183 (2012).

49. Esmaeilpour, Z. *et al.* Incomplete evidence that increasing current intensity of tDCS boosts outcomes. *Brain Stimulation* (2017). doi:10.1016/j.brs.2017.12.002

50. Brown, J. a, Lutsep, H. L., Weinand, M. & Cramer, S. C. Motor cortex stimulation for the enhancement of recovery from stroke: a prospective, multicenter safety study. *Neurosurgery* **58,** 464–73 (2006).

51. Lindenberg, R., Nachtigall, L., Meinzer, M., Sieg, M. M. & Floel, A. Differential effects of dual and unihemispheric motor cortex stimulation in older adults. *J Neurosci* **33,** 9176–9183 (2013).

52. Churchland, M. M. *et al.* Neural population dynamics during reaching. *Nature* **487,** 51–56 (2012).

53. Rousche, P. J. & Normann, R. A. A method for pneumatically inserting an array of penetrating electrodes into cortical tissue. *Ann. Biomed. Eng.* **20,** 413–422 (1992).

54. Kelly, R. C. *et al.* Comparison of Recordings from Microelectrode Arrays and Single Electrodes in the Visual Cortex. *J. Neurosci.* **27,** 261–264 (2007).

55. Simeral, J. D., Kim, S.-P. P. S.-P., Black, M. J., Donoghue, J. P. & Hochberg, L. R. Neural control of cursor trajectory and click by a human with tetraplegia 1000 days after implant of an intracortical microelectrode array. *J Neural Eng* **8,** 25027 (2011).

56. Fraser, G. W. & Schwartz, A. B. Recording from the same neurons chronically in motor cortex. *J. Neurophysiol.* **22,** 11–17 (2012).

57. Richardson, A. G., Borghi, T. & Bizzi, E. Activity of the same motor cortex neurons during repeated experience with perturbed movement dynamics. *J. Neurophysiol.* **107,** 3144–54 (2012).

58. Vaidya, M. *et al.* Ultra-long term stability of single units using chronically implanted multielectrode arrays. in *2014 36th Annual International Conference of the IEEE Engineering in Medicine and Biology Society, EMBC 2014* 4872–4875 (2014). doi:10.1109/EMBC.2014.6944715

59. Abeles, M., Goldstein, M. H., Skaggs, W. E. & McNaughton, B. L. Theta Phase Precession in Hippocampal Neurinak Populations abd the Compression of. *Hippocampus* **6,** 149–172 (1996).

60. Telenczuk, B. *et al.* Local field potentials primarily reflect inhibitory neuron activity in human and monkey cortex. *Sci. Rep.* **7,** (2017).

61. Brendel, W., Romo, R. & Machens, C. K. Demixed Principal Component Analysis. *Adv. Neural Inf. Process. Syst. 24* 2654–2662 (2011).

62. Kobak, D. *et al.* Demixed principal component analysis of neural population data. *Elife* **5,** (2016).

63. Litwin-Kumar, A., Harris, K. D., Axel, R., Sompolinsky, H. & Abbott, L. F. Optimal Degrees of Synaptic Connectivity. *Neuron* **93,** 1153–1164.e7 (2017).

64. Mazzucato, L., Fontanini, A. & La Camera, G. Stimuli Reduce the Dimensionality of Cortical Activity. *Front. Syst. Neurosci.* **10,** (2016).

65. Radman, T., Ramos, R. L., Brumberg, J. C. & Bikson, M. Role of cortical cell type and morphology in subthreshold and suprathreshold uniform electric field stimulation in vitro. *Brain Stimul.* (2009). doi:10.1016/j.brs.2009.03.007

66. English, D. F. *et al.* Pyramidal Cell-Interneuron Circuit Architecture and Dynamics in Hippocampal Networks. *Neuron* **96,** 505–520.e7 (2017).

67. Vigneswaran, G., Kraskov, A. & Lemon, R. N. Large Identified Pyramidal Cells in Macaque Motor and Premotor Cortex Exhibit 'Thin Spikes': Implications for Cell Type Classification. *J. Neurosci.* **31,** 14235–14242 (2011).

68. Horvath, J. C., Carter, O. & Forte, J. D. Transcranial direct current stimulation: five important issues we aren't discussing (but probably should be). *Front. Syst. Neurosci.* **8,** (2014).

69. Cheney, P. D. & Fetz, E. E. Functional classes of primate corticomotoneuronal cells and their relation to active force. *J. Neurophysiol.* **44,** 773–791 (1980).

70. Fetz, E. E. Are movement parameters recognizably coded in the activity of single neurons? *Behav. Brain Sci.* **15,** 679–690 (1992).

71. Thach, W. T. Correlation of neural discharge with pattern and force of muscular activity, joint position, and direction of intended next movement in motor cortex and cerebellum. *J. Neurophysiol.* **41,** 654–676 (1978).

72. Skaggs, W. E., McNaughton, B. L. & Gothard, K. M. in *Advances in Neural Information Processing Systems 5* (eds. Hanson, S. J., Cowan, J. D. & Giles, C. L.) 1030–1037 (Morgan-Kaufmann, 1993). doi:10.1109/PROC.1977.10559

73. Churchland, M. M. & Shenoy, K. V. Temporal Complexity and Heterogeneity of Single-Neuron Activity in Premotor and Motor Cortex. *J. Neurophysiol.* **97,** 4235–4257 (2007).

74. Shenoy, K. V., Sahani, M. & Churchland, M. M. Cortical Control of Arm Movements: A Dynamical Systems Perspective. *Annu. Rev. Neurosci.* **36,** 337–359 (2013).

75. Sadtler, P. T. *et al.* Neural constraints on learning. *Nature* **512,** 423–426 (2014).

76. Cunningham, J. P. & Yu, B. M. Dimensionality reduction for large-scale neural recordings. *Nature Neuroscience* **17,** 1500–1509 (2014).

77. Levy, R. B. & Reyes, A. D. Spatial Profile of Excitatory and Inhibitory Synaptic Connectivity in Mouse Primary Auditory Cortex. *J. Neurosci.* **32,** 5609–5619 (2012).

78. Cambiaghi, M. *et al.* Brain transcranial direct current stimulation modulates motor excitability in mice. *Eur. J. Neurosci.* **31,** 704–709 (2010).

79. Esmaeilpour, Z. *et al.* Notes on Human Trials of Transcranial Direct Current Stimulation between 1960 and 1998. *Front. Hum. Neurosci.* **11,** (2017).

80. Sasaki, K. & Gemba, H. Compensatory motor function of the somatosensory cortex for the motor cortex temporarily impaired by cooling in the monkey. *Exp. Brain Res.* **55,** 60–68 (1984).

81. Fetz, E. E., Finocchio, D. V, Baker, M. A. & Soso, M. J. Sensory and motor responses of precentral cortex cells during comparable passive and active joint movements. *J. Neurophysiol.* **43,** 1070–1089 (1980).

82. Soso, M. J. & Fetz, E. E. Responses of identified cells in postcentral cortex of awake monkeys during comparable active and passive joint movements. *J. Neurophysiol.* **43,** 1090–1110 (1980).

83. Wang, B. *et al.* Firing Frequency Maxima of Fast-Spiking Neurons in Human, Monkey, and Mouse Neocortex. *Front. Cell. Neurosci.* **10,** (2016).

84. Terzuolo, C. A. & Bullock, T. H. Measurement of Imposed Voltage Gradient Adequate to Modulate Neuronal Firing. *Proc. Natl. Acad. Sci.* **42,** 687–694 (1956).

85. Anastassiou, C. A., Perin, R., Markram, H. & Koch, C. Ephaptic coupling of cortical neurons. *Nat. Neurosci.* (2011). doi:10.1038/nn.2727

86. Ozen, S. *et al.* Transcranial Electric Stimulation Entrains Cortical Neuronal Populations in Rats. *J. Neurosci.* **30,** 11476–11485 (2010).

87. Isaacson, J. S. & Scanziani, M. How inhibition shapes cortical activity. *Neuron* **72,** 231–243 (2011).

88. Matsumura, M., Chen, D., Sawaguchi, T., Kubota, K. & Fetz, E. E. Synaptic interactions between primate precentral cortex neurons revealed by spike-triggered averaging of intracellular membrane potentials in vivo. *J. Neurosci.* **16,** 7757–7767 (1996).

89. Hendy, A. M., Teo, W. P. & Kidgell, D. J. Anodal Transcranial Direct Current Stimulation Prolongs the Cross-education of Strength and Corticomotor Plasticity. *Med. Sci. Sports Exerc.* **47,** 1788–1797 (2015).

90. Zhu, F. F. *et al.* Cathodal transcranial direct current stimulation over left dorsolateral prefrontal cortex area promotes implicit motor learning in a golf putting task. *Brain Stimul.* **8,** 784–786 (2015).

91. Rioult-Pedotti, M. S., Friedman, D. & Donoghue, J. P. Learning-induced LTP in neocortex. *Science (80-.).* **290,** 533–536 (2000).

92. Golub, M. D. *et al.* Learning by neural reassociation. *Nat. Neurosci.* **21,** 607–616 (2018).

93. Ajemian, R., D'Ausilio, A., Moorman, H. & Bizzi, E. Why professional athletes need a prolonged period of warm-up and other peculiarities of human motor learning. *J. Mot. Behav.* **42,** 381–8 (2010).

94. Ajemian, R., D'Ausilio, A., Moorman, H. & Bizzi, E. A theory for how sensorimotor skills are learned and retained in noisy and nonstationary neural circuits. *Proc. Natl. Acad. Sci. U. S. A.* **110,** E5078-87 (2013).

95. Edwards, D. *et al.* Physiological and modeling evidence for focal transcranial electrical brain stimulation in humans: A basis for high-definition tDCS. *Neuroimage* (2013). doi:10.1016/j.neuroimage.2013.01.042

96. Grossman, N. *et al.* Noninvasive Deep Brain Stimulation via Temporally Interfering Electric Fields. *Cell* **169,** 1029–1041 (2017).

97. Luu, P. *et al.* Slow-Frequency Pulsed Transcranial Electrical Stimulation for Modulation of Cortical Plasticity Based on Reciprocity Targeting with Precision Electrical Head Modeling. *Front. Hum. Neurosci.* **10,** (2016).

98. Brown, J. A., Lutsep, H., Cramer, S. C. & Weinand, M. Motor cortex stimulation for

enhancement of recovery after stroke: case report. *Neurol Res* **25,** 815–818 (2003).

99. Zanos, S., Richardson, A. G., Shupe, L., Miles, F. P. & Fetz, E. E. The Neurochip-2: an autonomous head-fixed computer for recording and stimulating in freely behaving monkeys. *IEEE Trans Neural Syst Rehabil Eng* **19,** 427–435 (2011).

100. Bi, G. Q. & Poo, M. M. Synaptic modifications in cultured hippocampal neurons: dependence on spike timing, synaptic strength, and postsynaptic cell type. *J. Neurosci.* **18,** 10464–10472 (1998).

101. Hebb, D. O. *The organization of behavior; a neuropsychological theory*. *The organization of behavior; a neuropsychological theory.* (Wiley, 1949).

102. Lucas, T. H. Activity-dependent motor cortex reorganization induced with recurrent intracortical stimulation triggered from forelimb muscles. (2009).

103. Nudo, R. J., Jenkins, W. M. & Merzenieh, M. M. Repetitive microstimulation alters the cortical representation of movements in adult rats. *Somatosens. Mot. Res.* **7,** 463–483 (1990).

104. Hess, G., Aizenman, C. D. & Donoghue, J. P. Conditions for the induction of long-term potentiation in layer II/III horizontal connections of the rat motor cortex. *J Neurophysiol* **75,** 1765–1778 (1996).

105. Jacobs, K. M. & Donoghue, J. P. Reshaping the Cortical Motor Map by Unmasking Latent Intracortical Connections. *Source Sci. New Ser.* **251,** 944–947 (1991).

106. Iriki, A., Pavlides, C., Keller, A. & Asanuma, H. Long-term potentiation in the motor cortex. *Science (80-.).* **245,** 1385–1387 (1989).

107. Bliss, T. V. P. & Lømo, T. Long-lasting potentiation of synaptic transmission in the dentate area of the anaesthetized rabbit following stimulation of the perforant path. *J. Physiol.* **232,** 331–356 (1973).

108. Monte-Silva, K. *et al.* Induction of late LTP-like plasticity in the human motor cortex by repeated non-invasive brain stimulation. *Brain Stimul.* **6,** 424–432 (2013).

109. Stefan, K., Kunesch, E., Benecke, R., Cohen, L. G. & Classen, J. Mechanisms of enhancement of human motor cortex excitability induced by interventional paired associative stimulation. *J. Physiol.* **543,** 699–708 (2002).

110. Pascual-Leone, A. *et al.* Effects of focal transcranial magnetic stimulation on simple reaction time to acoustic, visual and somatosensory stimuli. *Brain* **115,** 1045–1059 (1992).

111. Foltys, H. *et al.* Motor control in simple bimanual movements: A transcranial magnetic stimulation and reaction time study. *Clin. Neurophysiol.* **112,** 265–274 (2001).

112. Thabit, M. N. *et al.* Movement-related cortical stimulation can induce human motor plasticity. *J. Neurosci.* **30,** 11529–11536 (2010).

113. Asanuma, H. & Okuda, O. Effects of transcallosal volleys on pyramidal tract cell activity of cat. *J. Neurophysiol.* **25,** 198–208 (1961).

114. Ferbert, A. *et al.* Interhemispheric inhibition of the human motor cortex. *J. Physiol.* **453,** 525–546 (1992).

115. Pascual-leone, A., Brasil-neto, J. P., Valls-solé, J., Cohen, L. G. & Hallett, M. Simple reaction time to focal transcranial magnetic stimulation: Comparison with reaction time to acoustic, visual and somatosensory stimuli. *Brain* **115,** 109–122 (1992).

116. Bütefisch, C. M., Khurana, V., Kopylev, L. & Cohen, L. G. Enhancing encoding of a motor memory in the primary motor cortex by cortical stimulation. *J. Neurophysiol.* **91,** 2110–2116 (2004).

117. Kilavik, B. E., Zaepffel, M., Brovelli, A., MacKay, W. A. & Riehle, A. The ups and downs of beta oscillations in sensorimotor cortex. *Exp. Neurol.* **245,** 15–26 (2013).

118. Bremer, F. Physiology of the corpus callosum. *Res. Publ. Assoc. Res. Nerv. Ment. Dis.* (1958).

119. Jankowska, E., Padel, Y. & Tanaka, R. The mode of activation of pyramidal tract cells by intracortical stimuli. *J. Physiol.* **249,** 617–636 (1975).

120. Netz, J., Ziemann, U. & Hömberg, V. Hemispheric asymmetry of transcallosalinhibition in man. *Exp. Brain Res.* **104,** 527–533 (1995).

121. Murase, N., Duque, J., Mazzocchio, R. & Cohen, L. G. Influence of Interhemispheric Interactions on Motor Function in Chronic Stroke. *Ann. Neurol.* **55,** 400–409 (2004).

122. Hummel, F. C. & Cohen, L. G. Non-invasive brain stimulation: a new strategy to improve neurorehabilitation after stroke? *Lancet Neurology* **5,** 708–712 (2006).

123. Beaulé, V., Tremblay, S. & Théoret, H. Interhemispheric control of unilateral movement. *Neural Plasticity* **2012,** (2012).

124. Engel, A. K. & Fries, P. Beta-band oscillations--signalling the status quo? *Curr. Opin. Neurobiol.* **20,** 156–65 (2010).

125. Siegel, M., Donner, T. H. & Engel, A. K. Spectral fingerprints of large-scale neuronal interactions. *Nature Reviews Neuroscience* **13,** 121–134 (2012).

126. Seki, K. & Fetz, E. E. Gating of Sensory Input at Spinal and Cortical Levels during Preparation and Execution of Voluntary Movement. *J. Neurosci.* **32,** 890–902 (2012).

127. Heinrichs-Graham, E., Kurz, M. J., Gehringer, J. E. & Wilson, T. W. The functional role of post-movement beta oscillations in motor termination. *Brain Struct. Funct.* **222,** 3075–3086 (2017).

128. Khanna, P. & Carmena, J. M. Beta band oscillations in motor cortex reflect neural population signals that delay movement onset. *Elife* **6,** (2017).

APPENDIX

DATA AVAILABILITY

Data presented in chapters 1-3 is stored and available to Fetz group WaNPRC network members on the "R" drive (R\\research\Fetz Lab\abogaard). Raw data from chapter 1 is stored as PLX files (sorted SUA) and TDT files (LFP, snippets) and the naming of the file corresponds to experiment date (yyyymmdd). Meta-data regarding these sessions is stored in an excel file (meta-data.xls) in the "Spanky" directory (R\\research\Fetz Lab\abogaard\Spanky). Matlab compatible data are stored as <ExpID>.mat, where <ExpID> refers to the session name. The variable within each of these mat files is named "root" and corresponds to an OOARB.Session objects (see below).

CODE AVAILABILITY (THE OOARB TOOLBOX)

Code used to produce figures presented in Chapter 1 (with the exception of the population dynamics analysis, which used python) is available on the WaNPRC "R" drive (R\\research\Fetz Lab\abogaard\+OOARB and …\neurowest). The OOARB toolbox is an extensive library of object-oriented MATLAB code that defines three data classes (session, spike, lfp). Utah array recordings during a task are well suited for this toolbox.

The main utility of this toolbox is data-handling across multiple, simultaneously recorded streams that have different sample rates (or type, such as point process or continuous data). With this toolbox, a "session" object (a variable called "root" in the following examples) is created that has properties for spike objects, lfp objects, and behavioral data, among others. "State" properties (e.g. root.epoch and root.cel) are defined by the user and set epochs of time and neurons upon which the data properties are dependent. Thus, collecting all RU torques during

spikes from a given set of neurons between particular experimental time windows can be accomplished in a single line of code.

In addition to experiment-specific properties, the OOARB toolbox is home to many important function (called methods in the object-oriented language) that are useful for common analyses involving the correlation of SUA and behavioral or LFP data.

To use the OOARB toolbox, copy the +OOARB directory into a folder that is in MATLAB's path (in the current working directory). Code from within the toolbox may be imported as a library by typing "import OOARB.*", or run as individual functions ("OOARB.Spike.CrossCorr"). Documentation for the toolbox exists in the header of each .m file.